Progress in Oceanography 142 (2016) 72–104

Contents lists available at ScienceDirect

Progress in Oceanography

journal homepage: www.elsevier.com/locate/pocean

Seasonality, phytoplankton succession and the biogeochemical impacts of an autumn storm in the northeast Atlantic Ocean

Stuart C. Painter [a,*], Madelaine Finlay [a,b], Victoria S. Hemsley [a,c], Adrian P. Martin [a]

[a] National Oceanography Centre, European Way, Southampton SO14 3ZH, UK
[b] School of Biosciences and Medicine, Faculty of Health and Medical Sciences, University of Surrey, Guildford GU2 7XH, UK
[c] Ocean and Earth Science, University of Southampton, National Oceanography Centre, European Way, Southampton SO14 3ZH, UK

ARTICLE INFO

Article history:
Received 1 July 2015
Received in revised form 16 November 2015
Accepted 9 February 2016
Available online 17 February 2016

ABSTRACT

Phytoplankton chemotaxonomic distributions are examined in conjunction with taxon specific particulate biomass concentrations and phytoplankton abundances to investigate the biogeochemical consequences of the passage of an autumn storm in the northeast Atlantic Ocean. Chemotaxonomy indicated that the phytoplankton community was dominated by nanoplankton (2–20 μm), which on average represented 75 ± 8% of the community. Microplankton (20–200 μm) and picoplankton (<2 μm) represented 21 ± 7% and 4 ± 3% respectively with the microplankton group composed of almost equal proportions of diatoms (53 ± 17%) and dinoflagellates (47 ± 17%). Total chlorophyll-a (TCHLa = CHLa + Divinyl CHLa) concentrations ranged from 22 to 677 ng L^{-1}, with DvCHLa making minor contributions of between <1% and 13% to TCHLa. Higher DvCHLa contributions were seen during the storm, which deepened the surface mixed layer, increased mixed layer nutrient concentrations and vertically mixed the phytoplankton community leading to a post-storm increase in surface chlorophyll concentrations. Picoplankton were rapid initial respondents to the changing conditions with pigment markers showing an abrupt 4-fold increase in proportion but this increase was not sustained post-storm. 19′-HEX, a chemotaxonomic marker for prymnesiophytes, was the dominant accessory pigment pre- and post-storm with concentrations of 48–435 ng L^{-1}, and represented 44% of total carotenoid concentrations. Accompanying scanning electron microscopy results support the pigment-based analysis but also provide detailed insight into the nano- and microplankton communities, which proved to be highly variable between pre-storm and post-storm sampling periods. Nanoplankton remained the dominant size class pre- and post-storm but the microplankton proportion peaked during the period of maximum nutrient and chlorophyll concentrations. Classic descriptions of autumn blooms resulting from storm driven eutrophication events promoting phytoplankton growth in surface waters should be tempered with greater understanding of the role of storm driven vertical reorganization of the water column and of resident phytoplankton communities. Crucially, in this case we observed no change in integrated chlorophyll, particulate organic carbon or biogenic silica concentrations despite also observing a ~50% increase in surface chlorophyll concentrations which indicated that the surface enhancement in chlorophyll concentrations was most likely fed from below rather than resulting from in situ growth. Though not measured directly there was no evidence of enhanced export fluxes associated with this storm. These observations have implications for the growing practice of using chlorophyll fluorescence from remote platforms to determine ocean productivity late in the annual productivity period and in response to storm mixing.

© 2016 The Authors. Published by Elsevier Ltd. This is an open access article under the CC BY license (http://creativecommons.org/licenses/by/4.0/).

1. Introduction

Autumn phytoplankton blooms are considered a characteristic feature of the temperate North Atlantic Ocean (Longhurst, 1995; Martinez et al., 2011). Widely considered to result from storm induced deepening of the surface mixed layer or weakening thermal stratification due to general cooling of the water column, autumn blooms are classically considered as short lived periods of phytoplankton productivity following the entrainment of nutrients from depth (Russell and Yonge, 1928; Harvey et al., 1935; Margalef, 1969). Autumn blooms however receive far less attention than spring blooms due to greatly reduced productivity amplitudes, shorter durations, interannual variability in timing and

* Corresponding author. Tel.: +44 (0) 23 8059 6209; fax: +44 (0) 23 8059 6247.
E-mail address: stuart.painter@noc.ac.uk (S.C. Painter).

http://dx.doi.org/10.1016/j.pocean.2016.02.001
0079-6611/© 2016 The Authors. Published by Elsevier Ltd.
This is an open access article under the CC BY license (http://creativecommons.org/licenses/by/4.0/).

spatial variability in occurrence (Colebrook and Robinson, 1961); though the same factors may also be considered true of spring blooms.

Cyclonic weather systems are closely linked with autumn blooms but there is also growing interest in the biological impact of large cyclones particularly in the low latitude ocean where the occurrence of cyclones is expected to increase in frequency in future (Knutson et al., 2010). As most large cyclones studied to date approach hurricane force weather systems detailed supporting biological observations are rare, and studies have instead examined satellite derived surface fields of temperature and chlorophyll to identify post-storm impacts. Consequently, consensus over the biological effects remains equivocal and the attributable impacts can be highly variable between studies (e.g. Babin et al., 2004; Hanshaw et al., 2008; Foltz et al., 2015). In particular, in high latitude regions such as the Barents Sea, it has been shown that despite having a measurable impact on surface chlorophyll concentrations the overall significance of cyclones for annual productivity estimates was negligible due to the low frequency of cyclone occurrence during the annual growth period (Morozov et al., 2015).

In temperate latitudes the surface signature and duration of impact of cyclones and autumn blooms can be similar thus it raises the question of how one may be distinguished from the other in the temperate ocean. Both are commonly identified from increased surface chlorophyll concentrations, particularly in remote sensing datasets, with the duration of enhancement lasting from a few days to a few weeks at most. Through detailed in situ observation, several studies have revealed coincident increased diatom abundances during the autumn (Russell and Yonge, 1928; Harvey et al., 1935; Corlett, 1953), leading to widespread adoption of the idea that autumn blooms are synonymous with periods of increased diatom productivity in surface waters following storm induced nutrient entrainment. However, alternative mechanisms have been proposed including reduced grazing pressure due to dilution of plankton within a deeper mixed layer allowing phytoplankton growth to outpace grazing losses (Smayda, 1957; Cushing, 1959) and more recently, the vertical redistribution of an established subsurface chlorophyll maximum to shallower depths (Perry et al., 2008). Consequently, the irregularity in timing, or even complete absence, of autumn phytoplankton blooms in the temperate ocean suggests multiple factors are likely to be important and that greater detail of the impact of cyclones is needed.

Recent and continued debate about the mechanisms initiating the annual growth period has refocused attention on several basic assumptions in biological oceanography (Sverdrup, 1953; Behrenfeld, 2010; Taylor and Ferrari, 2011; Mahadevan et al., 2012; Behrenfeld and Boss, 2014). However, the pursuit of a single initiating physical mechanism (e.g. mixed layer depth) or biological control (e.g. grazing) has been criticized as being too simplistic with multiple complementary factors instead considered more likely (Lindemann and St-John, 2014). Similar basic assumptions accepted as explaining the autumn bloom are likely therefore to be open to scrutiny and reinvestigation. Few biogeochemical studies focus on the autumn period particularly in the open ocean. This may be due to perceived difficulties in capturing the period of destratification and mixing, as destratification is predominately driven by heat loss and autumn storms mixing the surface ocean, or by the interannual variability in storm track and frequency of storm occurrence precluding in situ observation of their impacts. More commonly, ship-based activities are largely curtailed during storms meaning that direct observation is limited.

In this study, we report biogeochemical and chemotaxonomic observations from the northeast Atlantic prior to, during and immediately after the passage of a significant autumn storm. This has allowed us to investigate the sequence of events leading to a post-storm increase in surface chlorophyll concentrations representative of an autumn bloom yet which was not associated with any change in integrated chlorophyll concentrations. First, though we begin with a brief review of the typical conditions in the northeast Atlantic in late summer.

1.1. Typical summer conditions in the northeast Atlantic

The seasonal cycle of the northeast Atlantic Ocean is relatively well understood (e.g. Longhurst, 1995, 1998; Körtzinger et al., 2001, 2008). In the region ~40–60°N a stratified water column with low surface nutrient concentrations is typical during the summer (Körtzinger et al., 2008; Steinhoff et al., 2010; Hartman et al., 2012). It is common for a diatom dominated subsurface chlorophyll maximum to form at the base of the mixed layer in late spring and persist throughout the summer (Lochte and Pfannkuche, 1987; Painter et al., 2010b). This subsurface chlorophyll maximum is dominated by cells >5 μm in size (whilst cells 1–5 μm in size dominate the waters of the mixed layer above (Joint et al., 1993)), and is closely associated with a fucoxanthin pigment maximum (a pigment marker for diatoms; Gibb et al., 2001). One predictable and therefore measureable consequence of deeper mixing in autumn would be to entrain diatoms from depth into the surface ocean (e.g. Corlett, 1953). Continuous Plankton Recorder (CPR) records do suggest a weak increase in diatom abundance in some areas of the northeast Atlantic in autumn (McQuatters-Gollop et al., 2007) but in the open waters of the northeast Atlantic (~40–43.5°N) Leblanc et al. (2005) estimated that diatoms accounted for only 2–4% of integrated (0–200 m) primary production during autumn due to continued Si limitation of the diatom community. Widely reported and significant latitudinal gradients in environmental conditions and community structure between 40°N and 60°N however suggest that a *de facto* assumption of Si limitation of the autumn diatom community is increasingly incorrect further north (e.g. North Atlantic Bloom Experiment (Ducklow and Harris, 1993); the Prime Study (Savidge and Williams, 2001) and references therein).

The surface waters of the mixed layer are dominated by nanoplankton throughout the summer with suggestions that the northeast Atlantic is essentially in steady state as microzooplankton herbivory rates broadly match daily productivity rates (Colebrook, 1984, 1986; Burkill et al., 1993). Joint et al. (1993) estimated that up to 49% of the chlorophyll and up to 51% of integrated production could be found in the 1–5 μm size fraction in July. Separately, chemotaxonomic studies based on photosynthetic and carotenoid pigment distributions reveal a nanoplankton dominance during the summer months with the pigment 19′-hexanoyloxyfucoxanthin (HEX; a widely used pigment marker for prymnesiophytes; Jeffrey et al., 2011) consistently found to be the dominant accessory pigment (Williams and Claustre, 1991; Barlow et al., 1993a, 1993b, 2002, 2004; Gibb et al., 2000, 2001). The resupply of nutrients to the mixed layer in autumn could therefore also lead to a secondary increase in prymnesiophytes, which typically succeed diatoms in the annual cycle of species succession (e.g. Barlow et al., 1993a, 1993b), but which, assuming a coccolithophore dominance, are argued to bloom under mid-summer conditions of high irradiance intensities, shallow mixed layers and high NO_3^-:PO_4^{3-} ratios (e.g. Tyrrell and Merico, 2004; Lessard et al., 2005).

The presence of latitudinal gradients implies that care must be taken in the interpretation of seasonal changes and in the comparison of different studies. Between 37 and 62°N Gibb et al. (2001) revealed a transition in the phytoplankton community from one dominated by prymnesiophytes in the north to one dominated by cyanobacteria and prochlorophytes in the south. A hydrographic front at ~52.5°N marked the approximate transition point. Pigment analyses conducted on Atlantic Meridional Transect (AMT)

cruises 3 and 5 (October 1996 and October 1997 respectively) also indicate a nanoplankton dominance at ~50°N giving way to picoplankton dominance in the south (Gibb et al., 2000; Aiken and Bale, 2000; Barlow et al., 2002; Robinson et al., 2006, 2009).

Despite these established summertime conditions comparatively little is known about the summer to autumn transition period. Karayanni et al. (2005) reported annual maximum abundances of *Prochlorococcus*, but annual minimum abundances of *Synechococcus*, pico- (<2 μm) and nanoeukaryote (<10 μm) phytoplankton in September/October and estimated that *Prochlorococcus* accounted for 43 ± 7% of integrated phytoplankton biomass in the <10 μm size fraction during the autumn period. In a related study by Maixandeau et al. (2005) the inclusion of larger microplankton (>10 μm) in their analysis did not alter the conclusion of a picoplankton dominance of the autumnal phytoplankton community biomass due to the low abundance of microplankton. These observations are consistent with the general autumnal reduction in microplankton (dinoflagellate and diatom) abundances relative to the spring and summer periods, reported from CPR data (McQuatters-Gollop et al., 2007), but apparently at odds with inferences made from the majority of summertime observations that consistently show a nanoplankton dominance of the phytoplankton community with only minor contributions from picoplankton. It is necessary however to interpret the observations of Karayanni et al. (2005) (and others) in the context of well established latitudinal gradients in phytoplankton community structure, sea surface temperature, nutrient concentrations and stratification (Savidge and Williams, 2001; van de Poll et al., 2013; Mojica et al., 2015). Specifically, over the latitude range of the study reported by Karayanni et al. (2005) (38–45°N) the typical spring to autumn seasonal increase in the picoplankton contribution to euphotic zone integrated production has been related to changes in seasonal stratification and sea surface temperature (van de Poll et al., 2013; Mojica et al., 2015). Further north the contribution from picoplankton to integrated production was considerably lower (<3%) (van de Poll et al., 2013). Thus, whilst the observations of Karayanni et al. (2005) are indicative of the latitude of that study and of the influence of the seasonal northward expansion of the North Atlantic subtropical gyre, they are unlikely to be comparable to studies conducted a few degrees further north where picoplankton abundance is markedly lower and the community is increasingly dominated by nanoplankton.

2. Materials and methods

2.1. Cruise overview

R.R.S. Discovery cruise D381 (August 28th to October 3rd 2012; year days 241–277) was the penultimate cruise prior to her retirement and replacement and represented the last time she was used by UK oceanographers to sample within the northeast Atlantic Ocean after 50 years of service. All samples reported in this study were collected within a small geographic region of approximately 70 km radius around 48.69°N, 16.19°W. This nominal position is ~40 km southeast of the Porcupine Abyssal Plain (PAP) sustained observatory (49°N, 16.5°W; Hartman et al., 2012), >250 km from the northwest European continental shelf break and >500 km from the nearest landmass (Fig. 1). During the cruise 21 stations were occupied and sampled for a variety of biogeochemical parameters and up to 297 underway samples were collected and processed (Fig. 1; note that data from station 5 (a shelf edge station) and station 13 (loss of CTD package) are not reported here resulting in a total of 19 stations). Due to logistical requirements for other shipboard activities the cruise was split into two legs, the first leg covered the period August 28th to September 13th (days 241–257) and the second leg covered September 14th to October 3rd (days 258–277) with the ship being off site between September 12th and September 17th (days 256–260). A significant autumn storm was encountered during the second leg of the cruise (maximum wind speeds on September 25th, day 269) and to compare and contrast pre- and post-storm conditions we distinguish stations that were sampled pre-storm (stations 6–12) from those sampled post-storm (stations 14–21).

2.2. Mixed layer depth

Mixed layer depths were determined at each station using a density threshold criterion of +0.125 kg m^{-3} relative to near surface densities (Monterey and Levitus, 1997).

2.3. Nutrient concentrations

Water samples for the measurement of the major macronutrients nitrate, ($NO_3^- + NO_2^-$, hereafter NO_3^-) orthosilicic acid ($Si(OH)_4$) and phosphate (PO_4^{3-}) were collected from both the ship's underway water system (nominal sampling depth 5 m) and all depths sampled via CTD casts. All samples were analysed using a Skalar *Sanplus* segmented flow autoanalyser following common methodologies (Kirkwood, 1996).

2.4. Water column particulate analyses

Water samples for particulate concentrations were collected from both the ship's underway water system and from CTD sampling bottles within the upper 60 m of the water column.

2.4.1. Particulate organic carbon and nitrogen analyses

For each particulate inorganic carbon (POC) and nitrogen (PON) sample up to 1 L of seawater was filtered on to pre-ashed (>450 °C for >4 h) 25 mm glass fibre filters (Whatman GF/F). After filtration samples were rinsed with a weak 1% solution of HCl to remove inorganic carbon residue. Filters were frozen at −20 °C onboard and later oven dried overnight at 40 °C, before being pelleted into tin capsules using a laboratory press and analysed for POC and PON content using a Carlo Erba CHN Analyzer.

2.4.2. Biogenic silica analysis

For biogenic silica (bSi) measurements 1 L of seawater was carefully measured and filtered on to a 25 mm diameter 0.8 μm polycarbonate filter. In instances where the full volume did not pass through the filter, the volume of the remaining unfiltered seawater was subtracted from the starting volume to obtain an accurate measure of the volume filtered. Filters and blanks (fresh filters washed with 0.2 μm filtered seawater) were oven dried at 40 °C and stored in 15 mL Falcon tubes until alkaline digestion and analysis for the Si content could be undertaken. In the laboratory, 5 mL of 0.2 M NaOH was added to each Falcon tube to digest the sample which was baked at 85 °C for at least 2 h (Ragueneau and Treguer, 1994). After returning to room temperature approximately 10 mL of 0.1 M HCl was added to neutralize the pH of the digested sample to pH 7–8. The solution was then analysed on a segmented flow autoanalyser using a routine methodology for Si analysis (Kirkwood, 1996). Results are reported as the measured molar concentration of $Si(OH)_4$, and have not been converted to the equivalent concentration of opal (SiO_2) (see Torres-Valdes et al. (2014) for discussion of this problem).

2.4.3. Particulate inorganic carbon analysis

Particulate inorganic carbon (PIC) concentrations were measured on 1 L seawater samples filtered on to 25 mm 0.2 μm polycarbonate filters. Each filter was rinsed with a weak solution of

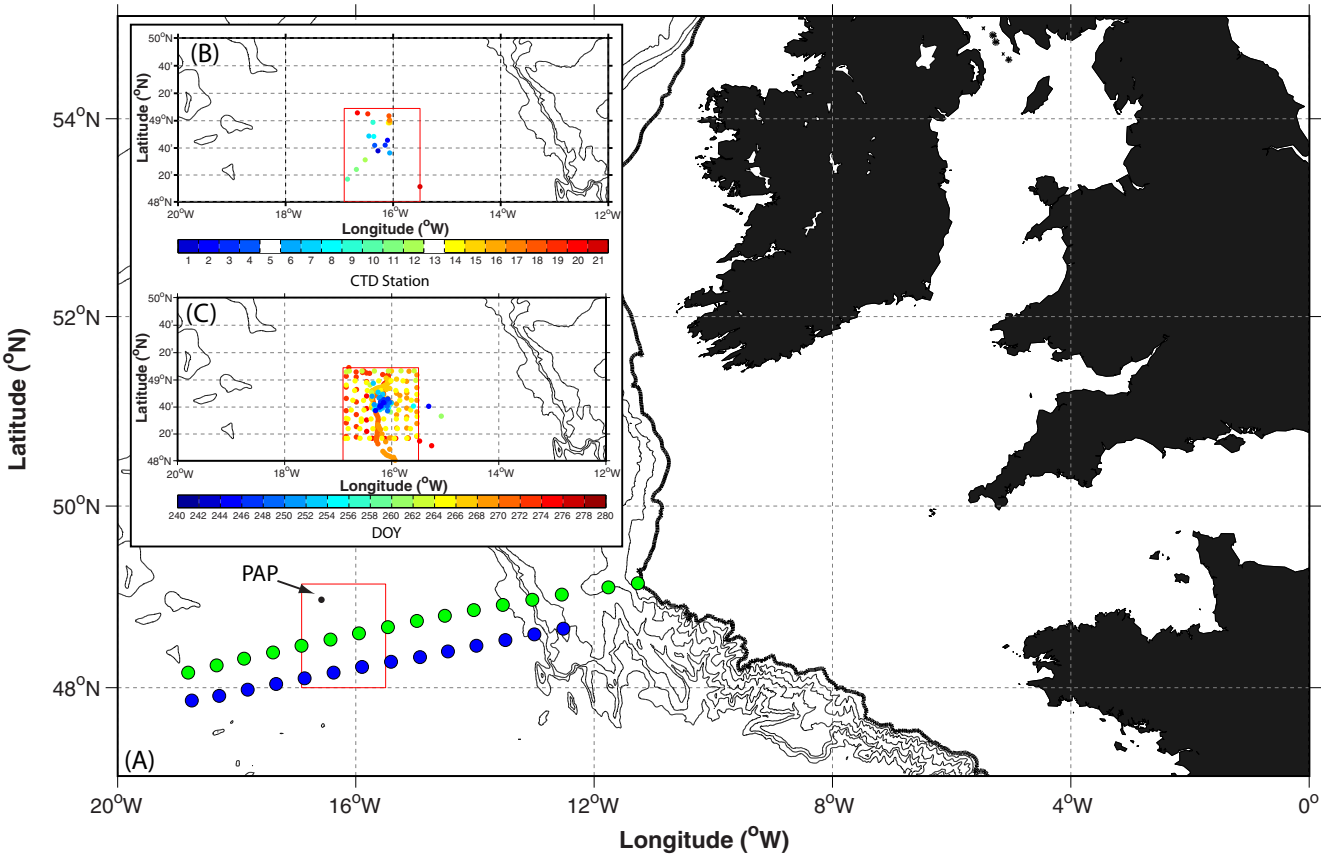

Fig. 1. Map showing (a) the location of the study site (red box) in relation to neighbouring landmasses and the sample positions from two Continuous Plankton Recorder transects conducted in September 2012 (green dots) and October 2012 (blue dots). Inset images show (b) the position of the CTD stations within the study site (colour coded by station number) and (c) underway sample positions within the study site (colour coded by sampling day of year). Note that CTD station 5, which was conducted at the shelf edge (~9.7°W), is not shown in the inset image and is not included in this study and CTD station 13 was terminated early and no data were returned. (For interpretation of the references to colour in this figure legend, the reader is referred to the web version of this article.)

analytical grade ammonium solution (pH ~ 9.7) to remove residual sea salt and placed in a 2 mL Eppendorf tube. Filters were oven dried at 40 °C and stored until analysis. Frequently, we were unable to filter the full litre so the volume of the remaining unfiltered seawater was subtracted from the starting volume to obtain an accurate measure of the volume filtered. In the laboratory all samples were weighed, extracted in 2% nitric acid and analysed using Inductively Coupled Plasma Atomic Mass Spectrometry (Green et al., 2003). Sample carbon content (as PIC) was calculated assuming a 1:1 molar equivalency with the measured calcium content (present as $CaCO_3$) of the sample (Van Bleijswijk et al., 1994).

2.5. Phytoplankton pigment analyses

2.5.1. Fluorometric chlorophyll analysis

Chlorophyll-a concentrations (CHLa; mg m^{-3}) were determined fluorometrically from 250 mL of seawater collected from the underway supply and filtered on to 25 mm Whatman GF/F filters (nominal pore size ~0.7 μm) before pigment extraction in 6 mL of 90% acetone at 4 °C over a subsequent 18–20 h period. Pigment extracts were measured on a Turner Designs "Trilogy" fluorometer calibrated against a pure chlorophyll-a standard (Sigma, UK) following Welschmeyer (1994).

Post cruise analysis revealed that the fluorometric chlorophyll measurements significantly overestimated total chlorophyll concentrations obtained via HPLC analysis (see next section). On average, HPLC derived total chlorophyll-a (TCHLa = Divinyl CHLa + CHLa) concentrations were 41% lower than fluorometric CHLa concentrations. Although this difference could be due to HPLC sample storage and pigment degradation we think this unlikely as it has been shown that with the appropriate storage pigment degradation is minimal (Mantoura et al., 1997). The higher fluorometric concentrations are more likely to be due to the presence of accessory pigments and phaeopigments. As the fluorometric dataset is larger than the HPLC dataset and thus provides greater temporal resolution in surface waters we have calibrated the underway fluorometric chlorophyll concentrations using the following equation derived from a Model II linear regression between the HPLC TCHLa and fluorometric CHLa datasets,

$$\text{HPLC [TCHLa]} = 0.3697 \times \text{Fluorometric [CHLa]} + 0.0140 \quad (n = 96,\ R^2 = 0.54,\ p < 0.001). \tag{1}$$

Although there is considerable scatter in the datasets and the correlation is relatively modest (R^2 = 0.54), the correction harmonizes the two datasets to an acceptable level. Note that in the following we make reference to both fluorometric CHLa and HPLC TCHLa observations.

2.5.2. High performance liquid chromatography (HPLC) pigment analysis

Phytoplankton pigments were quantitatively measured via high performance liquid chromatography (HPLC) analysis using the reverse-phase binary solvent method described by Barlow et al. (1997). Typically, 2 L water samples were collected from both the ship's underway water system (nominal sampling depth 5 m) and from CTD sampling bottles and filtered on to 25 mm glass fibre

filters (Whatman GF/F; nominal pore size 0.7 μm). Filters were immediately placed in cryogenic vials and frozen at −80 °C onboard ship. Samples remained frozen at −80 °C for several months before analysis though storage conditions were excellent and degradation is considered unlikely (Mantoura et al., 1997). Pigments were extracted in 3–5 mL of 90% HPLC grade acetone and sonicated on-ice for 30 s. All samples were analysed on a Thermo Finnigan SpectraSYSTEM 3 HPLC system fitted with a 3 μm Hypersil MOS-2 C-8 column and peak shapes analysed using ChromQuest software to provide pigment concentrations. Pigment identification was made through co-elution of pigment standards (Sigma, UK and DHI, Denmark). Measured pigments and abbreviations are reported in Table 1.

2.5.3. Diagnostic pigment analysis

Diagnostic pigment analysis (DPA; Vidussi et al., 2001; Uitz et al., 2006) was used to determine the taxonomic composition and size class structure of the phytoplankton community. We have used the definitions described by Aiken et al. (2009). Our diagnostic pigment (DP) index was based upon the sum of seven pigments selected for their taxonomic relevance (Table 1)

$$\mathrm{DP}\ (\mathrm{mg\ m^{-3}}) = \mathrm{ALLO} + \mathrm{BUT} + \mathrm{CHLb} + \mathrm{FUC} + \mathrm{HEX} + \mathrm{PER} + \mathrm{ZEA} \quad (2)$$

Following previous studies (e.g. Uitz et al., 2006; Aiken et al., 2009) we took a cautious approach to the interpretation of the pigment data and calculated the proportion of DP by plankton size class rather than by phytoplankton taxon given stated ambiguities in the derivation of phytoplankton functional types from pigment data using alternative methodologies such as CHEMTAX (Mackey et al., 1996; Aiken et al., 2009; Higgins et al., 2011). Note however that the pigment based size class definition used here is an approximation and that diatoms can formally be found in nano- and microplankton dimension based size classes.

2.6. Scanning electron microscopy analysis

In addition to pigment-based chemotaxonomy of the phytoplankton community we also collected a surface water sample (from 4 to 13 m depth) from each CTD cast primarily for examination and enumeration of the coccolithophore community. However, the nature of the analysis also provided a semi-quantitative assessment of other 'hard celled' plankton groups such as diatoms, dinoflagellates and silicoflagellates. The results for these latter groups are considered semi-quantitative due to the high magnification used to image coccolithophores and the limited area of the total sample filter analysed (approximately 1/300th of each sample).

Briefly, 1 L water samples were collected from the shallowest sampled depth on each CTD cast and filtered onto 25 mm 0.2 μm polycarbonate filters. Filters were washed with a weak solution of analytical grade ammonium solution (pH ~ 9.7) to remove residual sea salt, placed in labelled petrislides and dried at 40 °C overnight. For analysis a small section (~0.5 × ~0.5 cm) of filter was cut from the centre, mounted on an aluminium stub and coated in ~2 nm gold. A Leo 1450VP Scanning Electron Microscope (SEM) was used to automatically capture 225 images of consecutive fields of view arranged in a 15 × 15 grid at a magnification of ~×5000. Each image was visually examined for the abundance and species content of coccolithophores, and detached coccoliths as well as for any diatom, dinoflagellate and silicoflagellate cells using a range of taxonomic identification keys (Lebour, 1925, 1930; Dodge, 1985; Winter and Siesser, 1994; Hasle and Syvertsen, 1997; Heimdal, 1997; Steidinger and Tangen, 1997; Cros and Fortuno, 2002; Young et al., 2003). Cell abundances were estimated as described in Poulton et al. (2011).

2.7. Ancillary data

2.7.1. Jenkinson Gale Index

We make use of the Jenkinson Gale Index to assess storm frequency and storm intensity in the northeast Atlantic (Jenkinson

Table 1
Phytoplankton pigments and diagnostic pigment formulae used during this study, including pigment abbreviations and taxonomic significance (adapted from Aiken et al., 2009).

Pigment/pigment groups	Abbreviation	Taxonomic significance
Chlorophyll-a	CHLa	Photosynthetic pigment in algae
Chlorophyll-b	CHLb	Chlorophytes
Chlorophyll-c1 + c2	CHLc2	Diatoms, dinoflagellates, prymnesiophytes, chrysophytes
Chlorophyll-c3	CHLc3	Diatoms, dinoflagellates, prymnesiophytes, chrysophytes
Divinyl chlorophyll-a	DvCHLa	Prochlorophytes
Peridinin	PER	Dinoflagellates
19′-Butanoyloxyfucoxanthin	BUT	Chrysophytes
Fucoxanthin	FUC	Diatoms
19′-Hexanoyloxyfucoxanthin	HEX	Prymnesiophytes
Prasinoxanthin	PRA	
Violoxanthin	VIO	Green algae
Diadinoxanthin	DIA	Diatoms, prymnesiophytes
Alloxanthin	ALLO	Cryptophytes
Zeaxanthin	ZEA	Cyanobacteria
Lutein	LUT	Green algae
Gyroxanthin	GYRO	Dinoflagellates
β-Carotene	CAR	Photoprotective carotenoid
Total chlorophyll-a	TCHLa (CHLa + DvCHLa)	
Total carotenoids	TC (ALLO + BUT + CARO + DIA + FUC + HEX + LUT + PER + VIO + ZEA)	
Accessory pigments	AP (TCHLa + CHLb + CHLc2 + CHLc3)	
Total pigment	TP (TCHLa + AP)	
Diagnostic pigments	DP (ALLO + BUT + CHLb + FUC + HEX + PER + ZEA)	
Photosynthetic carotenoids	PSC (PER + BUT + FUX + HEX)	
Photoprotective carotenoids	PPC (VIO + DIA + ALLO + ZEA + CAR + LUT)	
Diatom proportion of DP	=FUC/DP	
Dinoflagellate proportion of DP	=PER/DP	
Microplankton proportion of DP	MICRO = diatom proportion of DP + dinoflagellate proportion of DP	
Nanoplankton proportion of DP	NANO = (ALLO + BUT + CHLb + HEX)/DP	
Prokaryote proportion of DP	PROK = ZEA/DP	

and Collison, 1977). The Jenkinson Gale Index is a classification scheme of daily atmospheric circulation based on Lamb Weather Types (Lamb, 1972) for the region 45–65°N, 20°W–10°E. An updated objective index for the period 1871–present based on climate reanalysis products (Kalnay et al., 1996; Compo et al., 2011) is described by Jones et al. (2013) and is available from the Climatic Research Unit, University of East Anglia (http://www.cru.uea.ac.uk/cru/data/lwt/). Briefly, the gale index term (G; unitless), is calculated from mean sea level atmospheric pressure measurements over the gridded domain as

$$G = \sqrt{[F^2 + (0.5Z)^2]} \quad (3)$$

where F is the resultant geostrophic wind flow (units hPa per 10° latitude) and Z the total geostrophic shear vorticity (units hPa per 10° latitude) (Jenkinson and Collison, 1977; Jones et al., 1993). Following Hulme and Jones (1991) we classify gales based on the exceedance of certain threshold values of G, thus $G > 30$ indicates a gale, $G > 40$ a severe gale and $G > 50$ a very severe gale.

2.7.2. MODIS Aqua remote sensing data

MODIS Aqua satellite data (R2013 processing) were analysed to provide the seasonal and interannual context for our cruise based observations. We examined the full satellite record of 4 km resolution 8-day composite images of chlorophyll and particulate inorganic carbon for the period 2002–2012. Significant cloud cover throughout the year over the locality of our study site reduced the total number of retrievals for individual pixels so to maximize data coverage we averaged all valid pixel retrievals for an area approximately 60×90 km in size (48.58–49.42°N, 16.08–16.92°W). We then produced a climatological annual cycle of chlorophyll and PIC from this time series by averaging all 8-day time periods together. This climatological timeseries was used to place the 2012 annual cycle of chlorophyll and particulate inorganic carbon in context.

Sea surface temperature (SST) data from the MODIS platform are also used in the following to provide additional detail regarding intra-cruise environmental variability for the period August 20th to October 14th 2012.

2.7.3. Continuous Plankton Recorder data

Data from the Continuous Plankton Recorder (CPR) survey were used to provide additional information on phytoplankton abundance and seasonality (Warner and Hays, 1994; Batten et al., 2003; Reid et al., 2003; Beaugrand, 2004; Richardson et al., 2006). Monthly average phytoplankton abundances from the standard E5 area of the northeast Atlantic for the period 2000–2012 were kindly supplied by the Sir Alister Hardy Foundation for Ocean Science, Plymouth, UK (Johns, 2014). Using the CPR monthly abundance data for 2000–2011 we constructed the mean annual cycle in abundance of total diatoms, total dinoflagellates and total coccolithophores and then examined the 2012 monthly abundance data in relation to the mean annual cycle to establish the normality of the 2012 year. In addition we also obtained data from two individual CPR tows that traversed our study site in September and October 2012 to provide support for our SEM based assessment of the phytoplankton community.

2.7.4. Shipboard irradiance measurements

Surface measurements of irradiance (400–700 nm; PAR) were made by a pair of ship-fitted PAR sensors (SKE510, Skye Instruments, UK). Integrated daily PAR and daily maximum surface PAR were derived from these data. Mean mixed layer PAR was estimated from these measurements using equations detailed in Kirk (2010) and an attenuation coefficient (Kd) of 0.1055 m^{-1} derived from MODIS Aqua products. This was necessitated by the loss of the entire CTD package at station 13 and only having nighttime CTD casts at earlier stations. Technical problems also resulted in data gaps in the afternoon after the solar maximum on days 273, 274 and 275 at the end of the cruise. These gaps could not reliably be interpolated over and as such integrated daily PAR and mean mixed layer PAR could not be estimated for these days. The depth of the euphotic zone was approximated as 4.6/Kd, providing a mean euphotic depth of 44 m. To account for inaccuracies in the estimation of Kd we assumed a 50 m euphotic depth.

3. Results

3.1. Mean annual cycle of irradiance and temperature in relation to chlorophyll and particulate inorganic carbon

The annual cycles in SST, surface PIC and chlorophyll concentrations in relation to day length, based on an astronomical model for the position of the PAP observatory (49°N, 16.5°W) are presented in Fig. 2. We include these data to set our observations in context. Day length varies from ~8 h of sunlight per day in December to a maximum of ~16 h of sunlight per day in June. Maximum PIC concentrations occur in May and precede maximum day length by 1 month but PIC concentrations for June and July are not too dissimilar with mean monthly values of 0.4–0.5 mmol m^{-3} at this time being quite distinct from mean values <0.35 mmol m^{-3} during the rest of the year. It is notable that PIC concentrations throughout August to November remain higher than concentrations seen between January and April. Mean monthly chlorophyll concentrations peak in June (>0.6 mg m^{-3}), coincident with maximum day length. The annual increase in chlorophyll from January to May is fairly linear with day length, whereas the increase/decrease towards/away from the annual maximum in June occurs at a markedly different rate. The post bloom decrease in surface chlorophyll concentration is distinctly non-linear between July and November with concentrations in September and October lying above a straight line linking July, August and November. This deviation is strongest in October and we interpret this as signifying the presence of recurrent autumn blooms in the northeast Atlantic Ocean (Martinez et al., 2011). The relationship between day length and SST describes a circular path with maximum SST occurring in August, some two months later than maximum day length. The May–July PIC peak typically occurs over a 3.5 °C temperature range but at times when the average day length is 15–16 h in duration. Similarly, maximum chlorophyll concentrations in June occur when mean day lengths are longest but approximately mid-way (~14.5 °C) within the seasonal temperature range (~12–17 °C).

3.1.1. 2012 annual cycle

The MODIS Aqua chlorophyll record indicated that 2012 was characterised with an unusually large chlorophyll peak in early June that was almost twice the magnitude of any previous bloom seen in the 2002–2012 instrumental record (Fig. 3). Peak chlorophyll concentrations reached almost 3 mg m^{-3}, with previous maximum concentrations being <1.4 mg m^{-3}. The climatological annual cycle of surface chlorophyll concentrations indicated that autumn 2012 was not dissimilar to typical conditions for this region at this time of year. However, because of the unusual magnitude of the 2012 spring bloom by September chlorophyll concentrations (~0.5 mg m^{-3}) were still higher than the climatological average concentration for the time of year (~0.3 mg m^{-3}). MODIS Aqua PIC concentrations were also relatively high during June reaching ~1 mmol m^{-3} but were not exceptional compared to previous years (Fig. 3). PIC concentrations during autumn 2012 were similar to the climatological mean concentration (~0.3 mmol m^{-3}) and well within the typical

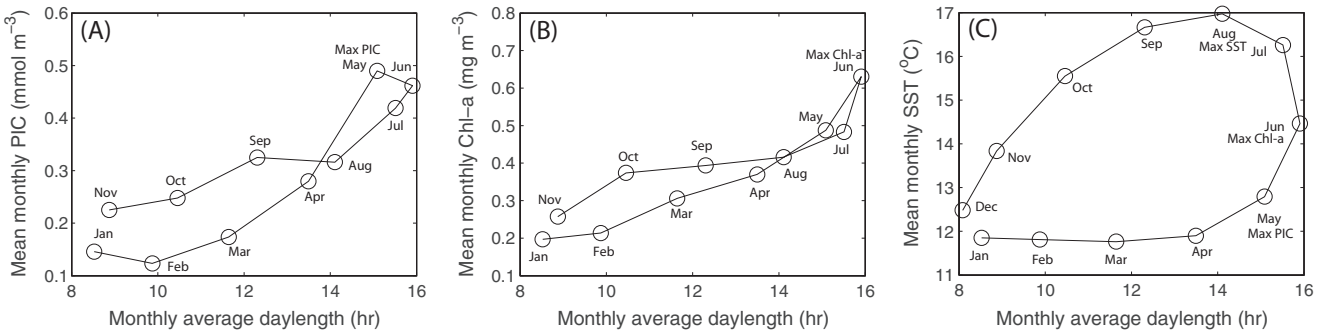

Fig. 2. Annual cycle and relationships between (a) mean monthly MODIS Aqua surface PIC concentrations and daylength, (b) mean monthly MODIS Aqua surface Chl-a concentrations and daylength and (c) mean monthly MODIS Aqua SST and daylength. The highest monthly maximum is indicated for each parameter. All data is provisionally based on a position of 49°N, 16.5°W.

range of previous autumn concentrations. Consequently, 2012 was characterised with an unusually intense spring bloom that was coincident with above average PIC concentrations, but by late summer/early autumn surface PIC concentrations were similar to typical autumn conditions whilst surface chlorophyll concentrations were above average.

3.2. Environmental conditions during the observation period

3.2.1. Satellite perspective

We present in Fig. 4 a series of 8-day MODIS-Aqua composite images to detail the spatial variability of surface environmental conditions during the cruise period. Strong north–south gradients in sea surface temperature (SST) and surface chlorophyll and PIC concentrations were present with lower SST (<16.5 °C), and higher chlorophyll (>0.4 mg m^{-3}) and PIC concentrations (>0.4 mmol m^{-3}) to the north than to the south. There was significant variability in these surface fields during the cruise, and in particular we note the large-scale southward movement (by >2° latitude) of the 16.5 °C isotherm during the week of 21st–28th September as well as the general decline in surface chlorophyll and PIC concentrations with time. Based on the general environmental conditions and spatial gradients there are indications that a hydrographic front ran through or close to the study site. Specific to the cruise survey area (red box in Fig. 4), SST was generally >16.5 °C, chlorophyll was generally <0.5 mg m^{-3}, and PIC < 0.4 mmol m^{-3} during the observation period. However, during 21st–28th September, SST decreased to <16 °C and both chlorophyll and PIC concentrations responded by decreasing/increasing respectively, reflecting wider regional changes.

3.2.2. In situ surface, meteorological and irradiance conditions

The dominant physical forcing event during the cruise related to the passage of a cyclonic storm through the study site when air pressure decreased to 997.5 mbar and northerly winds with maximum speeds of ~18 m s^{-1}, gusting to over 20 m s^{-1}, were experienced. Based on the period of sustained decreasing/increasing atmospheric pressure/wind speed we define the storm dates as year days 266–271 (see Fig. 10). In situ measurements from the ships thermosalinograph show the mean SST during the cruise was 17 ± 0.4 °C but a noticeable decrease of over 1 °C was recorded following the storm with post-storm SST remaining lower than the pre-storm temperatures (see Fig. 10).

The Jenkinson Gale index was used to characterise the storm event. Fig. 5 shows both the daily gale index for 2012 and the range in daily gale index values for the period 2000–2011. There are several features to note. Firstly, during 2012 there were 49 gale days (G > 30) and of those 8 were severe gale days (G > 40), and 1 was a very severe gale day (G > 50) (note we report gale days not the number of gales which can span multiple days). Secondly, of the 8 severe gale days identified in the 2012 record 4 took place between January and April (winter/spring) and 3 during November and December (late autumn). The remaining severe gale day occurred on September 25th 2012, and matched precisely the storm we endured at sea. Consequently, the Jenkinson Gale index indicates that the storm we encountered was one of the most severe of 2012 but more interestingly was an isolated event occurring ~5 months after the last G40 gale in April and 5 weeks before the next G40 gale at the start of November. Using the lower threshold of G30 however it can be seen that two G30 gales occurred in August (Fig. 5). Thirdly, viewed in the context of daily gale indices for the period 2000–2011 there is little to suggest that 2012 was in any way unusual as the majority of daily gale index values for 2012 lie well within the range of values for 2000–2011. There are inevitably a few instances of lower or higher values than the range for specific days (e.g. April 2nd) but there is no indication of any systematic difference. Fourthly, it is noteworthy that although some G40 storms have previously occurred in September storms of this severity are generally rare during this month and do not occur at all in August (at least for the period 2000–2011), thus the severity of the storm appears unusual. G40 storms are however increasingly common throughout November and December. Finally, it may be important that the gale index for 2012 dropped suddenly from values of ~20 to a value <10 on September 20th, indicating a weaker atmospheric circulation pattern (i.e. more stable conditions) before then climbing steadily to the maximum on September 25th. The magnitude of the climb from the minimum on September 20th to the maximum on September 25th is not in itself unusual (see a similar example in late October/early November 2012) but the duration of this steady increase (6 days) appears longer than other examples. Thus the fetch period may have implications for surface wind stress, upper-ocean mixing and biological impacts.

Irradiance conditions during the cruise are presented in Fig. 6. Integrated daily irradiance varied from 13 to 47.7 mol photons m^{-2} d^{-1}, averaging 31.7 mol photons m^{-2} d^{-1} over the cruise. We highlight the gradual reduction in integrated daily irradiance with time, which represented the gradual seasonal reduction in daylength, as an important environmental factor. The mean mixed layer irradiance, which varied from 2.8 to 14.4 mol photons m^{-2} d^{-1} with a cruise average of 7.9 mol photons m^{-2} d^{-1} also appeared to show a gradual reduction in time but in this case was due to changes in both surface irradiance and mixed layer depth. We also show in Fig. 6 the daily maximum surface irradiance, which was broadly constant although with some variability due to cloud cover.

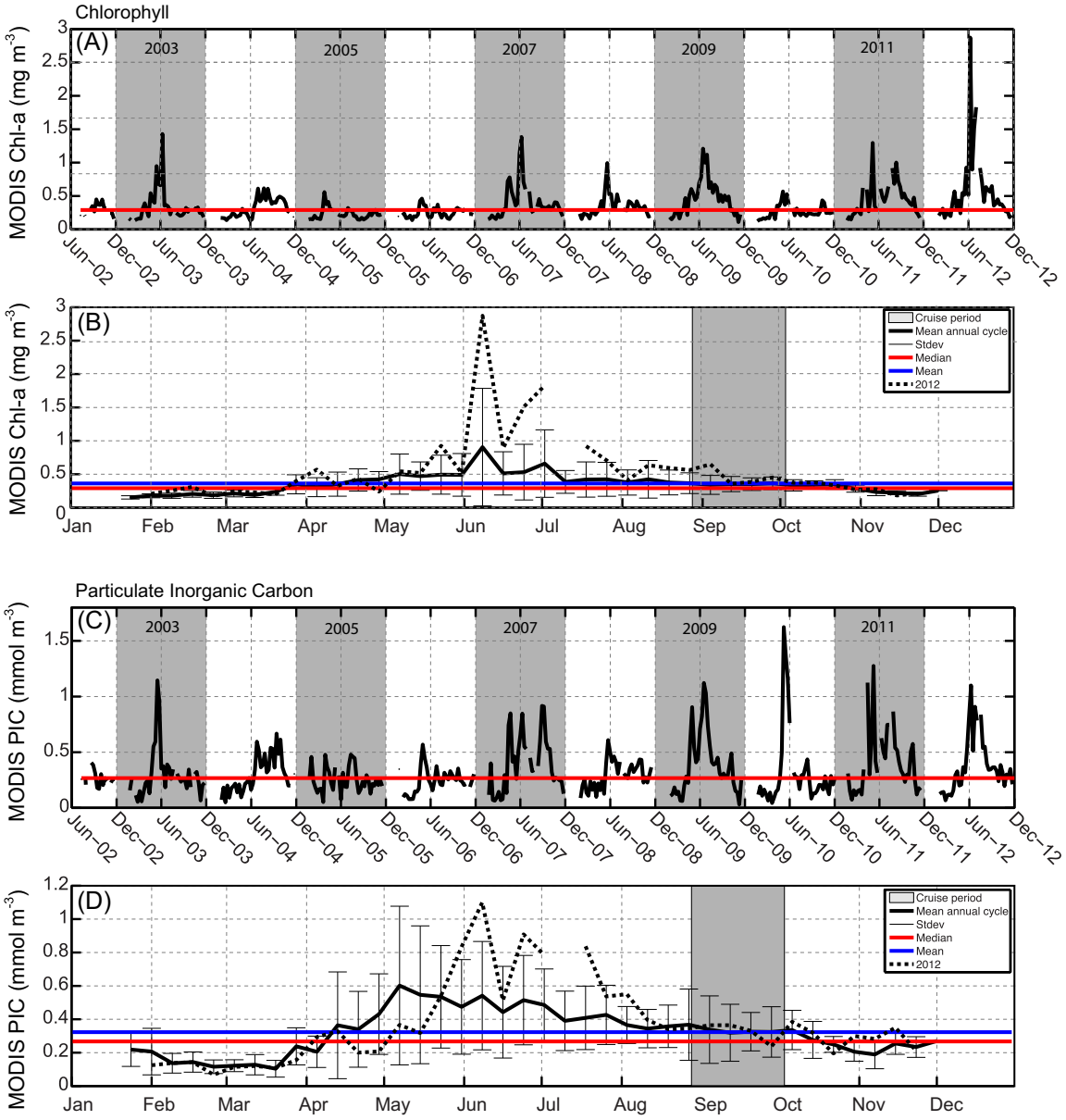

Fig. 3. MODIS Aqua measurements of (a) 2002–2012 surface chlorophyll time series based on averaged data for the geographic region 48.58–49.42°N, 16.08–16.92°W, (b) climatological annual cycle of chlorophyll based on 2002–2011 data (thick solid line with error bars) with 2012 annual cycle overlaid (dashed line), (c) 2002–2012 surface particulate inorganic carbon (PIC) time series based on averaged data for the geographic region 48.58–49.42°N, 16.08–16.92°W, (d) climatological annual cycle of particulate inorganic carbon based on 2002–2011 data (thick solid line with error bars) with 2012 annual cycle overlaid (dashed line). In all subplots the red horizontal line represents the median concentration and if present, the blue horizontal line represents the mean concentration. In panels (b and d) the cruise period is indicated by the grey shaded box. (For interpretation of the references to colour in this figure legend, the reader is referred to the web version of this article.)

3.3. Hydrography

Hydrographic stability was assessed via T/S analysis of the upper 400 m of the water column (Fig. 7). Eastern North Atlantic Central Water (ENACW) (Pollard et al., 1996) dominated the region but we were able to identify the presence of two closely related variants of ENACW based on temperature and salinity values. ENACWt which has salinity values >35.66 and is known as the subtropical variant and ENACWp which has salinity <35.66 and is known as the subpolar variant (Rios et al., 1992; Castro et al., 1998) were readily identifiable in our data. Following previous studies we used a temperature of 12.2 °C and a salinity of 35.66 to distinguish between these variants (Rios et al., 1992; Castro et al., 1998; Bode et al., 2002; Painter et al., 2010a). In general ENACWt was more prevalent but 7 CTD profiles with lower maximum salinities clearly sampled ENACWp (Table 2). These 7 profiles were loosely grouped to the northern half of the study site (Fig. 1) and covered the duration of the cruise. Profiles 1–4 were closely grouped in time and space and undertaken during the first leg of the cruise whereas profiles 9, 18 and 19 were undertaken during the second leg of the cruise. The variable presence of ENACWp supports the notion that a hydrographic front ran through the study site, with ENACWp predominately found in the north and ENACWt to the south. Further support for this is apparent in underway salinity measurements (not shown) which indicate higher salinities in the south and lower salinities in the north of the study site, however the data are insufficient to determine the position and movement of this front.

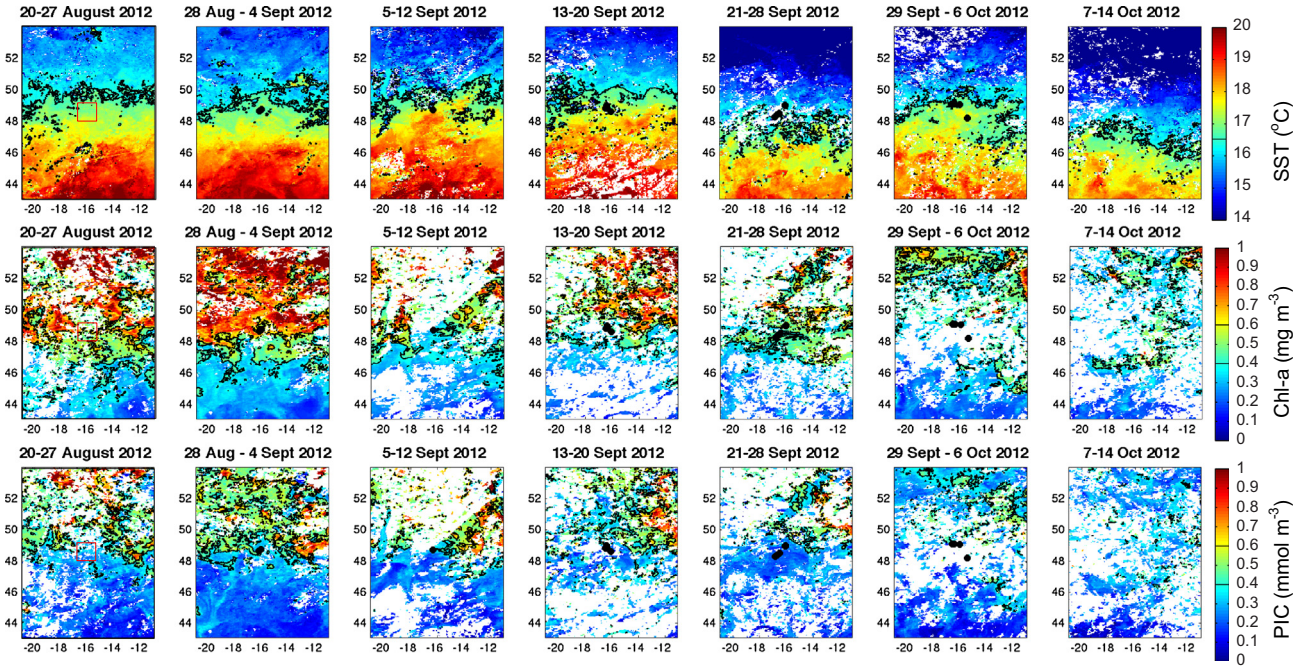

Fig. 4. MODIS Aqua 8-day composite maps showing the spatiotemporal variability for the period 20th August to 14th October 2012 in (top row) sea surface temperature (SST) (middle row) Chlorophyll (Chl-a), and (bottom row) particulate inorganic carbon (PIC). The red boxes in the panels of the left hand column denote the cruise survey area as shown in Fig. 1, whilst the black dots in the panels of columns 2–6 denote CTD positions. Where present contour lines signify values indicated on the respective colour bars. (For interpretation of the references to colour in this figure legend, the reader is referred to the web version of this article.)

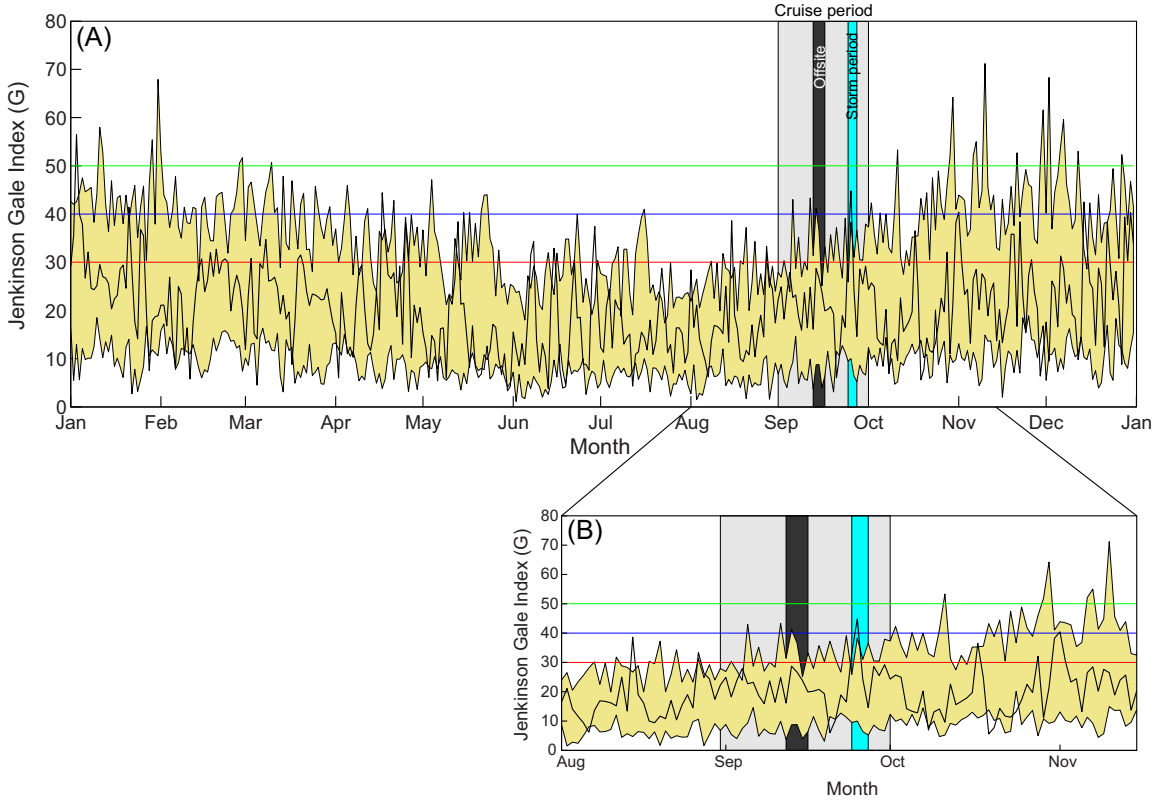

Fig. 5. Time series of storm occurrence in the Northeast Atlantic based on Jenkinson's Gale index. In (a) is presented the 2012 daily gale index (black line), the maximum–minimum range in daily gale index values for the period 2000–2011 (yellow shaded region) and indicators of gale severity (red, blue and green horizontal lines). The cruise period is denoted by the grey shaded box and storm peak based on in situ observations is denoted by the blue shaded box. In (b) is shown a close up of the same data for August to early November. The figure key is the same for both plots. (For interpretation of the references to colour in this figure legend, the reader is referred to the web version of this article.)

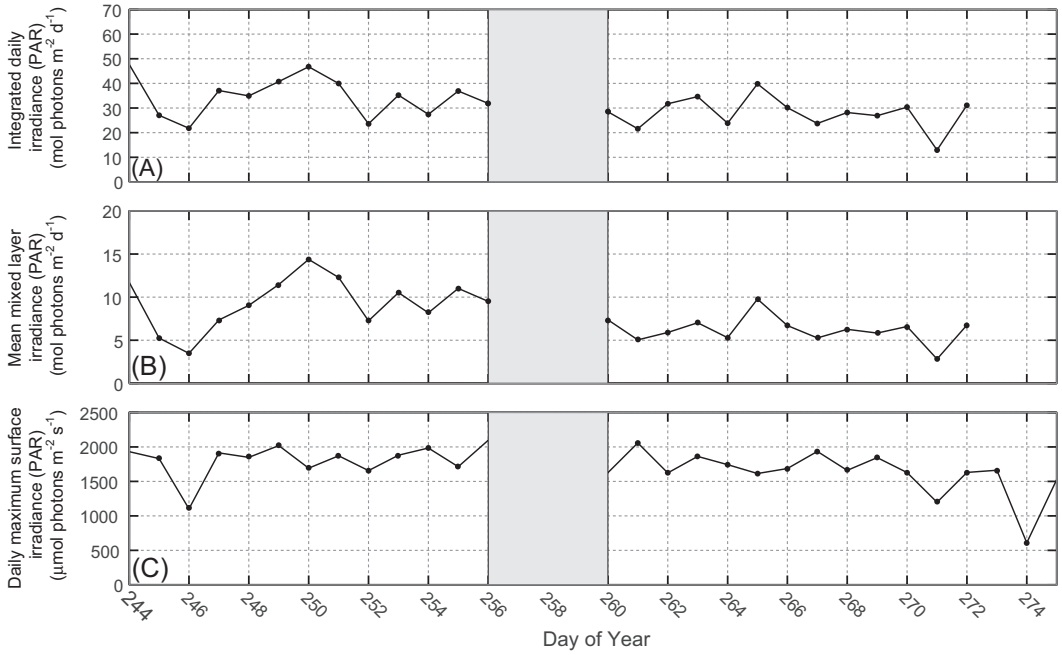

Fig. 6. Time series of irradiance during the observation period including (a) integrated daily PAR, (b) mean mixed layer irradiance, and (c) daily maximum surface PAR. Note that technical problems late in the cruise prevented calculation of integrated daily irradiance and mean mixed layer irradiance at this time. The grey box indicates the period when the ship was off site.

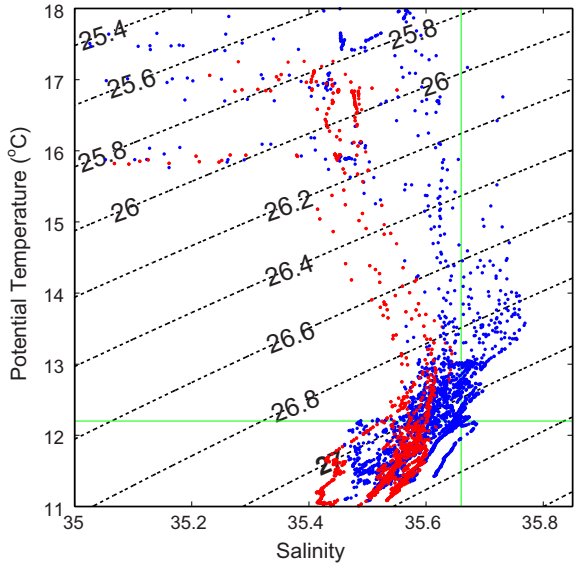

Fig. 7. T/S plot based on CTD profiles to 400 m depth. Profiles with maximum salinity values <35.66 are indicated by red dots and indicate the presence of Eastern North Atlantic Central Water subpolar (ENACWp) whilst blue dots indicate maximum salinities >35.66 indicative of Eastern North Atlantic Central Water subtropical (ENACWt). Green lines indicate typical defining criteria used in the literature. See Table 2 to identify which CTD profiles sampled which water mass variant. (For interpretation of the references to colour in this figure legend, the reader is referred to the web version of this article.)

3.4. Temporal variability in the surface ocean (underway data)

3.4.1. Nutrients and particulate biomass

Based on underway samples (Fig. 1) we present in Fig. 8 a time series of upper ocean biogeochemical parameters during the cruise. Initial surface nutrient concentrations were low and likely to have been limiting with NO_3^- concentrations <0.1 µmol L^{-1}, Si $(OH)_4$ concentrations <0.3 µmol L^{-1} and PO_4^{3-} concentrations <0.1 µmol L^{-1}. Late in the cruise around day 270 surface nutrient concentrations increased significantly as a result of storm induced mixing and a deepening of the mixed layer (see later sections/discussion) and at this time surface NO_3^- concentrations increased to ~0.6 µmol L^{-1}, $Si(OH)_4$ concentrations peaked at 0.2 µmol L^{-1} and PO_4^{3-} concentrations reached almost 0.15 µmol L^{-1}. Careful examination of the time series shows that surface nutrient concentrations oscillated in the days following the storm reaching a post-storm minimum around day 274 before then increasing again.

Fluorometrically determined surface chlorophyll concentrations (CHLa; Fig. 8) ranged from 0.07 to 0.81 mg m^{-3} with an average concentration of 0.27 ± 0.08 mg m^{-3}. The data indicated short-term temporal variability with a gradual decrease in surface chlorophyll concentrations from day 244 (~0.4 mg m^{-3}) to day 260 (~0.2 mg m^{-3}) followed by a equally gradual increase by ~50% thereafter to concentrations >0.3 mg m^{-3} peaking on day 272. HPLC TCHLa and MODIS-Aqua data are also shown, and the various datasets revealed consistent temporal patterns even though the MODIS Aqua chlorophyll concentrations were clearly higher. CHLa measurements also show a post-storm oscillation comparable to that described above for the surface nutrient concentrations. As CHLa concentrations decrease in tandem with the decreasing nutrient concentrations between days 272 and 274 it is unlikely that biological utilization explains the oscillation but may instead be due to spatiotemporal variability.

The range in surface particulate biomass concentrations was noticeably broader earlier in the cruise but all substrates tended to show a reduction in concentration with time. Concentrations of bSi were initially highly variable over days 244–250 with maximum concentrations of 0.8 µmol L^{-1} yet were rarely >0.1 µmol L^{-1} after day 260. Similarly, surface PIC concentrations reached a maximum of 1.4 µmol L^{-1} on day 244 but were generally <0.4 µmol L^{-1} thereafter. PON concentrations were generally >1.5 µmol L^{-1} over days 244–256 (mean ± sd 1.83 ± 0.45 µmol L^{-1}), and <1.5 µmol L^{-1} thereafter (1.22 ± 0.28 µmol L^{-1}). Although following the same temporal

Table 2
Summary table of station positions, sampling dates, integrated nutrient and particulate inventories and hydrographic character of each station.

Stn.	Date	Day of year	Lat (°N)	Lon (°W)	MLD (m)	$\int NO_3^-$ (mmol m^{-2})	$\int Si(OH)_4$ (mmol m^{-2})	$\int PO_4^{3-}$ (mmol m^{-2})	$\int TChla$ (mg m^{-2})	$\int bSi$ (mmol Si m^{-2})	$\int PIC$ (mmol m^{-2})	$\int POC$ (mmol C m^{-2})	$\int PON$ (mmol N m^{-2})	Water mass
1	31/08/2012	244.9	48.631	16.282	35	169.3	51.1	12.1	9.6	4.5	19.4	740.2	66.8	ENACWp
2	02/09/2012	246.9	48.762	16.106	55	6.2	19.3	4.8	9.9	5.8	18.0	789.7	79.8	ENACWp
3	04/09/2012	248.7	48.701	16.148	33	117.7	41.0	11.0	23.1	5.4	22.8	1139.0	124.6	ENACWp
4	06/09/2012	250.7	48.699	16.343	27	257.4	73.3	18.8	11	2.9	12.2	525.9	72.3	ENACWp
6	17/09/2012	261.6	48.606	16.065	43	14.9	6.0	5.3	11.1	4.8	10.9	572.2	71.0	ENACWt
7	17/09/2012	261.9	48.813	16.452	31	75.6	19.8	8.6	14.9	4.6	10.1	447.9	56.7	ENACWt
8	18/09/2012	262.7	48.808	16.361	47	6.1	2.1	5.0	14.0	2.2	9.5	508.2	61.4	ENACWt
9	19/09/2012	263.6	48.981	16.376	43	67.9	19.3	8.4	11.6	3.2	30.0	381.8	48.6	ENACWp
10	21/09/2012	265.8	48.283	16.850	35	20.9	9.5	7.2	18.8	4.4	17.2	424.7	54.9	ENACWt
11	21/09/2012	265.9	48.402	16.684	35	46.3	13.4	6.5	–	–	–	–	–	ENACWt
12	22/09/2012	266.1	48.521	16.520	39	20.6	8.4	5.8	8.8	4.1	13.8	398.0	51.9	ENACWt
14	28/09/2012	272.4	48.975	16.091	41	160.7	40.9	13.1	13.2	3.7	8.8	514.6	48.5	ENACWt
15	28/09/2012	272.5	48.976	16.062	45	76.1	23.7	11.1	–	–	–	487.5	54.6	ENACWt
16	28/09/2012	272.6	49.000	16.063	37	90.0	20.9	9.8	13.3	3.7	8.3	446.7	52.9	ENACWt
17	28/09/2012	272.7	49.008	16.068	35	85.5	18.2	9.7	–	–	–	468.5	55.9	ENACWt
18	29/09/2012	273.1	49.060	16.078	53	55.3	11.0	9.7	12.3	4.3	15.8	452.2	61.3	ENACWp
19	29/09/2012	273.2	49.084	16.472	57	37.8	10.4	6.6	13.9	4.6	13.3	441.1	61.6	ENACWp
20	29/09/2012	273.3	49.097	16.665	55	66.1	12.9	9.8	12.6	3.6	8.7	383.3	53.3	ENACWt
21	30/09/2012	274.4	48.190	15.500	65	94.2	23.6	9.7	12.7	10.6	16.5	412.8	54.6	ENACWt

pattern as the other particulates, POC concentrations exhibited the clearest signal of a decrease in time from values of >10 μmol L^{-1} at the start to values typically <10 μmol L^{-1} by the end of the cruise. Collectively the particulate data indicate a biological system that was in decline with reductions in the concentration of several different particulate pools, some of which reflect different algal groups. Despite the late cruise enhancement of surface nutrient concentrations to a maximum on day 272 there were no indications of coincident increases in any particulate pool concentrations at this time despite an increase in chlorophyll concentrations (see later sections).

3.4.2. Pigments

3.4.2.1. Total Chl-a. Total chlorophyll-a (TCHLa = DvCHLa + CHLa) concentrations in surface waters from HPLC analysis varied from 22 to 677 ng L^{-1} (Fig. 9). TCHLa concentrations, which were typically around 300 ng L^{-1}, nevertheless revealed a temporal pattern including a decrease in surface TCHLa concentrations from ~400 ng L^{-1} on day 244 to the mid-cruise minimum of ~100 ng L^{-1} around day 260. A gradual increase in TCHLa thereafter resulted in a maximum of ~400 ng L^{-1} on day 272. Note that throughout the record there can be significant sample-to-sample variability which is likely due to spatial variability. Although there are minor differences in absolute concentrations between the HPLC derived TCHLa concentrations and the calibrated fluorometric CHLa concentrations (Fig. 8) the general patterns are the same, with both datasets indicating a mid-cruise minimum around day 260 followed by an increase of 0.1–0.3 mg m^{-3} leading to a late cruise maximum around day 272.

3.4.2.2. Significance of DvChl-a. Despite being a pigment marker for prochlorophytes (Goericke and Repeta, 1992), which are typically found in warmer lower latitude waters, DvCHLa was detectable in a number of samples. Concentrations were nevertheless extremely low and typically <10 ng L^{-1}. DvCHLa was thus not prevalent during our cruise and usually represented <1% of total chlorophyll-a (DvCHLa + CHLa). However, during the latter part of the cruise DvCHLa concentrations increased to ~26 ng L^{-1} and whilst still low, the contribution DvCHLa made to TCHLa increased to almost 13% in some samples, suggesting both an important change in community composition but also in the contribution prochlorophytes made to total phytoplankton biomass. The increase in DvCHLa concentrations occurred at a time when the surface mixed layer deepened. The 13% contribution made by DvCHLa to TCHLa was comparable to autumnal estimates of up to 20% reported by Gibb et al. (2000, 2001) between 45 and 50°N.

We observed DvCHLa in waters with temperatures ranging from 15.9 to 17.8 °C. Previously, Gibb et al. (2000, 2001) reported temperature thresholds of 15.2–18 °C, below which DvCHLa was absent from waters in this region of the northeast Atlantic Ocean.

3.4.2.3. Accessory pigments. Concentrations of individual photosynthetic and photoprotective pigments are also shown in Fig. 9. Concentrations of HEX, which was the dominant accessory pigment in surface waters and taken as a marker for prymnesiophytes, ranged from 48 to 435 ng L^{-1}. Peridinin (PER) and fucoxanthin (FUC) concentrations, pigment markers for dinoflagellates and diatoms respectively, were generally <60 ng L^{-1} and <40 ng L^{-1} respectively but both pigments displayed a sharp reduction during the first few days of sampling. Initial concentrations of PER for days 244–246 ranged from 59 to 108 ng L^{-1}, with concentrations thereafter ranging from 2 to 70 ng L^{-1}. In contrast FUC concentrations were elevated between days 244–247 generally being in the range 40–80 ng L^{-1} and with a maximum concentration of 148 ng L^{-1} at this time. FUC concentrations thereafter were generally <40 ng L^{-1}. Concentrations of BUT, a marker for chrysophytes/pelagophytes,

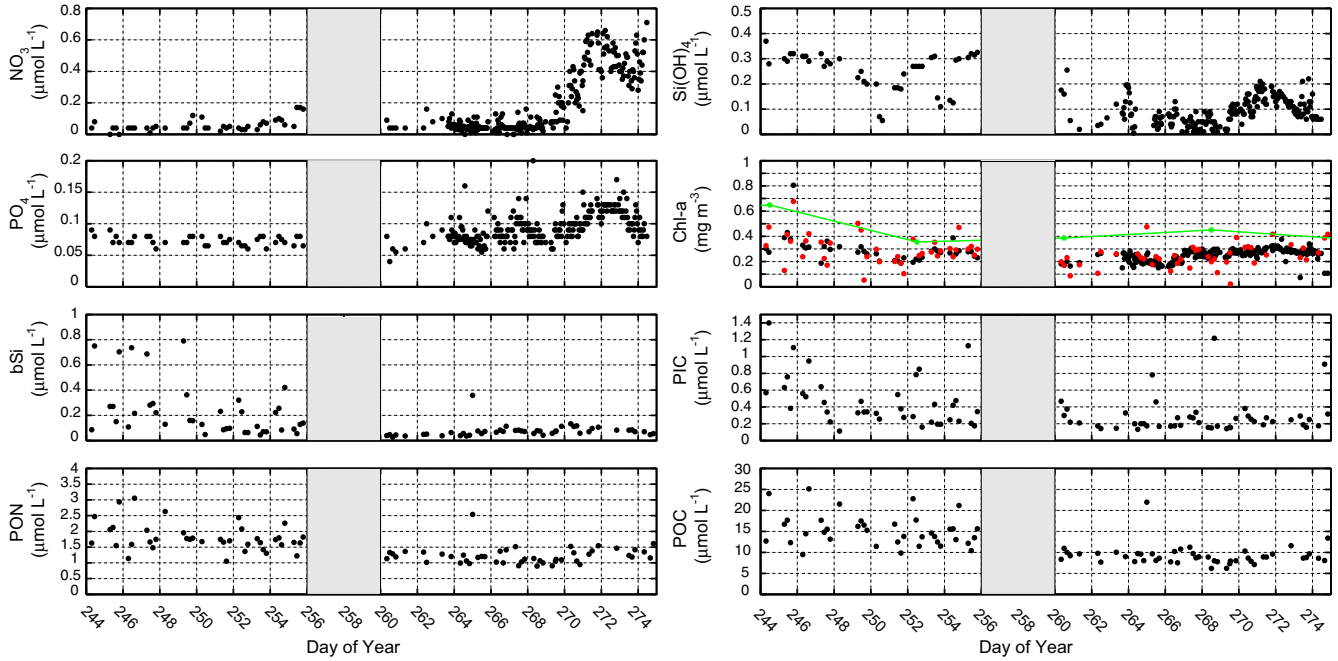

Fig. 8. Time series plots of surface biogeochemical parameters including (a) nitrate (NO_3^-) concentrations, (b) silicate ($Si(OH)_4$) concentrations, (c) phosphate (PO_4^{3-}) concentrations, (d) chlorophyll concentrations, (e) biogenic silica (bSi) concentrations, (f) particulate inorganic carbon (PIC) concentrations, (g) particulate organic nitrogen (PON) concentrations and (h) particulate organic carbon (POC) concentrations. Note that in panel (d) we present calibrated fluorometric chlorophyll (black symbols) and HPLC total chlorophyll (red symbols) concentrations. Also shown is the MODIS Aqua surface chlorophyll estimate (green line and symbols) averaged from 8-day composite images for the region 48.5–49.5°N, 15.5–17°W with data points positioned for the mid-time point of each 8 days composite period. The grey box in each panel indicates the period when the ship was off site. (For interpretation of the references to colour in this figure legend, the reader is referred to the web version of this article.)

were typically between 20 and 80 ng L^{-1} throughout the cruise. VIO, a marker for chlorophytes, was resolved to varying degrees during analysis, and was frequently just above base line levels suggesting imperfect resolution of this pigment. A number of samples however, produced clear peaks and VIO concentrations ranged from 18 to 77 ng L^{-1} with an exceptional peak of 136 ng L^{-1} observed at the start of sampling (day 245). The photosynthetic pigment, CHLb, which is a marker for chlorophytes, prochlorophytes and prasinophytes, was generally below 25 ng L^{-1} with the occasional sample having concentrations of up to 44 ng L^{-1}. Overall, the general pattern displayed by theses pigments was similar; concentrations were low, largely invariant and there were no strong temporal gradients.

The time history of photoprotective pigments is shown in Fig. 9. Concentrations of DIAD, a pigment present in diatoms, prymnesiophytes and chrysophytes, were highly variable and appeared to show a gradual reduction with time. DIAD concentrations at the start of the cruise exceeded 80 ng L^{-1}, but rarely exceeded 60 ng L^{-1} during the middle of the cruise and were <40 ng L^{-1} by the end. ALLO concentrations were low throughout the sampling period and typically <10 ng L^{-1}. ZEA, a photoprotective carotenoid (PPC) in cyanobacteria was present at low concentrations <35 ng L^{-1} throughout but there are indications of higher concentrations becoming more prevalent during the latter stages of sampling when concentrations >20 ng L^{-1} were more common. Finally, the time history of CARO concentrations in the surface ocean revealed no significant trend or pattern and concentrations were generally constant between 4 and 14 ng L^{-1}.

3.4.2.4. Photosynthetic and photoprotective pigments. Photosynthetic carotenoids (PSC) and photoprotective carotenoids (PPC) were grouped following the definitions used by Barlow et al. (2004) and Aiken et al. (2009) (Table 1) to allow for Diagnostic Pigment Analysis (DPA) of phytoplankton size classes. Amongst the PPC, VIO and DIA represented the largest constituents with average contributions of 22% and 41% respectively, though both were highly variable. Other individual PPC generally contributed <16% to total PPC concentrations. Within the pool of PSC, HEX represented the dominant carotenoid and averaged 56 ± 6% (range 41–68%). The next most abundant photosynthetic carotenoid was BUT (21 ± 4%) with PER and FUC both contributing 12%. Overall HEX was the dominant carotenoid representing 44 ± 5% of the total carotenoid pool (PSC + PPC). BUT, PER and FUC were the next largest contributors and represented 16 ± 3%, 9 ± 5% and 9 ± 2% respectively.

The proportion of total carotenoid pigments represented by PSC and PPC was also determined. PSC represented 79% on average of the total carotenoids (range 65–93%) whilst PPC represented only 21% (range of 7–35%). Given the latitude of our observations it is perhaps not surprising that PSC dominated but the mean contribution was lower than the 90% estimated by Barlow et al. (2004) from observations collected in this region in May and June 1998. However, the relative proportions of PSC and PPC were not fixed and a clear trend of increasing PSC dominance of the total carotenoid pool was evident within the data (not shown). Based on a regression between PSC or PPC contribution and time, the PSC contribution increased from 76% on day 244 to 81% on day 275 whilst the PPC contribution fell from 24% to 19%. This increased dominance by PSC was most likely a seasonal attribute of the data, and it is noteworthy that both mean daily surface irradiance decreased (Fig. 6) and surface mixed layers deepened during the cruise. These factors could each explain the increased proportion of PSC within the total carotenoid pool as phytoplankton responded to seasonally weakening irradiance intensities and lower mean mixed layer irradiance intensities.

The DPA indicated that the phytoplankton community was dominated by nanoplankton, which represented 75 ± 8% of the community on average. Microplankton and picoplankton made modest contributions of 21 ± 7% and 4 ± 3% respectively (Fig. 10). A temporal trend was evident within the data and microplankton,

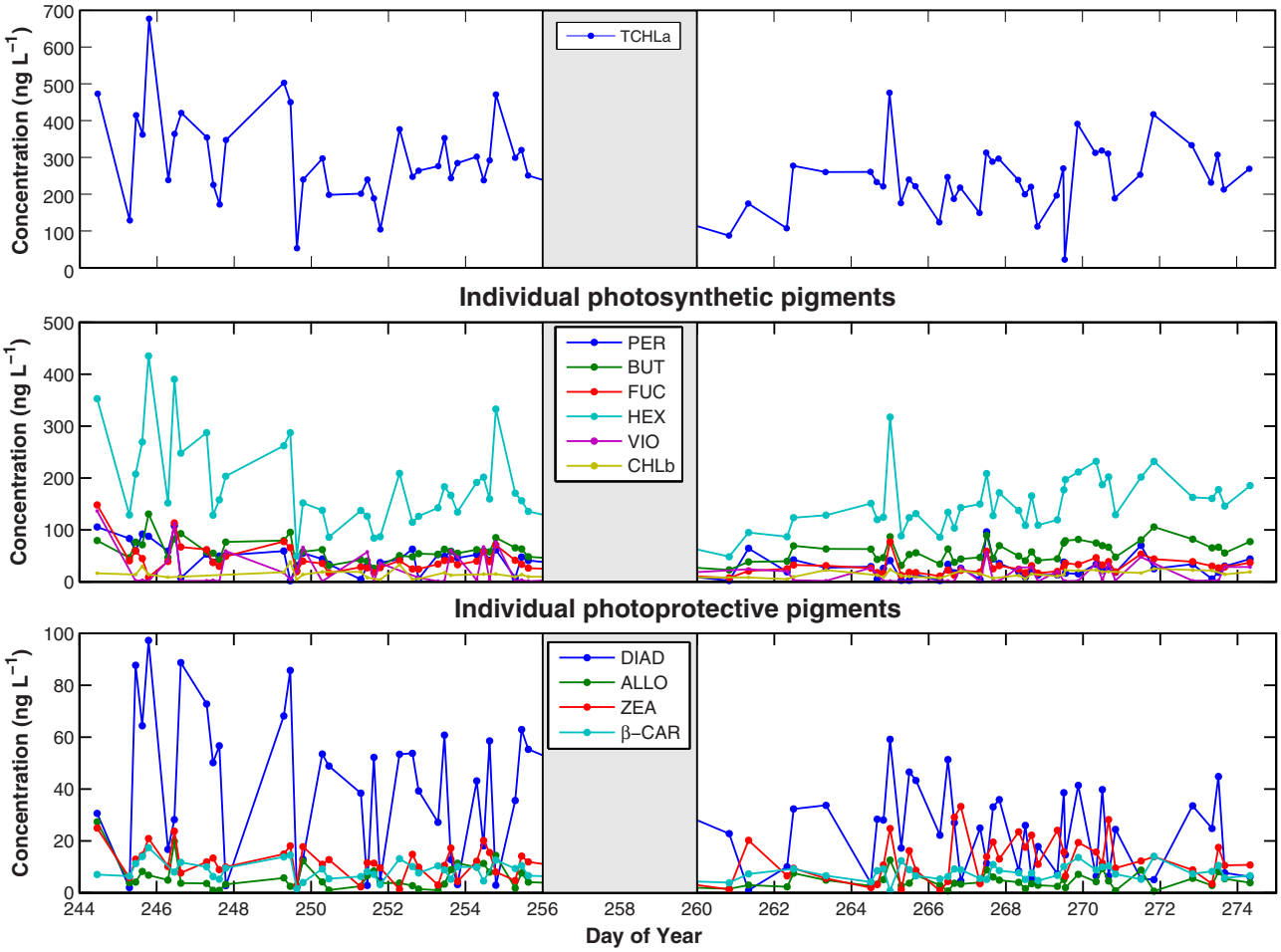

Fig. 9. Time series plot of HPLC derived pigment concentrations in the surface ocean including (a) total chlorophyll-a (chlorophyll-a + divinyl chlorophyll-a) concentrations, (b) concentrations of the major photosynthetic pigments and (c) concentrations of the major photoprotective pigments. See Table 1 for pigment abbreviations. In all panels the grey box represents the period the ship was off site.

which represented closer to 30% of the population at the start of the cruise, were found to represent <20% by the end of the cruise. Similarly, the nanoplankton contribution increased from <70% to ~80% of the population over the same period. The picoplankton contribution was always <9% but significant variability was evident and at times the picoplankton proportion could increase or decrease 2–4-fold. The mean contribution made by diatoms and dinoflagellates to the microplankton community in surface waters was approximately equal at 53 ± 17% and 47 ± 17% respectively, but within individual samples the contribution from each group could range from <10% to >90%. The near equivalence of the average contribution by both groups is suggestive of a community equally balanced to access resources yet the wide range in contributions on a per sample basis suggests either patchy distributions of species and/or active competition between taxa.

3.4.3. Phytoplankton community (Continuous Plankton Recorder and SEM)

3.4.3.1. Continuous Plankton Recorder. Monthly averaged total abundances of diatoms, dinoflagellates and coccolithophores for 2012 in relation to the 2000–2011 monthly climatological average are presented in Fig. 11. Although there are a few data gaps in 2012 due to the irregular passage of CPR equipped ships through the area there are notable differences for the 2012 dataset compared to the climatological mean for each plankton group. Diatoms were less abundant during the 2012 spring bloom (March–June) than normal, whilst dinoflagellate and coccolithophore abundances appeared significantly higher during the summer and early autumn (June to October). During September–October 2012, the CPR data suggest that diatoms were present at near typical abundances, whilst dinoflagellates, and in particular coccolithophores, were more abundant than normal for the time of year. The significant increase in coccolithophore abundance at this time agrees with the pigment chemotaxonomic analysis and the dominance of HEX within the carotenoid pool (Fig. 9). Interestingly, the unusually high abundances of dinoflagellates and coccolithophores during the summer of 2012 most likely explains both the elevated surface chlorophyll and PIC concentrations seen between June and August 2012 in the satellite record (Fig. 3).

Two CPR transects passed through the E5 standard area of the CPR survey and through the middle of our study site on 22nd September and 19th/20th October 2012 (Fig. 1). The 30 samples resulting from these transects were examined for further information on the phytoplankton community accepting the limitations provided by CPR collection methodologies and the semi-quantitative nature of the resulting abundance data (Richardson et al., 2006). A number of diatom species were identified in the CPR data (Table 3), but none could be considered geographically widespread or abundant as estimated abundances were at or below (i.e. absent) the lowest CPR abundance criteria. *Pseudo-nitzschia* spp., *Thalassiosira* spp., and *Thalassiothrix longissima* were the most common diatom species recorded appearing in 5–7 of the 30 individual CPR samples. Dinoflagellates were more common and more widespread in the CPR transects though were noticeably

more common in the September transect than in the October transect. Species of the *Ceratium* genus were the most common but were not particularly abundant with typical cell densities of ~5000 cells m^{-3} and patchy maximum abundances of ~20,000 cells m^{-3} in the case of *Ceratium fusus*. *Prorocentrum* spp., were the most common, appearing in over half of the samples but abundances were variable ranging from ~5000 cells m^{-3} to ~30,000 cells m^{-3}. *Prorocentrum* spp., were particularly common in September but far less common in October.

The CPR record also provided estimates of total coccolithophore and silicoflagellate abundances though species level identification was not recorded in the CPR archive. Coccolithophores were present in 22 of the 30 CPR samples, and were perhaps slightly less frequent in October than September. Abundances exceeded ~30,000 cells m^{-3} in some samples but were usually <12,000 cells m^{-3}. The CPR record independently demonstrates that coccolithophores were the most abundant phytoplankton group during our cruise. Silicoflagellates, were also comparatively common, appearing in 21 of the 30 samples with approximate abundances ranging from ~5000 to ~12,000 cells m^{-3}.

Finally, we note in passing the unexpected presence of *Trichodesmium* spp. in 1 single sample along both CPR transects at latitudes of 49.17°N in September and 48.34°N in October. Northward advection from further south is the most likely explanation for the presence of *Trichodesmium* spp. at these latitudes and at this time of year. Extant observations of *Trichodesmium* spp. distributions do show the occasional presence at such northerly latitudes though usually earlier in the year (Tyrrell et al., 2003; Luo et al., 2012).

3.4.3.2. Scanning electron microscopy analysis of the surface ocean phytoplankton community. In total we identified 30 species of coccolithophore, 16 species of dinoflagellate, and 1 species of silicoflagellate in surface water samples though abundances of taxa and species were highly variable (Tables 4 and 5). Diatoms were typically present in pennate form (mainly *Pseudo-nitzschia* spp.) and only rarely were small centric forms observed. A notable exception to this was the presence of *Chaetoceros atlanticus*, identified in a single sample (station 20; 0.93 cells mL^{-1}) and two chains of *Leptocylindrus mediterraneus* at stations 3 and 18. Due to limitations in identification markers we present the pennate diatom abundances on the basis of size, denoting small pennate diatoms as <15 μm and large pennate diatoms as >15 μm (n.b. we could not acid wash the sample prior to gold coating and SEM analysis due to our desire to examine the coccolithophore community thus many taxonomic features used to identify diatoms were obscured by organic detritus in the SEM micrographs).

The abundance of small pennate diatoms varied over 50-fold during the cruise with abundances ranging from 0.62 (station 10) to 35.76 (station 18) cells mL^{-1}. Although highly variable there was nevertheless a temporal trend, which saw a step-up in abundances from <20 cells mL^{-1} at stations 1–12 to >20 cells mL^{-1} from station 14 onwards. The highest abundances were therefore seen late in the cruise during the post-storm period.

Large pennate diatom abundances were far less variable varying <20-fold during the observation period. Total abundances ranged from a maximum of 99.5 cells mL^{-1} (station 1) to a minimum of 5.75 cells mL^{-1} (station 12). Initial abundances at stations 1–3 were >70 cells mL^{-1}, but abundances rapidly decreased to more typical concentrations of <20 cells mL^{-1} thereafter. There was no subsequent temporal trend in abundance and no significant increase post-storm.

Dinoflagellates were identified at all stations except station 8 where they were entirely absent. Total dinoflagellate abundances were low but nevertheless varied over 14-fold with abundances ranging from 8.98 (station 1) to 0.62 (station 10) cells mL^{-1}. The most frequently observed dinoflagellates were *Prorocentrum balticum* (identified at 12 of 15 stations), *P. minimum* (9 of 15 stations), *Gonyaulax polygramma* (7 of 15 stations) and *Oxytoxum scolopax* (6 of 15 stations) with other notable species such as *Ceratium furca* and *Mesoporus perforatus* being less common. There was no temporal trend in either total abundance or species diversity but note that the nature of the SEM analysis provides only

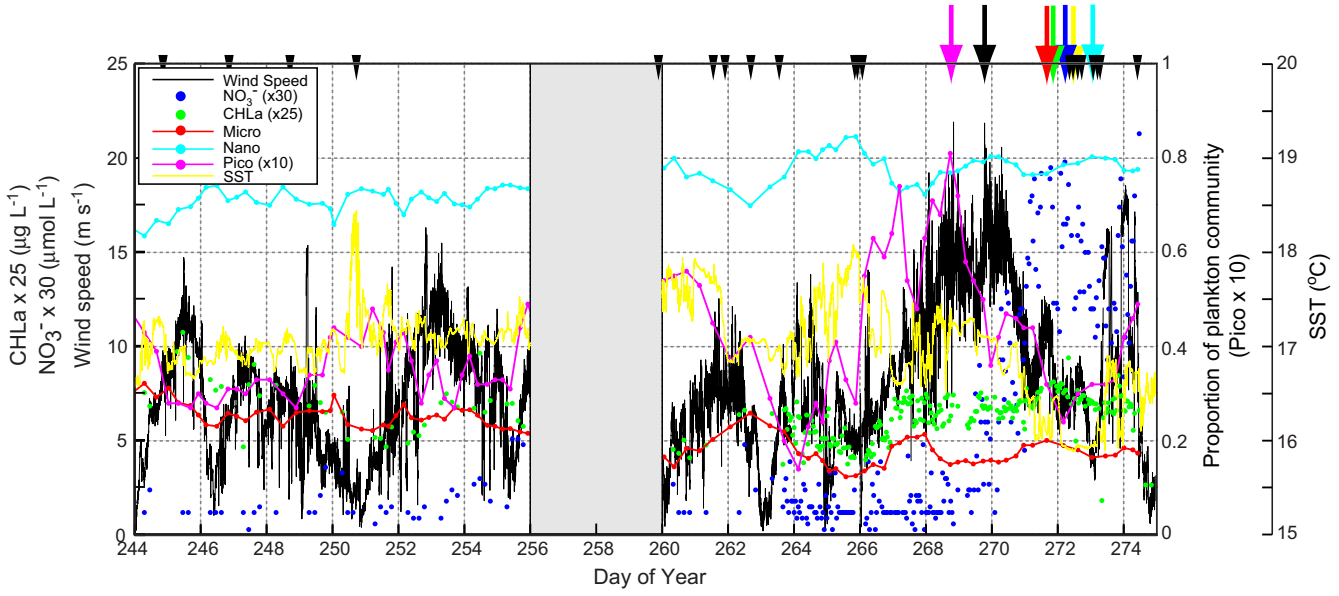

Fig. 10. Time series of wind speed (black line), nitrate concentrations (blue dots), chlorophyll concentrations (green dots), sea surface temperature (SST; yellow line), and phytoplankton community size class distributions (red, cyan, purple lines). Note the use of different scaling factors for different parameters on their respective *y*-axis. Coloured arrows along the top *x*-axis denote the timing of the maximum/minimum value of each parameter. The timing of each CTD cast is indicated by the inverted black triangles along the top *x*-axis. The grey box represents the period the ship was off site. In this study we consider the start of the storm to be late on day 265 and the storm peak to be on day 269 (indicated by black arrow on top *x*-axis). (For interpretation of the references to colour in this figure legend, the reader is referred to the web version of this article.)

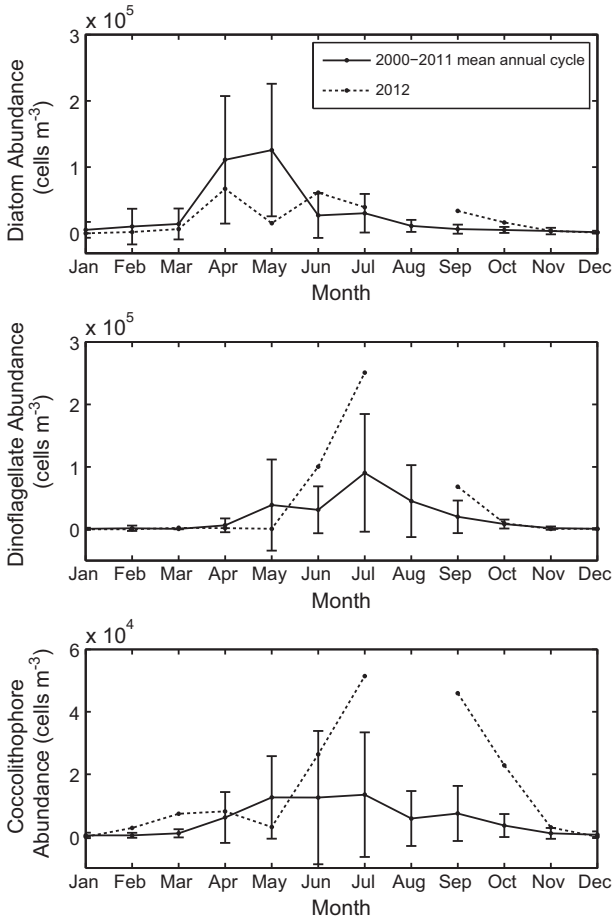

Fig. 11. Continuous Plankton Recorder (CPR) mean monthly total abundances of (a) diatoms, (b) dinoflagellates and (c) coccolithophores from the E5 standard area for 2000–2011 (solid line) and actual monthly abundances for 2012 (dashed line). Gaps in 2012 time series due to gaps in CPR coverage of the E5 standard area.

semi-quantitative information on abundances and examination of larger sample cross sections would likely increase both abundances and total species counts.

The silicoflagellate *Dictyocha fibula* was identified at 7 of 15 stations sampled but was never present in high abundance. Other than two specimens being identified at station 6 the presence of *D. fibula* was clearly restricted to the late cruise period and was identified from station 14 onward. Maximum abundance peaked at station 14 (2.18 cells mL^{-1}) but then steadily decreased. The distinct (near) absence of *D. fibula* before station 14 and its consistent presence thereafter argues for the entrainment of *D. fibula* from depth and its subsequent sinking out of surface waters in the days after resulting in the gradual decrease in abundance. *Dictyocha* spp. are known to have comparatively high sinking velocities of almost 0.5 m d^{-1} which supports the observed pattern (Bach et al., 2012).

The coccolithophore community was comparatively rich with 30 distinct species identified in total, though loose coccoliths from >30 species were present (Table 5). The number of species present at any particular station however was far lower ranging from 4 to 17. We present in the Appendix A further details of the station-to-station variability in the coccolithophore community restricting ourselves here to broad temporal changes. Coccolithophore species diversity appeared to increase with time from ~10 to 12 species per station at the start of the cruise to 13–15 species per station by the end of the cruise though the trend was not statistically significant.

Table 3
Phytoplankton species identified in CPR samples collected in September and October 2012 in the CPR E5 standard area along 2 transects running northeast to southwest through the study site (see Fig. 1). Total abundances per m^{-3} have been obtained from the CPR data as detailed by Richardson et al. (2006). Note that we present the minimum–maximum range of abundances for all CPR samples shown in Fig. 1 for each transect and that the quoted abundances do not reflect typical abundances for each CPR sample. Frequently, CPR samples returned zero abundance for the species listed.

Species	CPR abundance per m^{-3} (September)	CPR abundance per m^{-3} (October)
Diatoms		
Skeletonema costatum	Up to 5000	–
Thalassiosira spp.	Up to 5000	Up to 5000
Chaetoceros (Hyalochaete) spp.	Up to 5000	–
Chaetoceros (Phaeoceros) spp.	–	Up to 5000
Thalassiothrix longissima	5000–11,666	–
Thalassionema nitzschioides	–	Up to 5000
Cylindrotheca closterium	–	Up to 5000
Coscinodiscus spp. (unidentified)	Up to 5000	Up to 5000
Nitzschia spp. (unidentified)	–	Up to 5000
Nitzschia bicapitata	–	Up to 5000
Pseudo-nitzschia delicatissima complex	5000–11,666	5000–11,666
Pseudo-nitzschia seriata complex	–	Up to 5000
Dinoflagellates		
Ceratium fusus	5000–31,666	Up to 5000
Ceratium furca	5000–11,666	Up to 5000
Ceratium macroceros	Up to 5000	Up to 5000
Dinoflagellate cysts (total)	Up to 5000	–
Ceratium candelabrum	Up to 5000	–
Ceratium trichoceros	Up to 5000	Up to 5000
Gonyaulax spp.	Up to 5000	Up to 5000
Oxytoxum spp.	Up to 5000	–
Protoperidinium spp.	Up to 5000	–
Scrippsiella spp.	–	Up to 5000
Leptocylindrus mediterraneus	5000–31,666	–
Prorocentrum spp. ('Exuviaella' type)	5000–31,666	Up to 5000
Silicoflagellates	5000–21,666	5000–43,333
Coccolithaceae (Total)	5000–56,666	5000–56,666
Other notables		
Trichodesmium spp.	Up to 5000	Up to 5000

Emiliania huxleyi was generally the most abundant coccolithophore but its contribution to total coccolithophore abundance varied significantly between stations. On average *E. huxleyi* represented 39 ± 20% of total coccolithophore abundance, but the actual contribution varied from 15% to 71% at individual stations (Appendix Fig. A1). Furthermore, at several stations (stations 3, 4, 6, 7 and 12) *E. huxleyi* was not the dominant species but was outnumbered by *Syracosphaera halldalii* which was the second most abundant species recorded on average (mean 18 ± 12%), but which could represent over 30% of total coccolithophore abundances at some stations. *Gephyrocapsa muellerae* and *G. ericsonii* were the third and fourth most abundant species on average representing 6 ± 7% and 4 ± 5%, though either species could be entirely absent, or present at individual stations with maximum contributions to total coccolithophore abundances of ~20%.

The rarer coccolithophore species (defined as individually contributing <5% to total coccolithophore abundance), when aggregated collectively represented between 7% and 30% of total coccolithophore abundance (mean 15 ± 7%) indicating that rarer

Table 4
Diatom, dinoflagellate and silicoflagellate abundances (cells mL^{-1}).

Species	Station															
	1	2	3	4	6	7	8	9	10	12	14	16	18	19	20	21
Diatoms																
Small pennate (<15 μm)	13.47	0.73	3.11	18.44	0.78	6.26	7.70	6.20	0.62	2.49	21.82	21.16	35.76	27.48	16.63	19.90
Large pennate (>15 μm)	99.50	76.09	73.07	12.80	6.37	21.79	17.62	11.38	6.53	5.75	16.91	6.38	8.08	12.49	8.24	20.83
Dinoflagellates																
Protoperidinium sp.	0.35	0	0	0	0	0	0	0	0	0	0	0	0	0	0	0
Protoperidinium divergens	0	0	0	0	0.31	0	0	0	0	0	0	0	0	0	0	0.62
Prorocentrum (small)	0.69	0	0	0	0	0.69	0	0	0	0	0	0	0	0	0	0
Prorocentrum minimum	2.07	2.19	1.55	0.61	0.62	0.34	0	0.81	0	0.62	0.73	0	0	0	0	1.24
Prorocentrum balticum	2.07	1.46	0.78	1.83	0	1.03	0	1.22	0	0.62	1.36	0.73	3.11	1.25	0.62	0.62
Prorocentrum compressum	0	0	0	0.61	0	0	0	0	0	0	0	0	0	0	0	0
Prorocentrum triestinum	0	0	0	0	0.62	0	0	0	0	0	0	0	0	0	0	0
Mesosporus perforatus	0.69	0	0	0	0.31	0	0	0	0	0.62	0.36	0.36	1.24	0	0	0
Gonyaulax polygramma	1.73	0.73	0	0.61	1.55	1.72	0	0	0	0	0	1.46	0.31	0	0.31	0
Ceratium fusus	0.69	0	0	0	0	0.34	0	0	0	0	0	0	0	0	0	0
Ceratium furca	0	0	0	0	0.31	0	0	0	0	0.62	0.36	0	0	0	0.16	0
Oxytoxum scolopax	0.69	0	0	0.61	0	0.69	0	0.41	0	0.62	0.36	0	1.24	0	0	0
Goniodoma	0	0	0	0	0	0	0	0	0	0	0	0	0	0	0	0
Dinophysis	0	0	0	0	0.31	0	0	0	0	0	0	0	0	0	0	0
Phalacroma rotundata	0	0	0	0	0	0	0	0	0.62	0	0	0.36	0	0	0	0
Ceratium gibberum	0	0	0	0	0	0	0	0	0	0.62	0	0	0	0	0	0
Total abundance	8.98	4.39	2.33	4.27	4.04	4.80	0	2.44	0.62	3.73	3.18	2.92	5.91	1.25	1.09	2.49
Silicoflagellate																
Dictyocha fibula	0	0	0	0	0.62	0	0	0	0	0	2.18	1.09	0.62	0.62	0.31	0.62

species were an important contributor to the coccolithophore community at this time of year. Notable minor species were *Calcidiscus leptoporus*, *Acanthoica quattrospina*, *Rhabdospaera clavigera*, *Helicosphaera carteri*, *Palusphaera vandelii* and the holococcolithophores *Anthosphaera* sp. and *Homozygosphaera spinosa*. A summary of the coccolithophore community based on contributions to total coccolithophore abundance at each station is presented in Appendix Fig. A1 where we have condensed the total number of species to 17 having grouped the rarer species together under the heading 'other'. A full listing of identified species with abundances is provided in Table 5.

Despite broad similarities in the composition (but not species abundances) of the coccolithophore community between stations, it is worth noting that two stations do not fit comfortably into this generalization. Station 8 was unusual because we did not identify a single coccosphere from any *Syracosphaera* species, which was remarkable given the ubiquity of the *Syracosphaera* genus throughout the rest of the dataset. Furthermore even loose *Syracosphaera* liths were at unusually low abundances of just 8.29 coccoliths mL^{-1} (aggregated total) at this station. We also identified a major contribution of 26% to total coccosphere abundance at this station from *Calcidiscus leptoporus* (Appendix Fig. A1). Station 9 was also unusual as rare species (aggregated total) made a significant (30%) contribution to total coccolithophore abundance, with the remaining 70% made up from just 2 species, *E. huxleyi* (58%) and *S. halldalii* (12%) (Appendix Fig. A1). Interestingly, although stations 8 and 9 were sampled sequentially and close together station 8 was hydrographically influenced by ENACWt whilst station 9 by ENACWp (Table 2).

Despite these differences our samples are consistent with the temperate North Atlantic coccolithophore group described previously (McIntyre and Bé, 1967; Okada and McIntyre, 1977; Winter et al., 1994).

3.5. Vertical variability in the surface ocean (profile data)

3.5.1. Temperature, nutrients and chlorophyll

Individual profiles of temperature, density, chlorophyll fluorescence and nitrate all show a consistent homogenization of the upper ocean related to upper ocean mixing and the deepening of the surface mixed layer (Fig. 12). This reorganization of the water column followed the passage of a storm through the study site on days 266–271 (Fig. 10), which in addition to decreasing SST also increased surface nutrient concentrations (Fig. 8) most likely due to wind-driven nutrient entrainment from depth (Rumyantseva et al., 2015). The most prominent biological change was the loss of the sub-surface chlorophyll maximum and its replacement with a homogenous chlorophyll profile (Fig. 12). The average mixed layer depth deepened from 38 ± 8 m prior to the storm to 49 ± 11 m after the storm (Table 2). Associated with this was a large and significant change to the average mixed layer temperature which decreased by ~1.3 °C from 17.38 ± 0.5 °C to 16.02 ± 0.3 °C (*t*-test, $p < 0.001$), and significant increases in average mixed layer nutrient concentrations. Average mixed layer NO_3^- concentrations rose from 0.1 ± 0.1 to 1.6 ± 1.0 μmol L^{-1} (*t*-test, $p < 0.001$), $Si(OH)_4$ concentrations rose from 0.2 ± 0.1 to 0.4 ± 0.3 μmol L^{-1} (*t*-test, $p < 0.01$), and PO_4^{3-} concentrations rose from 0.1 ± 0.02 to 0.2 ± 0.05 μmol L^{-1} (*t*-test, $p < 0.001$). The larger changes to mean mixed layer nutrient concentrations compared to surface values (Fig. 8), particularly for NO_3^-, appears to be driven by the presence of vertical nutrient gradients within the lower mixed layer possibly due to overestimation of the mixed layer depth with the criterion used here (Section 2.2). Mixed layer average chlorophyll concentrations however showed no significant change with average concentrations before the storm of 0.25 ± 0.07 and 0.27 ± 0.1 μg L^{-1} after the storm (*t*-test, $p > 0.05$). The lack of any significant change in average mixed layer chlorophyll concentrations indicates a lack of any significant growth and supports our supposition that the increase in surface chlorophyll concentrations (Figs. 8 and 9) was the result of supply from below.

To rule out any significant change occurring at depths beneath the mixed layer but above the base of the deeper euphotic zone we examined 50 m integrated stocks (Table 2). Integrated nutrient concentrations ranged from 6.1 to 257.4 mmol m^{-2} for NO_3^-, from 2.1 to 73.3 mmol m^{-2} for $Si(OH)_4$ and from 4.8 to 18.8 mmol m^{-2} for PO_4^{3-}. Nutrient inventories were surprisingly variable throughout the cruise, which suggests active supply from below, patchy distribution within the mixed layer or possibly the influence of

Table 5
Results of coccolithophore identification and enumeration from SEM micrographs including coccolithophore species abundance (cells mL^{-1}), selected abundances of loose coccoliths for the most dominant species (coccoliths mL^{-1}) and the coccolith:coccosphere ratio.

Species	Station															
	1	2	3	4	6	7	8	9	10	12	14	16	18	19	20	21
Emiliania huxleyi coccospheres	11.75	20.12	13.99	4.88	4.66	4.46	6.51	20.53	4.35	9.64	52.37	8.39	32.96	32.17	27.21	26.43
Emiliania huxleyi coccoliths	481.24	644.53	698.03	195.09	200.86	189.78	238.67	790.52	210.81	187.18	1154.97	614.41	729.43	807.02	544.12	689.01
Coccolith:coccosphere ratio	40.97	32.04	49.89	40.0	43.07	42.54	36.64	38.51	48.43	19.42	22.06	73.22	22.13	25.09	20.0	26.07
Syracosphaera spp. (unidentified)		0.73	3.89	5.49	3.11	1.37	0	1.22	2.49	1.87	1.82	0.36	2.49	3.12	2.80	9.02
Syracosphaera halldalii coccospheres	6.22	12.44	19.04	12.80	8.08	7.04	0	4.27	2.80	9.95	8.55	2.92	1.87	3.75	7.62	16.48
Syracosphaera halldalii coccoliths	183.10	256.06	358.34	206.67	122.50	132.13	1.18	244.27	255.73	237.55	302.56	185.71	202.72	201.13	134.94	517.38
Coccolith:coccosphere ratio	29.44	20.59	18.82	16.14	15.15	18.78	–	57.24	80.67	23.88	35.40	63.63	108.67	53.67	17.71	31.40
Syracosphaera moshlii coccospheres	4.15	3.66	3.50	4.88	1.24	0.69	0	0.81	0.62	1.24	0.73	0.36	0.62	0.62	1.24	8.08
Syracosphaera moshlii coccoliths	54.58	18.29	49.75	27.43	7.77	11.33	4.74	10.97	8.08	4.35	8.36	9.85	11.82	18.11	4.04	49.13
Coccolith:coccosphere ratio	13.17	5.0	14.22	5.63	6.25	16.50	–	13.5	13.0	3.5	11.50	27.0	19.0	29.0	3.25	6.08
Syracosphaera nodosa	2.07	2.19	0	0.61	0.31	0.34	0	0	0	0	0	0	0.62	1.25	1.24	9.33
Syracosphaera borealis	0	0.73	0	0	0.78	0	0	0.41	0	0	0	0	0	0	0	1.24
Syracosphaera c.f. *tumularis*	0	0	0.78	1.22	0	1.37	0	0.41	0	0	0	0	2.49	0	0	0
Syracosphaera ossa	0	0	0	0	0	0	0	0.81	0	0	0	0	0	0	0	0
Syracosphaera pulchra	0	0	0	0	0	0	0	0.41	0.62	0	0.55	0	0	0.62	0.93	0
Gephyrocapsa muellerae coccospheres	8.98	2.19	3.89	1.22	2.18	1.03	1.18	1.22	2.49	6.53	1.45	0.36	3.11	1.87	2.80	13.68
Gephyrocapsa muellerae coccoliths	29.71	10.24	7.77	21.34	37.31	19.22	16.58	10.57	30.47	23.01	13.82	4.74	6.84	12.49	6.84	68.40
Coccolith:coccosphere ratio	3.31	4.67	2.00	17.50	17.14	18.67	14.0	8.67	12.25	3.52	9.50	13.0	2.20	6.67	2.44	5.0
Gephyrocapsa ericsonii coccospheres	0.69	2.93	3.11	0.61	4.97	0.69	0.59	1.22	1.87	2.49	1.82	1.46	0	1.87	0.62	19.90
Gephyrocapsa ericsonii coccoliths	4.15	0	3.11	0	4.66	1.72	0	0.41	11.19	0.62	0.36	0	0	0	0.62	10.57
Coccolith:coccosphere ratio	6.0	–	1	–	0.94	2.50	–	0.33	6.0	0.25	0.2	–	–	–	1	0.53
Calcidiscus leptoporusi coccospheres	1.38	0	0	0	0	0	2.96	0.81	0	0	3.64	0	1.24	5.00	0	0
Calcidiscus leptoporus coccoliths	4.84	2.93	23.32	7.32	2.80	4.46	4.44	4.27	3.73	1.24	6.18	3.28	11.29	10.62	3.11	1.24
Coccolith:coccosphere ratio	3.50	–	–	–	–	–	1.5	5.25	–	–	1.70	–	9.0	2.13	–	–
Acanthoica quattrospina	1.38	0	0	0	0	0	0	0	0	1.24	0.73	0.73	0	1.25	1.55	11.19
Anthosphaera sp.	0.69	0.73	1.55	0	0	0	0	0	1.24	1.24	0	0	0	0	0	3.11
Homozygosphaera spinosa	1.38	0	0.78	1.22	0.62	0.69	0	0.81	1.87		0	0	0	0	0	0
Corisphaera sp.	2.76	2.93	1.55	3.66	1.24	0	0	0.41	1.87	1.24	0.73	0	1.87	3.12	0	7.46
Rhabdospaera clavigera	0	2.93	0	0	1.24	0.34	0	0.81	0	0	0	0	1.87	0	1.55	0.62
Anacanthoica acanthos	0	0	0.78	0	0	0	0	0	0	0	0	0	0	0	0	0
Michaelsarsia sp.	0	0	0	0	0	0	0	0.41	0	0	0	0.36	0	2.50	0.93	4.35
Helicosphaera carteri	0	0	0	0	0.31	0	0	0.41	0	0	0.73	0.36	0	0.62	0.31	0
Palusphaera vandelii	0	0	0	0	2.80	0.34	0	0	4.35	0.62	0.36	0	1.87	0.62	0	0
Ophiaster sp.	0	0	0	0	0	0.69	0	0	0	0	0	0	0	0	0	0
Cyrtosphaera aculeata	0	0	0	0	0	1.37	0	0.41	0	0	0	0	0	0	0	0
Calcisolenia brasiliensis	0	0	0	0	0	0	0	0	0.62	0	0	0	0	0	0	0.62
Pappomonas sp.	0	0	0	0	0	0	0	0	0	0.62	0	0	0	0	0	0
Rhabdosphaera xiphos	0	0	0	0	0	0	0	0	0	0.62	0	0	0	0	0	0
Papposphaera sp.	0	0	0	0	0	0	0	0	0	0	0	0	1.87	0	0	0
Pontosphera c.f. *syracusana*	0	0	0	0	0	0	0	0	0	0	0	0	0.62	0	0	0
Reticulofenestra sp.	0	0	0	0	0	0	0	0	0	0	0	0	0	0.62	0	0
Canistrolithus sp.	0	0	0	0	0	0	0	0	0	0	0	0	0	0	0	0.62

internal waves, eddies and fronts. Integrated nutrient concentrations were however distinctly higher at station 14 (day 272) following the storm and at stations thereafter than at stations immediately before the storm. Integrated NO_3^- concentrations rose from an average pre-storm value of 36 mmol m^{-2} to a maximum post-storm value of 160 mmol m^{-2}, an increase of over 400%, but more generally post-storm concentrations were >70 mmol m^{-2}, an increase of ~200%. Similarly, integrated $Si(OH)_4$ concentrations rose from ~11 mmol m^{-2} to ~41 mmol m^{-2}, a rise of just less than 400%, whilst PO_4^{3-} concentrations rose from ~7 mmol m^{-2} to 13 mmol m^{-2}, a smaller ~200% increase. Changes to integrated total chlorophyll concentrations were more muted than changes to nutrient inventories. Integrated chlorophyll concentrations ranged from 8.8 to 23.1 mg m^{-2} (Table 2), and were generally lower than summertime (June–August) concentrations reported previously (e.g. 22.8–69 mg m^{-2} (Joint et al., 1993); 13.2–59.5 mg m^{-2} (Painter et al., 2010b); 12.2–48.5 mg m^{-2} (Painter, unpublished data July/August 2009)). Integrated chlorophyll concentrations averaged 13.2 ± 3.5 mg m^{-2} at stations immediately before the storm. After the storm however average integrated chlorophyll concentrations were 13.0 ± 0.6 mg m^{-2}, thus there was no indication of any significant growth following the addition of nutrients in either integrated chlorophyll concentrations (which also included waters beneath the mixed layer) or mixed layer averaged chlorophyll concentrations.

Estimates of the Ekman layer depth (h), the depth of wind penetration, calculated as

$$h = 7.12 * \frac{1}{\sqrt{\sin \varphi}} * V \quad (4)$$

where φ equals the latitude and V the wind speed (Chen and Tang, 2012), indicate that prior to the storm the mean Ekman layer depth was 48 ± 20 m, comparable to the mean pre-storm mixed layer depth (~38 m), but this deepened to a short-lived maximum of 195 m at the height of the storm. For a sustained maximum wind speed of ~18 m s^{-1} the Ekman layer depth would have been ~150 m thus in the absence of stratification it is likely that this cyclonic storm could have entrained water from significant depths. In reality stratification was present and would have limited the entrainment depth but this calculation demonstrates that perturbations to a significant depth may have been possible.

Nutrient ratios were generally conservative throughout the water column. In Fig. 13 we present summary plots showing the nutrient ratios within the upper 120 m of the water column (n.b. 97% of observations were from <60 m depth). This clearly revealed an important difference between waters of the mixed layer and those immediately below. At depths <50 m the NO_3^-:Si ratio was ~5:1, but below 50 m this decreased to ~2:1. This indicated the mixed layer was depleted in Si relative to NO_3^- compared to subjacent waters beneath the mixed layer. NO_3^-:PO_4^{3-} was conservative across all sampled depths at 18:1, though there was a positive intercept on a linear regression, suggesting that residual PO_4^{3-} would have remained once NO_3^- was exhausted. Similarly, Si:PO_4^{3-} was broadly constant at 5:1, yet again a positive intercept was observed on a linear regression suggesting that PO_4^{3-} concentrations would have remained around 0.095 μmol L^{-1} once Si was exhausted. Previous summertime (June/July) observations reported by Painter et al. (2010b) also demonstrated a significant change in NO_3^-:Si within (6:1) and beneath (1:1) the mixed layer, but also revealed NO_3^-:PO_4^{3-} values of 15:1, and Si:PO_4^{3-} values of 10:1 beneath the mixed layer and significant removal of PO_4^{3-} (relative to Si) within the mixed layer (leading to a positive intercept on a linear regression). Thus our autumn results are not that dissimilar to previous observations.

3.5.2. Particulate biomass profiles

Integrated particulate biomass concentrations are presented in Table 2. Concentrations of bSi ranged from 2.2 to 10.6 (mean ± sd, 4.5 ± 1.9) mmol m^{-2}, though concentrations were generally <5 mmol m^{-2}, with the exception of station 21 where they were >10 mmol m^{-2}. PIC concentrations ranged from 8.3 to 30 mmol m^{-2}, though were arguably closer to 10 mmol m^{-2} than 30 mmol m^{-2} in the majority of cases, and there were indications of a gradual and sustained decrease in integrated PIC with time. POC concentrations were notable for the step-like decrease in integrated concentrations that followed the first 3 stations, where integrated pools sizes were 740–1140 mmol C m^{-2}, and the lack of variability thereafter, with concentrations ranging from 381 to 572 mmol C m^{-2}. A similar, though more muted step-like decrease was also evident in the integrated PON concentrations. Initial integrated concentrations at the first three stations were 66.8–124.6 mmol N m^{-2}, with concentrations thereafter ranging from 48.5 to 72.3 mmol N m^{-2}.

A comparison of integrated particulate pool sizes before the storm (stations 6–12) and after the storm (stations 14–21) indicated that there was little or no difference between the two time periods. For example, average integrated bSi concentrations changed from 3.9 to 5.1 mmol m^{-2}, POC from 455.5 to 450.8 mmol C m^{-2}, PON from 57.4 to 55.3 mmol N m^{-2} and PIC from 15.2 to 11.9 mmol C m^{-2}. None of these differences were significant. Against this background of low level variability however a short-lived period of significant variability was observed over days 272–273 (stations 14–19). At this time integrated PON concentrations increased by ~16% from an average of 53 to 61.5 mmol N m^{-2} (two-sample t-test, $p < 0.05$). This suggests firstly a lag between the disturbance of the system and any biological response, and secondly that the biological response was short-lived given that in general pre- and post-storm conditions were similar. It is also evident that the response in the particulate pools was not consistent. There was no coincident increase in integrated POC concentrations at this time, which would be indicative of phytoplankton growth and instead integrated POC concentrations appeared to decrease by 7% though this change was not statistically significant ($p > 0.05$). This implies that phytoplankton cellular nitrogen content increased separately to increases in cellular carbon content. Integrated C:N ratios, which were greater than 6.6:1 at all stations, decreased at this time from values >8 on day 272 to values <8 on day 273 supporting this conjecture, but note that overall C:N ratios were broadly stable in time. Larger apparent changes to integrated bSi and PIC pools over days 272–273 when the bSi pool increased by 19% from 3.7 to 4.4 mmol Si m^{-2} and the PIC pool increased by 70% from 8.6 to 14.5 mmol C m^{-2} were not significant ($p > 0.05$). Note again however that in general there was little evidence of sustained pre- and post-storm differences thus these short-lived changes, if genuine biological responses and not inter-station variability, are ephemeral responses that will be hard to study in detail.

We present in Fig. 14 pre- and post-storm profiles of the particulate fractions based on a 10 m depth binned average of all data points, which are also shown in Fig. 14 for reference. This serves both to highlight the limited variability between observation periods and to identify general vertical patterns in the data. The bSi observations ranged from 0.02 to 0.25 μmol L^{-1}, and the mean profiles show a subsurface maximum at 25 m (representing the average of all measurements between 20 and 30 m depth) which may have been enhanced post-storm. The subsurface maximum lies above the mean mixed layer depth (43 ± 10 m). PON concentrations varied from 0.27 to 2.37 μmol L^{-1} and whilst largely uniform within the mixed layer decreased beneath the mixed layer. The mean profiles revealed uniform concentrations within the mixed layer, and minimum concentrations at 45–55 m close to the cruise mean mixed layer depth. A similar pattern was evident in the POC

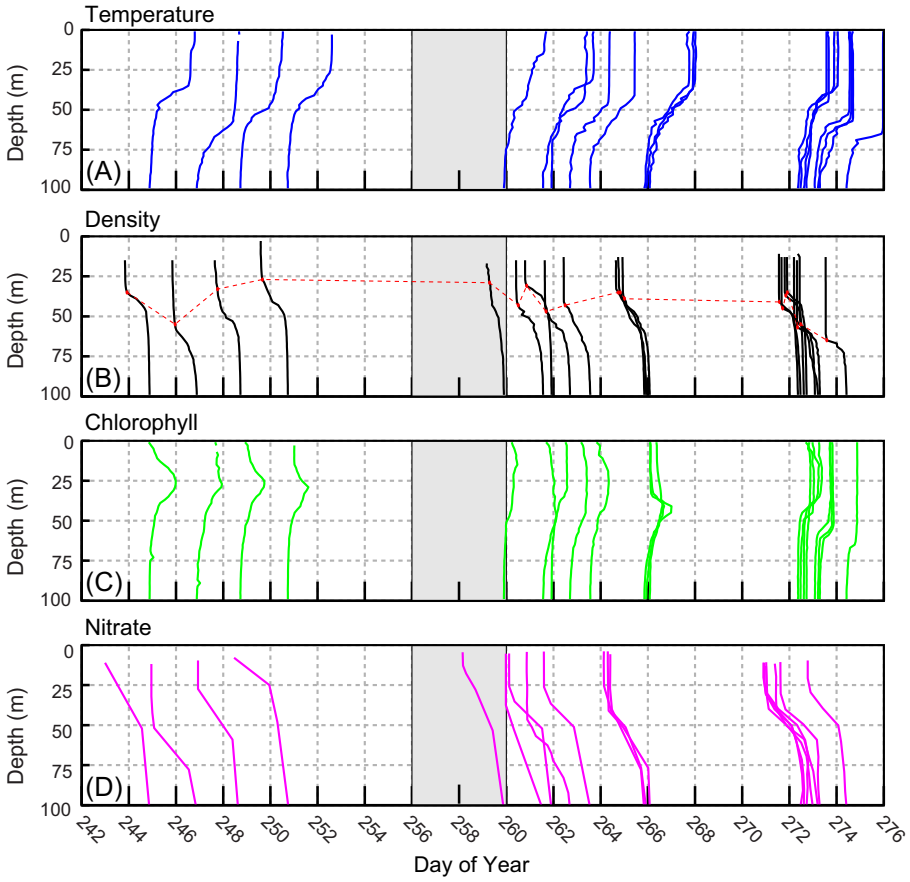

Fig. 12. Time series of vertical profiles of (a) temperature (°C), (b) density (kg m^{-3}), (c) chlorophyll fluorescence (mg m^{-3}), and (d) nitrate (μmol L^{-1}). The base of each profile on the *x*-axis has been positioned according to sampling date and time. The red dashed line indicates the depth of the mixed layer. The grey box in each panel indicates the period when the ship was off site. (For interpretation of the references to colour in this figure legend, the reader is referred to the web version of this article.)

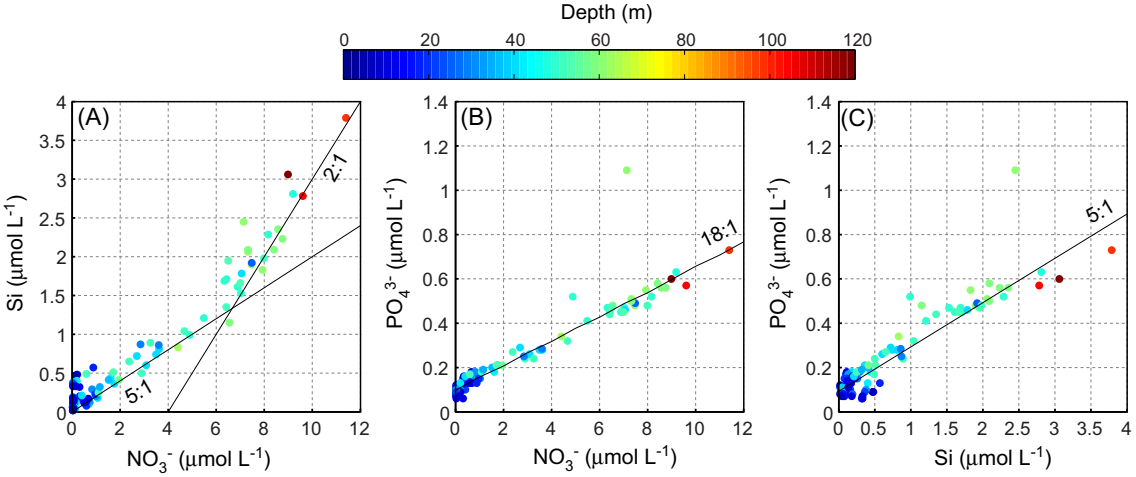

Fig. 13. Nutrient stoichiometries in the upper ocean including (a) silicate (Si) and nitrate (NO_3^-) relationships, which reveal marked difference above and below the mixed layer, (b) phosphate (PO_4^{3-}) and nitrate relationship which shows no variation with depth from a ratio of 18:1, and (c) phosphate and silicate relationship which also shows no variation with depth from a ratio of 5:1.

data though the mean profiles indicate a local POC maximum at 25 m depth coincident with the bSi maximum. This remained but was not enhanced post-storm. The PIC data ranged from 0.09 to 0.67 μmol L^{-1} with an extreme value of 1.5 μmol L^{-1} recorded at station 9. Lower values were generally found at the base of the mixed layer. Mean concentrations within the mixed layer were very similar for both pre- and post-storm periods and there was a weak reduction in PIC concentrations beneath the mixed layer. Collectively there was little to suggest any significant change to any particulate pool after the storm.

3.5.3. Pigments and chemotaxonomic trends

Integrated pigment concentrations are presented in Table 6. Despite the small spatial extent of sampling (~70 km radius), there was a high degree of variability between stations for some pigments. For example, integrated concentrations of ZEA (1.65 mg m^{-2}), CHL-b (1.96 mg m^{-2}), DVCHL-a (1.71 mg m^{-2}) and CARO (1.15 mg m^{-2}) were significantly elevated at station 10 being 2–3-fold higher than the next highest station (various by pigment). Concentrations of HEX (10.32 mg m^{-2}) at station 10 were also elevated. This combination of pigments suggests that station 10 was located in a region of elevated cyanobacterial abundance. Station 10 was located in the southwest corner of the study site (48.28°N 16.85°W; Fig. 1) and recorded the highest salinity (35.7691 at a depth of 75 m) seen amongst the CTD profiles suggesting a lower latitude influence. Interestingly, the most southerly station (station 21; 48.19°N) had the next highest integrated concentration of CHLb (1.02 mg m^{-2}), supporting a lower latitude influence in the south of our study site. In contrast, station 3 (48.7°N) contained high integrated concentrations of PER (1.85 mg m^{-2}), VIO (0.86 mg m^{-2}), DIAD (6.18 mg m^{-2}) and GYRO (0.29 mg m^{-2}) pigments which most likely resulted from a higher dinoflagellate abundance.

The DPA based on vertical sampling indicated that the phytoplankton community was dominated by nanoplankton (76 ± 9%), with microplankton (21 ± 9%) and picoplankton (5 ± 5%) making modest contributions (Fig. 15). On average, changes of <2%, were seen in the contribution of each group between pre- and post-storm periods. These mean contributions match those derived from surface underway sampling (Section 3.4) suggesting that equivalent approximations of the proportion of the phytoplankton community represented by each group can be derived from either sampling strategy. However, unlike the surface underway samples the mean contributions made by diatoms and dinoflagellates to the microplankton community were not equal, with diatoms representing 66 ± 19% and dinoflagellates 34 ± 19% respectively due to important changes at depth. Depth binned contributions of diatoms and dinoflagellates to the microplankton community revealed a clear and distinct vertical distribution (Fig. 15) with increased diatom dominance at the base of the mixed layer. In the surface depth bin (0–10 m), diatoms and dinoflagellates represented 55 ± 15% and 45 ± 15% of the microplankton community, similar to estimates from underway surface sampling (53 ± 17% and 47 ± 17% respectively; Fig. 10). Indeed, these proportions were fairly consistent over the upper 30 m (i.e. above the base of the mixed layer). Below 30 m depth (i.e. at the base of and below the mixed layer) the diatom proportion steadily increased representing an average of 84 ± 11% of the microplankton community between 50 and 60 m depth (Fig. 15). Meanwhile, the dinoflagellate contribution to the microplankton community decreased to a minimum of 16 ± 11% between 50 and 60 m depth. This particular distribution pattern is consistent with the seasonal downward migration of diatoms and the establishment of a subsurface maximum in response to nutrient limitation in surface waters (Lochte and Pfannkuche, 1987; Painter et al., 2010b). However, following the storm there was a shift towards greater diatom dominance within the microplankton size class at all depths and in the surface 0–10 m depth bin diatoms may have represented up to 91% of the microplankton.

We also determined the proportion of total carotenoid pigments represented collectively by photosynthetic and photoprotective carotenoids (Fig. 15). Photosynthetic carotenoids represented 84 ± 7% on average of the total carotenoid pool (range 63–95%) whilst photoprotective carotenoids represented only 16 ± 7% (range 5–37%). These estimates are similar to those derived from surface samples indicating that there were no significant subsurface influences that could alter the interpretation derived from surface samples alone. Indeed, the dominance by photosynthetic carotenoids was strongly conservative with depth pre- and post-storm (Fig. 15). The only station that did not conform to these general conditions was station 10, which as noted above contained significantly elevated concentrations of ZEA, DVCHLa, CHLb and CARO. As a result, the proportion of photoprotective carotenoids increased to >30% in some individual samples.

Amongst the individual photoprotective carotenoids DIA made the largest mean contribution (48 ± 20%) with ZEA and CARO contributing 20 ± 13% and 21 ± 15% respectively. Other individual photoprotective carotenoids represented <12% of the total photoprotective carotenoid concentration. There are indications in the data that contributions from VIA and CARO both increased at depths >40 m with contributions of >20% and >30% becoming more common in individual samples.

HEX (54 ± 10%) represented the dominant photosynthetic carotenoid in the upper ocean with a proportion similar to that obtained from surface samples. Contributions by BUT (23 ± 5%), PER (8 ± 7%) and FUC (15 ± 9%) were also similar to estimates obtained from surface samples. The dominant vertical trend in photosynthetic carotenoids however was in the contribution FUC made to the total photosynthetic carotenoid pool. The FUC contribution increased from ~<15% in the upper 30 m to a maximum of 47% at 50 m.

Unsurprisingly, HEX was the dominant carotenoid representing 40 ± 9% of the total carotenoid pool (PSC + PPC). BUT, FUC, DIA and PER were the next largest contributors and represented 19 ± 6%, 13 ± 9%, 12 ± 12% and 7 ± 6% respectively. All other carotenoids contributed <4% on average.

Presented in Table 7 are the mean ratios for selected diagnostic pigments to TCHLa and mean TCHLa and accessory pigment concentrations based on CTD profile data averaged over the upper 50 m and surface underway samples. Both datasets provide comparable mean estimates but there are nonetheless several significant differences. The mean TCHLa concentration derived from underway data (0.27 mg m^{-3}) was similar to that derived from profile data (0.24 mg m^{-3}) but the difference was not significant (*t*-test, $p > 0.05$). The mean accessory pigment concentration however was significantly different (*t*-test, $p < 0.01$) between the underway (0.4 mg m^{-3}) and CTD profile samples (0.3 mg m^{-3}). Consequently there was also a significant difference in the accessory pigment: TCHLa ratio (*t*-test, $p < 0.01$). As the accessory pigment pool represents the sum total of CHLa, CHLb and CHLc2 + c3 (Table 1), the reason for the difference in the accessory pigment: TCHLa ratio must lie within either the CHLb or CHLc2 + c3 pools, given the lack of significant differences in TCHLa concentrations. The ratio of both CHLb:TCHLa and CHLc:TCHla both showed significant differences between the underway and CTD profile data with a more significant difference in the CHLb:TCHLa ratio. It is probable that the vertical distribution of CHLb more likely explains the existence of a significant difference in the accessory pigment: TCHLa ratio between underway and profile data.

Surprisingly, despite a prominent subsurface maximum in FUC concentrations (that is reflected in the microplankton dominance at depth – Fig. 15) there was no significant difference in the FUC: TCHLa ratio calculated from underway (0.13 ± 0.06) or profile data (0.16 ± 0.12). The HEX:TCHLa ratio meanwhile was different with a higher ratio in surface waters (0.63 ± 0.15) compared to the profile data (0.51 ± 0.21), reflecting, in part, the vertical distribution of nanoplankton (Fig. 15). Ratios of photosynthetic and photoprotective carotenoids to TCHLa also displayed significant differences between the underway and profile data, with higher ratios in underway compared to profile data (Table 7). An increase in the proportion of photosynthetic carotenoids in surface waters is not unexpected during periods of seasonally declining irradiance intensities and can easily explain the elevated PSC:TCHLa value

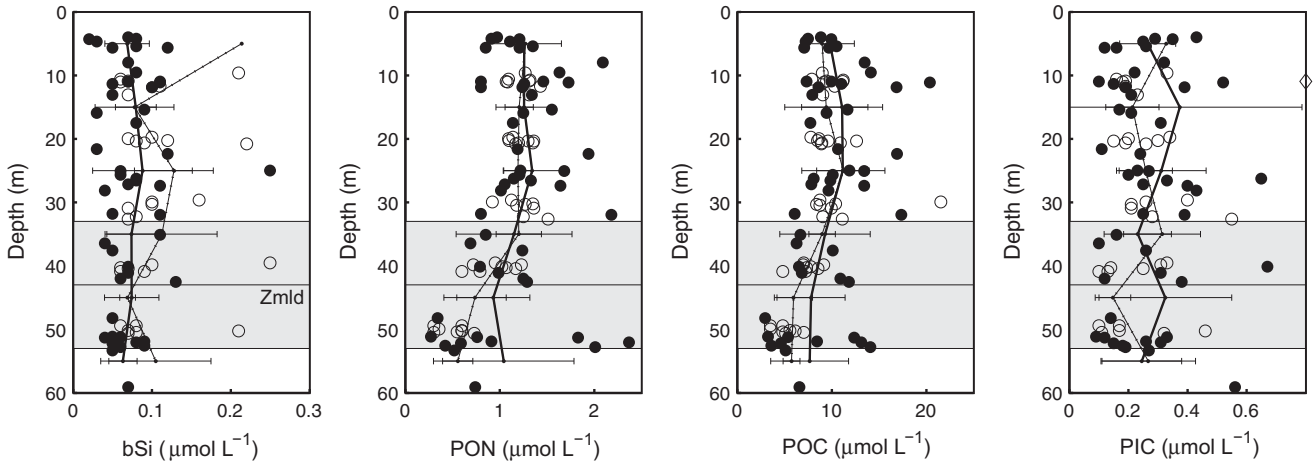

Fig. 14. Pre-storm (stations 1–12; thick black line) and post-storm (stations 14–21; thin black line) mean vertical profiles (±stdev) of (a) biogenic silica (bSi), (b) particulate organic nitrogen (PON), (c) particulate organic carbon (POC) and (d) particulate inorganic carbon (PIC). The mean profile for each period is based on 10 m depth binned averaging of available measurements. In each panel the observations are split by sampling period with pre-storm observations indicated by the black filled circles and post-storm observations by black open circles. The cruise mean mixed layer depth (Zmld), is indicated by the horizontal black line with grey shading used to indicate the standard deviation of the mean mixed layer depth.

observed (Table 7). Elevated PPC:TCHLa in the underway data meanwhile suggests that irradiance intensities were still high enough to damage cellular photosynthetic apparatus.

We also present in Table 7 similar estimates of mean pigment ratios based on pre-storm and post-storm classification of stations. None of the apparent differences between these two time periods were statistically significant indicating that there were no dramatic changes in pigment ratios as a result of environmental disturbance due to the passage of the storm.

We also present the results of log-linear regression models between TCHLa and accessory pigment concentrations in Table 7 to allow comparison of our pigment dataset to recent global syntheses of HPLC observations (Trees et al., 2000; Peloquin et al., 2013). Although there was generally a poorer fit in the underway data ($r^2 = 0.683$) compared to the profile data ($r^2 = 0.922$) both models were highly comparable to existing global relationships (Trees et al., 2000; Peloquin et al., 2013) and to the range of values reported from individual studies conducted across a range of environments (Trees et al., 2000). This indicates that our observations are consistent with previous assessments of the relationship between accessory pigments and TCHLa.

3.6. Particulate ratios as indicators of post-storm biogeochemical changes

The ratio of PIC to POC can be used to infer aspects of coccolithophore bloom state or calcite turnover rates (Balch et al., 2005) and upper ocean carbon fluxes mediated by PIC as a ballast material (Koeve, 2002). In Fig. 16 we present PIC:POC ratios derived from underway data (Fig. 8) and in integrated form for each station. We also include for reference summer and autumn seasonal estimates of the PIC:POC ratio for Longhurst's North Atlantic Drift (NADR) and northeast Atlantic shelf biogeochemical provinces (Longhurst, 1998) derived from a global analysis of PIC and POC distributions from MODIS Terra data by Balch et al. (2005).

Surface underway PIC:POC ratios ranged from 0.005 to 0.153. The majority of ratios were generally lower than the NADR mean summer (July–September) value of 0.043 and closer to the NADR mean autumn (October–December) value of 0.017 derived from Balch et al. (2005). Interestingly, a number of individual samples returned high PIC:POC values that appeared similar to the mean autumn value of 0.130 derived from Balch et al. (2005) for the northeast Atlantic shelf province. This raises the possibility that transport from the shelf, which was ~250 km away, had reached the sampling site but as only 2 underway samples had PIC:POC values >0.1 this is considered unlikely. A significant downward trend in surface PIC:POC ratios was identified ($t(93) = -2.36$, $p < 0.05$) reflecting reductions in both PIC and POC concentrations and indicating that the two parameters were not reducing at a constant rate.

A similar comparison between 50 m integrated PIC:POC ratios and those derived from the euphotic zone integrals reported by Balch et al. (2005) also show good agreement (Fig. 16). As with individual surface values we find a better agreement between our integrated PIC:POC values and the NADR mean autumn value of 0.017 than to the NADR mean summer value of 0.04, though our integrated results encapsulate both mean seasonal estimates. Integrated PIC:POC ratios averaged 0.029 ± 0.015, and whilst generally <0.030 did reach a value of 0.078 at station 9, which is notable for the unusual coccolithophore community observed at this station (Appendix Fig. A1).

The close agreement between our in situ observations and those derived from MODIS indicate that the current algorithms for deriving PIC and POC appear broadly correct for the region of our study. However, many of our surface PIC:POC ratios and water column integrated ratios were more correctly represented by the mean autumn estimates (October–December) than the mean summer estimates (July–September) reported by Balch et al. (2005) despite slight differences in the temporal periods analysed (our cruise in September technically falls within the summer time frame used by Balch et al. (2005))

In Table 8 we present a comparison of both in situ surface and integrated PIC and POC estimates with those reported by Balch et al. (2005). Surface PIC concentrations were similar, though the mean value was higher than either of the mean NADR summer or autumn concentrations. This was also reflected in our integrated PIC results, which for our data were 70% larger on average than the mean summer value or ~350% larger than the mean autumn value. Surface POC concentrations were also considerably higher than the mean seasonal estimates derived from MODIS, being ~175% or ~290% higher than the mean NADR summer and autumn estimates respectively. Due to the method of interpolating surface POC to the euphotic zone depth it is likely that vertical variability in POC was

Table 6
Integrated pigment concentrations (mg m^{-2}) presented by station. Note that there are no pigment data for stations 11, 15 or 17 (represented by –). In cases where pigments were not detectable the corresponding cell is left blank.

Stn.	Chl_{c3}	Chl_{c2}	PER	BUT	FUC	HEX	PRAS	VIO	DIAD	ALLO	ZEA	LUT	GYRO	Chl_b	DVChla	Chl a	B-CARO
1	0.05	0.03	0.32	2.12	1.92	4.56	0.11	0.06	1.79	0.13	0.07	0.11		0.54		9.59	0.24
2	0.06	0.04	0.35	1.18	0.75	4.04	0.55	0.41	3.00	0.10	0.18	0.05		0.15	0.12	9.81	0.17
3	0.00	0.10	1.85	3.49	1.33	7.42	0.51	0.86	6.18	0.20	0.35	0.22	0.29	0.95	0.66	22.42	0.63
4	0.10	0.06	0.75	2.51	1.95	7.10	0.25	0.07	1.19	0.33	0.18	0.09		0.66	0.00	10.94	0.27
6	0.09	0.05	0.87	2.83	1.33	6.23	0.24	0.50	0.82	0.12	0.50	0.04		0.21	0.40	10.71	0.40
7	0.14	0.02	1.70	3.57	2.12	7.02	0.46	0.04	0.82	0.36	0.30	0.19		0.53	0.58	14.32	0.60
8	0.13	0.09	1.86	3.79	2.10	7.05	0.44	0.09	1.63	0.17	0.36	0.78	0.03	0.83	–	14.00	0.38
9	0.02	0.05	0.97	2.39	1.15	5.77	0.16	0.59	2.28	0.11	0.18	0.13	0.31	0.39	0.09	11.51	0.25
10	0.10		0.80	4.81	1.86	10.32	0.60	0.06	1.40	0.30	1.65	0.16	0.04	1.96	1.71	17.11	1.15
11	–	–	–	–	–	–	–	–	–	–	–	–	–	–	–	–	–
12			0.39	1.44	0.60	3.00	0.08	0.13	1.53	0.30	0.54	0.29		0.18	0.70	8.14	0.48
14	0.02		1.40	3.06	1.96	6.27	0.77	0.16	1.20	0.09	0.18	0.17		0.31	0.81	12.43	0.51
15	–	–	–	–	–	–	–	–	–	–	–	–	–	–	–	–	–
16	0.35	0.18	1.32	3.24	2.08	7.38	0.53	0.17	0.96	0.30	0.36	0.19	–	0.96	0.10	13.24	0.47
17	–	–	–	–	–	–	–	–	–	–	–	–	–	–	–	–	–
18	0.04	0.02	1.03	2.71	1.45	6.59	0.43	0.54	3.37	0.29	0.38	0.11	0.08	0.60	0.37	11.94	0.33
19	0.02	0.20	0.87	3.70	1.87	8.44	0.23	0.20	1.34	0.19	0.18	0.08		0.31	0.04	13.89	0.42
20	0.13	0.05	0.63	3.46	1.68	7.28	0.47	0.07	1.09	0.30	0.26	0.16	0.06	0.91	0.04	12.60	0.32
21	0.01	0.04	0.47	3.18	1.80	7.33	0.62	0.03	0.67	0.16	0.45	0.17	–	1.02	0.35	12.37	0.40
Mean ± sd	0.08 ± 0.09	0.07 ± 0.06	0.92 ± 0.54	2.90 ± 0.93	1.55 ± 0.54	6.5 ± 1.73	0.44 ± 0.24	0.27 ± 0.25	1.74 ± 1.39	0.21 ± 0.09	0.38 ± 0.35	0.18 ± 0.17	0.09 ± 0.12	0.69 ± 0.46	0.37 ± 0.45	12.66 ± 3.3	0.44 ± 0.22

missed, a fact Balch et al. (2005) clearly acknowledge, yet our in situ observations do not indicate a prominent sub-surface POC maximum (Fig. 16). Nevertheless our integrated POC concentrations were over 2-fold higher on average than either NADR mean summer or autumn estimates.

PIC:PON molar ratios are presented in Fig. 16. In surface waters the PIC:PON ratio ranged from 0.04 to 1.14 (mean ± sd 0.26 ± 0.18) and exhibited a weak but significant downward trend with time that was significantly different from zero ($t(93) = -3.52$, $p < 0.05$). Integrated PIC:PON molar ratios were comparable to surface values, ranging from 0.15 to 0.62 (mean ± sd 0.24 ± 0.11), suggesting that surface values may provide a suitable proxy for the PIC:PON ratio of the upper ocean. However, in integrated form station 9, which had a PIC:PON ratio of 0.62 and which was twice that of the next highest station (station 10, 0.31), was noticeably different to all other stations. Given important underlying differences in the coccolithophore community at this station (see Section 3.4.3.2) it suggests that the integrated PIC:PON ratio is sensitive to coccolithophore community composition and in this particular case, the relative contribution made by rarer coccolithophore species to total coccolithophore abundance. This in turn likely reflects the variability in calcite content between different coccolithophore species. bSi:POC molar ratios are presented in Fig. 16. In surface waters the ratio of bSi to POC ranged from 0.03 to 0.051 (mean ± sd 0.011 ± 0.008) and displayed a complex temporal pattern. Overall the data show a significant gradual reduction with time in bSi:POC ($t(94) = -3.75$, $p < 0.05$) suggesting that either the relative proportion of bSi decreased or the proportion of POC increased. In reality (Fig. 8) both bSi and POC concentrations decreased but at different rates and it is the relatively faster reduction in bSi concentrations that appears to drive the overall reduction in the bSi:POC ratio. Closer examination of the temporal trend in bSi:POC however reveals that between days 260 and 271 bSi:POC actually increased in surface waters. This was driven by a small increase in bSi concentrations as POC concentrations continued to decrease at this time (Fig. 8). We consider it likely therefore that the increase in surface bSi concentrations and in bSi:POC at this time is linked to the increase in abundance of small pennate diatom and silicoflagellates recorded in the SEM analyses (Section 3.4.3.2).

When integrated over 50 m the ratio of bSi to POC ranged from 0.004 to 0.026 (mean ± sd 0.009 ± 0.005) but unlike the trend in surface waters integrated bSi:POC exhibited a gradual and significant increase with time ($t(14) = 2.23$, $p < 0.05$). Station 21 was notable for having the highest integrated bSi:POC ratio of any station, but even with this station omitted from the statistical regression the gradual increase remained significant. The existence of opposing trends in bSi:POC ratios between surface waters and integrated ratios suggests either that a subsurface addition to the bSi pool or a rapid removal from the POC pool was taking place. Irrespective of this, it is evident that surface bSi:POC does not provide accurate information on the vertical bSi:POC ratio as is the case for PIC:PON, a finding that is self-evident given subsurface diatom distributions and abundances.

The ratio of bSi to PON is also shown in Fig. 16, and appears qualitatively similar to bSi:POC, varying more broadly during the first half of the cruise than the second, reaching a minimum (~0.04) around day 260, and displaying a late cruise peak with values ~0.1 around day 270/271. The reduction in bSi:PON with time was significant ($t(94) = -4.53$, $p < 0.05$). Integrated values were broadly similar between stations with values around ~0.05 but ranged from 0.04 to 0.19. Station 21 again provided a significant deviation from the overall general pattern. There was no significant trend in integrated bSi:PON with time either with or without station 21 included.

PIC and bSi are both considered important ballast minerals aiding the sequestration of carbon into the ocean interior (Klass and

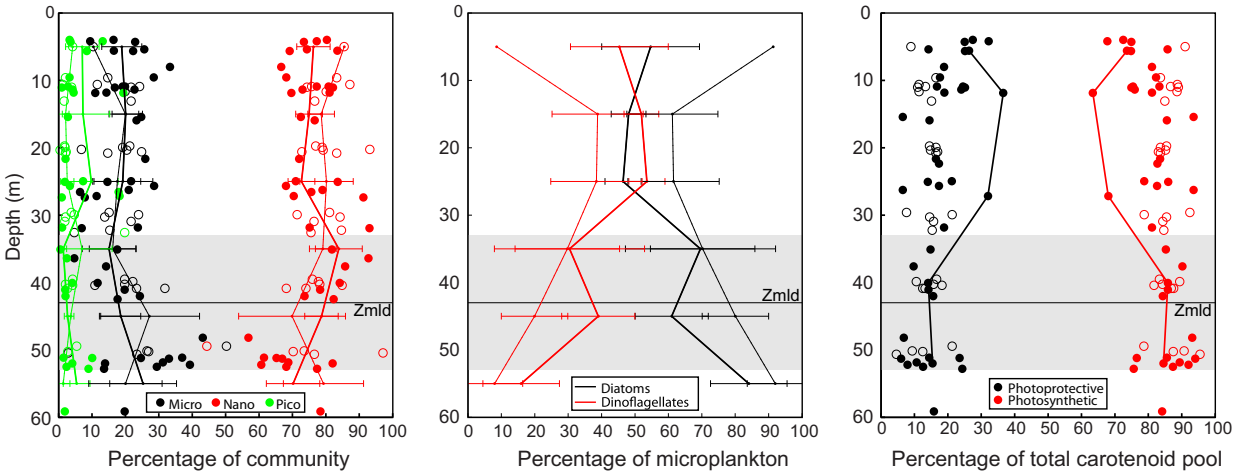

Fig. 15. Summary results of diagnostic pigment analyses including (a) pigment based size class assessment of the phytoplankton community revealing the dominance by nanoplankton and far smaller contributions by pico- and microplankton to the phytoplankton community, (b) relative mean percentage of diatoms and dinoflagellates within the microplankton size class and (c) relative percentage of photoprotective and photosynthetic carotenoids within total measurable carotenoid pools by depth. In panels (a and c) we indicate pre-storm samples with filled circles and post-storm samples with open circles. In panels (a and b) we include mean profiles with standard deviation of the mean based on 10 m depth averaging of available measurements for pre-storm (thick lines) and post-storm (thin lines) periods. Note that in panel (c) we highlight the profile from station 10 due to its unusual relative contributions of photoprotective and photosynthetic carotenoids. In all panels the cruise mean mixed layer depth (Zmld) is indicated by the horizontal black line with grey shading used to indicate the standard deviation of the mean mixed layer depth.

Table 7
Cruise mean values (±standard deviation) of total Chl *a* (TCHLa) and total accessory pigments (mg m^{-3}) by dataset (underway or CTD profile data) and the mean ratios of selected diagnostic accessory pigments to TCHLa, see Table 1 for definitions. Note that CTD profile data are simply averaged over the upper 50 m for the entire cruise and also on the basis of pre- and post-storm station timing. The resulting mean values are tested for significant differences using a *t*-test, with *p*-values reported. Also shown are the log-linear regression models between TCHLa and accessory pigments for each dataset (underway and entire cruise profile data).

	Total Chl *a*	Accessory	Accessory:TCHLa	CHLc:TCHLa	CHLb:TCHLa	FUC:TCHLa	HEX:TCHLa	ZEA:TCHLa	PSC:TCHLa	PPC:TCHLa
Underway data	0.27 ± 0.11	0.40 ± 0.17	1.53 ± 0.46	0.06 ± 0.12	0.05 ± 0.02	0.13 ± 0.06	0.63 ± 0.15	0.05 ± 0.03	1.14 ± 0.31	0.30 ± 0.10
CTD profile data	0.24 ± 0.14	0.30 ± 0.17	1.28 ± 0.43	0.02 ± 0.02	0.08 ± 0.04	0.16 ± 0.12	0.51 ± 0.21	0.04 ± 0.04	0.98 ± 0.42	0.24 ± 0.14
Significant difference	ns	$p < 0.01$	$p < 0.01$	$p < 0.05$	$p < 0.01$	ns	$p < 0.01$	ns	$p < 0.01$	$p < 0.01$
CTD stn 6–12 (pre-storm)	0.25 ± 0.14	0.31 ± 0.18	1.28 ± 0.22	0.02 ± 0.02	0.08 ± 0.04	0.14 ± 0.09	0.50 ± 0.12	0.06 ± 0.05	0.97 ± 0.27	0.26 ± 0.13
CTD stn 14–21 (post-storm)	0.26 ± 0.13	0.33 ± 0.14	1.34 ± 0.6	0.02 ± 0.02	0.10 ± 0.04	0.16 ± 0.10	0.56 ± 0.26	0.04 ± 0.02	1.04 ± 0.54	0.22 ± 0.14
Significant difference	ns	ns	ns	ns	ns	ns	ns	ns	ns	ns
Underway data	Log(Accessory pigments) = 0.762 ∗ log(TCHLa) + 0.028 $n = 74$, $r^2 = 0.683$									
CTD profile data	Log(Accessory pigments) = 0.968 ∗ log(TCHLa) + 0.0679 $n = 77$, $r^2 = 0.922$									

Archer, 2002). The ratio of PIC to bSi in surface waters, which reveals the relative importance of bSi and PIC as potential ballast, showed no strong temporal trend with values ranging from 0.4 to 19.2 but values were generally >1:1. There was a suggestion of reduced variability in PIC:bSi with time with values of 2–4:1 later in the cruise (Fig. 16). PIC therefore appeared more important as potential ballast material than bSi. This observation is consistent with the surface concentrations of both bSi and PIC (Fig. 8) which both exhibited reduced variability in concentration throughout the cruise but with molar concentrations of PIC that were at least twice those of bSi. We also present in Fig. 16 integrated PIC:bSi ratios which were broadly comparable to surface measurements. Integrated PIC:bSi ranged from 1.6 to 9.4 (mean 3.5 ± 1.8) but were <5:1 at all stations except station 9, when a ratio of 9.4 was measured due to a significant increase in the concentration of PIC in the water column at this station (Table 2). The elevated PIC:bSi ratio at station 9, indicative of greater PIC relative to bSi, is consistent with the elevated PIC:POC and PIC:PON ratios for the same station (Fig. 16). Given that typical integrated PIC:bSi ratios were between 2 and 4.5, this suggests that PIC was 2–4.5 times more abundant than bSi and thus potentially more important as a vector for export.

POC:PON ratios in the surface ocean exhibited a clear temporal trend (Fig. 16). C:N ratios were initially between 8 and 10 and consistently larger than the Redfield ratio of 6.6:1 (Redfield et al., 1963). However, a consistent reduction in the C:N ratio was observed such that by day 274 C:N ratios were close to or just below Redfield with a range of 6–8. Few observations revealed C:N ratios >10. This trend was significantly different from zero ($t(93) = -6.41$, $p < 0.05$). Much has been written about the topic of phytoplankton carbon overconsumption since elevated C:N ratios were first reported in the northeast Atlantic (Sambrotto et al., 1993a, 1993b; Toggweiler, 1993; Banse, 1994; Kahler and Koeve, 2001; Körtzinger et al., 2001; Koeve, 2004, 2006). Carbon overconsumption has often been explained as a response to nutrient stress and seems to be most prevalent during the summer months in the northeast Atlantic Ocean (Körtzinger et al., 2001). Our observations indicate that particulate C:N ratios in the surface mixed layer were elevated compared to the Redfield ratio but the data also show that the C:N ratio was decreasing in a gradual manner during the observation period. Given the abrupt nature of nutrient resupply to the surface ocean observed from day 270 onwards (Fig. 8), it is unlikely that the steady reduction in the particulate C:N ratio over days 244–275 can be linked to nutrient resupply as there is no abrupt

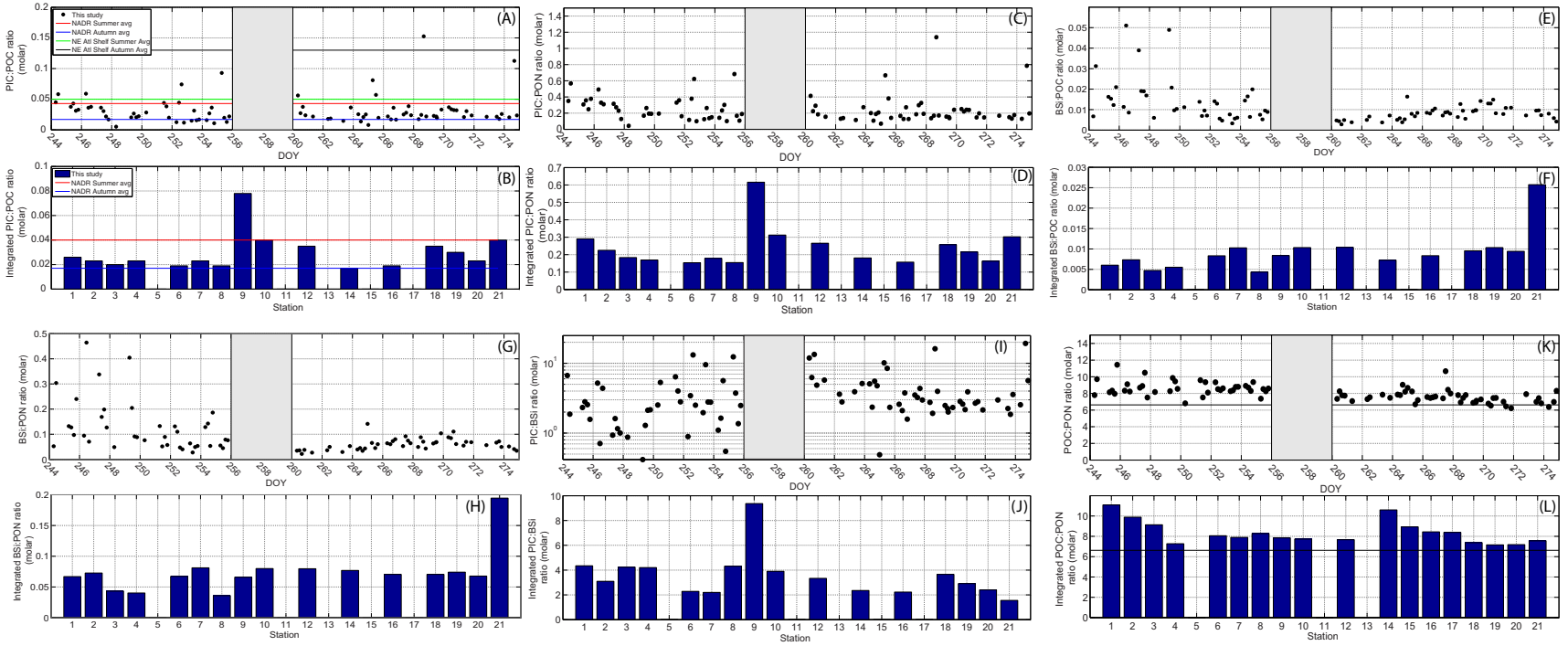

Fig. 16. Particulate molar ratios in surface underway samples and based on 50 m integrated pools for (a) surface PIC:POC ratio, (b) integrated PIC:POC ratio, (c) surface PIC:PON ratio, (d) integrated PIC:PON ratio, (e) surface bSi:POC ratio, (f) integrated bSi:POC ratio, (g) surface bSi:PON, (h) integrated bSi:PON ratio, (i) surface PIC:bSi ratio (note log-scale), (j) integrated PIC:bSi ratio, (k) surface POC:PON ratio and (l) integrated POC:PON ratio. Note that in panels (a and b) we also show the summer and autumn seasonal average PIC:POC ratios derived from Balch et al. (2005) for the North Atlantic Drift (NADR) and northeast Atlantic Shelf biogeochemical provinces of Longhurst (1998) and in panels (k and l) we provide the Redfield C:N ratio of 6.6:1 for reference (horizontal black line). Where present the grey box represents the period the ship was off site.

Table 8
Comparison of the mean seasonal concentrations of PIC and POC in the NADR province derived from remote sensing methods by Balch et al. (2005) and those sampled in this study.

Variable (units)	Remote sensing data		Field data
	Mean summer (July–September)	Mean autumn (October–December)	This study mean ± std (range)
Surface PIC (mg m^{-3})	2.34 ± 1.1	0.65 ± 0.21	4.4 ± 3.4 (1.35–16.79)
Surface POC (mg m^{-3})	54.03 ± 6.74	38.24 ± 2.15	148.36 ± 61.03 (74.4–402.8)
Integrated PIC (mg m^{-2})	103.83 ± 37.27	39.41 ± 11.62	176.4 ± 70.8 (99.6–360)
Integrated POC (mg m^{-2})	2566.18 ± 107.9	2341.62 ± 42.36	6356.4 ± 2262 (4581–13,668)

reduction in C:N ratios to support this. Instead we suggest that irradiance may be a more likely explanation as it is one of the few environmental factors to also exhibit a slow gradual change (Fig. 6).

Despite the consistent temporal changes to surface particulate C:N ratios the same was not true of integrated C:N pools which were all consistently >6.6:1 (Fig. 16). The majority of stations (9) had C:N ratios between 6 and 8, whilst 7 stations had C:N ratios between 8 and 10, and 2 stations produced C:N ratios >10.

4. Discussion

The passage of a significant early autumn storm of unusual intensity through the study site deepened the mixed layer, entrained nutrients from depth and increased surface nutrient concentrations. The storm also resulted in complex perturbations to the plankton community. Most surprising was the lack of any change in either mixed layer average chlorophyll concentrations or euphotic zone integrated chlorophyll concentrations, despite a ~50% increase in surface chlorophyll concentrations and a 200–400% increase in integrated nutrient concentrations. This strongly suggests that the observed increase in surface chlorophyll concentrations was the result of input from below, most notably from the vertical redistribution of an established subsurface chlorophyll maximum (Fig. 12), rather than from in situ growth following the addition of nutrients. This observation, and a similar report from the temperate northeast Pacific by Perry et al. (2008), suggest that this mechanism for what may otherwise be perceived as an autumn bloom may be more prevalent than previously realized.

Chemotaxonomic analysis of the phytoplankton community revealed that the nanoplankton size class dominated the community during September/October. Both individual pigment concentrations (particularly of the accessory pigment HEX) and scanning electron microscopy analysis support the conclusion that prymnesiophytes/coccolithophores were dominant at this time. Our taxonomic analyses however were restricted and most notably our insight into the picoplankton population was limited to pigment densities. The broader conclusion reached from our chemotaxonomic analysis of a prymnesiophyte dominance is supported by previous studies (e.g. Gibb et al., 2001; Barlow et al., 1993a, 1993b) suggesting that our observations are representative of the northeast Atlantic Ocean and consequently they extend the period of nanoplankton dominance into the early autumn.

Our data also demonstrate an increase in surface DVCHLa concentrations and in the contribution made by DVCHLa to TCHLa (up to 13%) which is consistent with an emerging autumnal *Prochlorococcus* abundance maximum; though relative to other pigments the concentrations of DVCHLa were low and the chemotaxonomic analysis indicated picoplankton accounted for only ~5% of the phytoplankton community both in surface waters (Fig. 10) and with depth (Fig. 15). Previously, Gibb et al. (2000) noted a greater contribution of DvCHLa to TCHLa during autumn months whilst Karayanni et al. (2005) identified greater *Prochlorococcus* abundance in autumn so collectively such observations indicate an important seasonal aspect of prochlorophyte ecology in the northeast Atlantic.

Despite canonical descriptions of the seasonal evolution and succession of plankton genera in temperate waters (e.g. Margalef, 1978) the DPA revealed that all major taxa were still present in the northeast Atlantic though many were vertically separated from one another. In keeping with seasonal resource limitation theory there was a strong emphasis on smaller nano- rather than larger microplankton size classes coincident with low and limiting nutrient concentrations within the surface mixed layer due to the competitive advantage gained from smaller cell size under such conditions.

Before discussing the chronology of events in detail and determining the biogeochemical impacts of this storm it is worth restating one important factor. The TS analysis of CTD data suggests that we sampled related but ultimately different water masses during the cruise, thus it is not improbable that some of the temporal variability seen in our datasets was driven by these subtle changes in water mass. However, the pigment data and the electron microscopy data clearly revealed a large and significant change coincident with the passage of the storm through the site irrespective of water mass and as the spatial extent of typical autumn storms is large (100s to 1000s of km) relative to our study area this would likely mean that no one water mass would be impacted in isolation thus the overall impacts should be similar.

4.1. Chronology of the impact of an autumn storm on phytoplankton biomass and community composition

The late cruise TCHLa maximum seen on year day 272 (Fig. 9) was coincident with increased nutrient concentrations (Fig. 8) and intriguing responses within the phytoplankton (Fig. 10). To clarify which component of the plankton community responded at this time we combined the various datasets to clarify the temporal patterns (Fig. 10). Over days 266–275 a number of trends were evident. Most surprisingly, the picoplankton contribution increased reaching a cruise maximum of 8% of the phytoplankton community late on day 268. This increase, which initially started on day 264 and may have been triggered by an earlier wind event, tracked the increase in wind speed that began on day 266 but during the plateauing of maximum wind speeds over days 269–270 the picoplankton contribution fell sharply to <4%. Wind speeds reached maximum values (gusting to >20 m s^{-1}) late on day 269 approximately 1 day after the picoplankton maximum. Maximum surface NO_3^- concentrations (based on the highest concentration measured) were observed on day 272, though it is arguable that maximum concentrations were reached in the preceding 24 h due to a plateauing of measured concentrations over this time period. The minimum SST however occurred at approximately the same time as the maximum NO_3^- concentration suggesting that the indicated timing for maximum NO_3^- is correct. Maximum surface CHLa concentrations were measured late on year day 271, thus maximum CHLa and NO_3^- concentrations were almost coincident (within 12 h). This time period is too short for the increase in

chlorophyll to have resulted from phytoplankton growth following increased nutrient availability and further supports our argument that supply from below provides the most likely explanation. Changes to the microplankton and nanoplankton contributions were rather muted but they were clearly offset from one another. The microplankton fraction increased from 15% to 20% of the population between days 270 and 271, before decreasing back to ~16% by day 273. Maximum microplankton contributions were seen late on day 271 after wind speeds had started to decrease and very shortly after peaks in both CHLa and NO_3^- concentrations, suggesting that microplankton most likely contributed to the post-storm increase in chlorophyll. The nanoplankton proportion displayed two peaks. The first peak was coincident with maximum wind speeds on day 270 but decreased thereafter from 80% to 76% of the population between days 270 and 271, coincident with decreasing wind speeds. There was a subsequent 4% increase in the nanoplankton fraction back to 80% on day 273 when the post storm maximum contribution was reached (Fig. 10). Collectively, the data indicate that picoplankton responded rapidly to wind mixing but that their response was short lived, whereas the microplankton, and particularly the nanoplankton, which represented the majority of the community (Fig. 15), were slower to respond with their respective community maximums occurring after the period of maximum wind speed. Two observations immediately arise from this. Firstly, the picoplankton peak preceded the maximum in CHLa and NO_3^- concentrations whereas the microplankton peak was almost coincident. Secondly, the peak in nanoplankton occurred coincident with peak wind speed and again 1 day after maximum nutrient and chlorophyll concentrations, thus nanoplankton appeared temporarily less important than microplankton in contributing to the post-storm maximum in surface chlorophyll.

Can the component of the microplankton community that responded be identified? A careful analysis of the microplankton pigment data indicated that the diatom contribution to the microplankton size class fell from >60% on day 269 (peak wind speed) to 43% on day 271.5 (peak CHLa) whilst the dinoflagellate contribution increased from <40% to 57% over the same time period. The post-storm peak in microplankton occurred on day 271.5 (Fig. 10) and the surprising conclusion therefore is that dinoflagellates not diatoms were largely associated with this post-storm maximum. This is surprising as dinoflagellates were generally the minor contributor to the microplankton pool in surface waters and contributed less with depth (Fig. 15) despite the water column clearly mixing to depth (Fig. 12) and entraining nutrients and presumably diatoms. There is nevertheless a very small temporal offset of ~6 h between the dinoflagellate dominance of the microplankton size class and peak chlorophyll concentration due to differences in sampling resolution and it is not therefore evident if the increase in chlorophyll can be attributed solely to dinoflagellates. By day 271.8, 8 h after the dinoflagellate dominance diatoms had rebounded to >60% of the microplankton size class and would also therefore have contributed to the chlorophyll peak.

The surprising dinoflagellate dominance in the period immediately after maximum wind speed is also unexpected as the SEM dataset presents a rather different conclusion. Station 14 was the first post-storm station but conducted on day 272, almost a full day after the events detailed in the underway data, hence the profile results are not inconsistent with the above. At this station total dinoflagellate abundance had decreased slightly from 3.73 to 3.18 cells mL^{-1} compared to station 12 (Table 4). A subsequent dinoflagellate maximum was observed at station 18 (day 273). There is no indication from the SEM data therefore that dinoflagellate abundances had increased immediately after the storm. In contrast, both small and large pennate diatom abundances at station 14 were higher than observed at station 12 (Table 4) with a subsequent maximum in the small pennate diatom group observed also at station 18. Consequently the SEM data derived from CTD casts indicates that diatoms were more abundant immediately after the storm.

The contrary conclusions derived from high temporal resolution underway observations and lower temporal resolution profile data strongly imply that different phytoplankton types respond over different time scales and that the time scale of observation needed to correctly observe the immediate impacts of storms is of the order of hours or less. Consequently, despite our best efforts the profile data is likely to bias interpretations of short-term (0–1 day) storm impacts as the sampling resolution is too crude. Longer-term impacts (1–4 days), which may prove to be more biogeochemically relevant given typical phytoplankton growth rates, may also be biased by sampling interval as they increasingly fail to fully resolve rapid short-lived changes.

Using automated flow cytometry sampling systems with sub-hourly sampling rates Thyssen et al. (2008) described rapid changes to phytoplankton communities following wind events and introduced the concept of response functional types – groups of plankton that respond over different time-scales to the same forcing event. Subsequent work across a range of environments has shown that picoplankton respond almost immediately to wind-driven perturbations with several fold increases in abundance not uncommon (Dugenne et al., 2014; Thyssen et al., 2014; Lomas et al., 2009b). As was observed in this study however, such responses are short lived.

4.2. Summary of changes attributable to storm activity

In Table 9 we present a summary of changes attributable to the passage of the first major storm of the 2012 autumn season in the northeast Atlantic Ocean. Many significant changes were observed despite these changes being derived from profile data, yet for some parameters such as the particulate pools, there was no change (see also Table 2). On average this one storm deepened the mixed layer by 26%, decreased average temperatures by 8% and increased average nutrient concentrations by ~100–1400% (n.b. note that average mixed layer changes appear larger than integrated changes possibly due to overestimation of mixed layer depths). Despite apparent changes of between 1% and 33% in the average mixed layer concentrations of chlorophyll, bSi, PIC, POC or PON these changes were not significant due to the level of variability between stations. More interestingly, there was a ~500% increase in the abundance of small pennate diatoms whereas the large pennate diatoms barely changed in abundance (+5%). We also note a ~900% increase in the abundance of silicoflagellates and a ~300% increase in *E. huxleyi* coccosphere abundance.

In previous studies the magnitude and sign of storm-induced changes depended greatly on the duration of the post-storm sampling period, the resolution of sampling and the parameter measured. For example, Koeve et al. (2002) reported ~3-fold increases in integrated chlorophyll and bSi concentrations over a 7-day period following a pre-spring bloom storm in April in the northeast Atlantic. POC concentrations meanwhile increased less than 1-fold (36%). This time period of observation (7 days) was over twice as long as we were able to sample the post-storm water column in our study (3 days) implying that we could have missed the greatest observable change in the post-storm period thereby providing an alternative explanation for the lack of any significant change in integrated chlorophyll or particulate pool concentrations (i.e. we did not sample for long enough). However, we consider this unlikely as there is no indication from the satellite record of subsequent increases in surface chlorophyll concentrations after the cruise (Fig. 3) and the removal of the subsurface chlorophyll

Table 9
Summary table of mixed layer changes attributable to storm action. We report the mean pre- to post-storm change for a variety of parameters based on mixed layer average values for stations 6–12 (pre-storm) and 14–21 (post-storm) or surface taxonomic data from those same stations. An estimate of the relative change is also provided. Note that the sign of each value is used to infer an increase (positive change) or decrease (negative change).

Parameter	Average change and units	Relative change (%)
Mixed layer depth	+11 m	+26
Average mixed layer temperature	−1.35 °C	−8
Average mixed layer nutrient concentrations	NO_3^-: +1.5 μmol L^{-1}	+1400
	$Si(OH)_4$: +0.31 μmol L^{-1}	+374
	PO_4^{3-}: +0.11 μmol L^{-1}	+117
Average mixed layer biogenic silica (bSi)[a]	+0.02 μmol L^{-1}	+33
Average mixed layer particulate inorganic carbon (PIC)[a]	−0.05 μmol L^{-1}	−15
Average mixed layer particulate organic carbon (POC)[a]	+0.07 μmol L^{-1}	+1
Average mixed layer particulate organic nitrogen (PON)[a]	+0.02 μmol L^{-1}	+2
Average mixed layer chlorophyll concentration[a]	+0.03 mg m^{-3}	+14
Small pennate diatom abundance (surface waters)	+19.78 cells mL^{-1}	+494
Large pennate diatom abundance (surface waters)	+0.58 cells mL^{-1}	+5
Silicoflagellate abundance (surface waters)	+0.81 cells mL^{-1}	+877
Dinoflagellate abundance (surface waters)	+0.2 cells mL^{-1}	+8
E. hux coccolith:coccosphere ratio (surface waters)	−15	−39
E. hux coccosphere abundance (surface waters)	+25.87 cells mL^{-1}	+309
E. hux coccolith abundance (surface waters)	+482 liths mL^{-1}	+159

[a] Change is not statistically significant – see text for details.

maximum by the storm (Fig. 12) argues against significant subsurface production.

From studies in the Sargasso Sea it has also been shown that the biological response to storms can vary enormously depending upon whether there is rapid destratification/stratification following a single storm event or continuous mixing following multiple storm events. In the former case a doubling of euphotic zone chlorophyll and bSi concentrations, rapid succession of phytoplankton types and increased export fluxes were observed 1–4 days after the storm (Krause et al., 2009; Lomas et al., 2009a, 2009b; Maiti et al., 2009). In the latter case integrated chlorophyll concentrations increased slowly over 8–9 days, there was no significant change in integrated bSi concentrations but bSi export fluxes doubled, and there was no obvious succession of phytoplankton types (Krause et al., 2009; Lomas et al., 2009a, 2009b).

Our results appear qualitatively similar to those following slow continuous mixing rather than following a shorter finite period of mixing despite the storm itself being an isolated event. One possible explanation for this lies in the interaction of post-storm inertial currents with surface wind stress which when aligned lead to enhanced shear instabilities at the pycnocline and temporarily enhanced turbulence (Pollard, 1980; Rippeth et al., 2009; Rumyantseva et al., 2015). This process has been shown to increase turbulent nutrient supply by an order of magnitude (Rippeth et al., 2009) and in relation to this particular storm nutrient fluxes were 25 times higher than background levels during post-storm alignment periods (Rumyantseva et al., 2015). It is not improbable therefore that these short-lived periods of inertial current-wind stress alignment provided additional mixing that impacted phytoplankton community dynamics and nutrient distributions.

4.3. Ballast minerals and relevance to export fluxes

A number of studies have suggested that export fluxes can be significantly enhanced in the aftermath of a storm (Koeve et al., 2002; Lomas et al., 2009b). Given the close association between cyclones and autumn blooms, such export fluxes may be mistaken for autumn bloom export pulses. Export fluxes were not measured in this study but possible impacts on export fluxes were assessed via examination of the relationships between bSi, PIC and POC. Although bSi and PIC were both positively correlated with POC, bSi had the stronger relationship indicating that siliceous organisms (e.g. diatoms, silicoflagellates) were likely the dominant source of POC in the surface ocean (Fig. 17). On average diatoms represented 66% of the microplankton size class in the upper 50 m (Section 3.5.3) but as microplankton represented only ~20% of the phytoplankton community (Fig. 15) this would imply that diatoms retained a disproportionate influence over potential POC export fluxes. The ratio of the ballast minerals PIC:bSi was not strongly correlated with POC (Fig. 17) and the inverse relationship reported by Balch et al. (2010) was not evident, possibly due to the temperate latitude of our study site versus the lower latitude focus of Balch et al. (2010).

Spearman-rank correlations between bSi, FUC, PIC and HEX against various environmental variables are shown in Table 10 for surface underway and profile datasets and compared to recent similar analyses for the northeast Atlantic Ocean. In the underway data bSi was positively and significantly correlated with POC (Rs = 0.68) and PON (Rs = 0.67). PIC was correlated with POC (Rs = 0.44) and PON (Rs = 0.43) but the correlations were weaker than for bSi. PIC was significantly but weakly correlated with HEX in underway data (Rs = 0.26), but was not correlated in the profile data. This discrepancy was previously noted by Gibb et al. (2001) who suggested that the decoupling between PIC and HEX could be due to the presence of *Phaeocystis*, a suggestion in keeping with known distributions of *Phaeocystis* in the North Atlantic (Vogt et al., 2012). FUC and bSi were weakly correlated in underway data (Rs = 0.47) and not correlated in the profile data. Finally we note that FUC and HEX were significantly and strongly correlated in both underway and profile data indicating the co-occurrence of diatoms and prymnesiophytes, an observation supported by the other datasets presented here. To our knowledge only Gibb et al. (2001) and Leblanc et al. (2009) have undertaken similar correlation analyses in the northeast Atlantic with both studies being conducted in June/July (also shown in Table 10). Similar correlations are reported by these studies, which compare favorably to our results but note that the results from Gibb et al. (2001) come from underway observations whilst those from Leblanc et al. (2009) come from profile data.

To infer export fluxes we examined chlorophyll fluorescence profiles over the upper 200 m for any indication of higher chlorophyll fluorescence at depth following the storm, which would be indicative of the convective export of fresh organic matter (Koeve et al., 2002). As is evident from Fig. 12 the largest changes occurred between 40 and 80 m depth in response to the deepening of the mixed layer and there is some suggestion of a downward

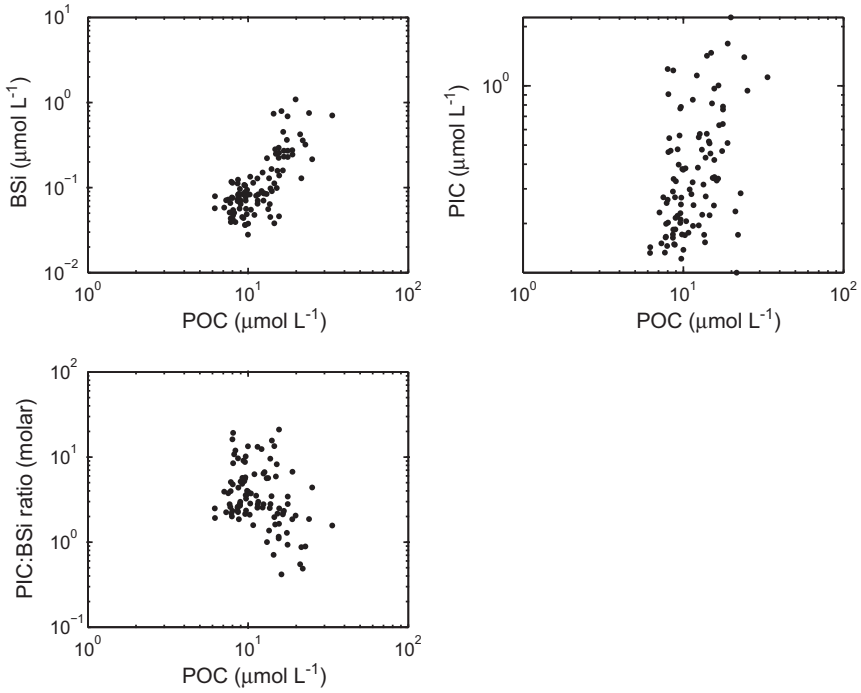

Fig. 17. Relationships between ballast minerals and organic carbon including (a) biogenic silica (bSi) and particulate organic carbon, (b) particulate inorganic carbon (PIC) and particulate organic carbon, and (c) the PIC:bSi ratio and particulate organic carbon.

Table 10
Spearman-rank correlation coefficients (r_s) between key diatom and coccolithophore pigment and particulate pools and nutrients and other pigments and particulate pools. Non-significant correlations are indicated by ns, whilst significant correlations ($p < 0.01$) are further sub-divided into weak ($r_s < 0.5$) and strong ($r_s > 0.5$; bold font) groups. Included are results from similar assessments conducted by Leblanc et al. (2009) and Gibb et al. (2001).

	Si	NO_3	PO_4	Fuco	HEX	POC	PON	PIC	bSi	TCHLa
Underway										
bSi	0.4883	ns	ns	0.4691	**0.5357**	**0.6754**	**0.6694**	0.3899	–	0.4157
Fuco	0.3403	ns	ns	–	**0.7433**	0.449	**0.5219**	0.3566	0.4691	**0.6487**
PIC	**0.5747**	ns	ns	0.3566	0.2638	0.4445	0.4268	–	0.3899	0.3956
HEX	0.2886	ns	ns	**0.7433**	–	0.4419	**0.5183**	0.2638	**0.5357**	**0.7578**
Profile										
bSi	ns	ns	ns	ns	ns	ns	ns	0.335	–	ns
Fuco	ns	ns	ns	–	**0.7754**	ns	ns	ns	ns	ns
PIC	ns	ns	ns	ns	ns	ns	0.3016	–	0.335	ns
HEX	−0.373	ns	ns	**0.7754**	–	ns	0.3927	ns	ns	**0.5952**
Leblanc et al. (2009)										
bSi	−0.343	ns	ns	**0.599**	0.129	ns	ns	ns	–	ns
Fuco	**−0.684**	**−0.545**	0.478	–	**0.876**	**0.86**	**0.838**	ns	**0.599**	**0.904**
PIC	ns	ns	ns	ns	ns	ns	ns	–	ns	ns
HEX	**−0.818**	**−0.728**	**−0.677**	**0.876**	–	**0.777**	**0.827**	ns	ns	**0.949**
Gibb et al. (2001)										
bSi	–	–	–	**0.71**	–	–	–	–	–	–
Fuco	–	–	–	–	–	–	–	–	**0.71**	–
PIC	–	–	–	–	0.49	–	–	–	–	–
HEX	–	–	–	–	–	–	–	0.49	–	–

movement of chlorophyll. There is however no indication of elevated chlorophyll fluorescence below 100 m after the storm when typically <1% of integrated chlorophyll fluorescence was located deeper than 100 m. We conclude therefore that there is no evidence of an export pulse in the 100–200 m depth range in the immediate aftermath of the storm.

4.4. Consequences

Based on a conservative post-storm increase of 20 mmol NO_3^- m^{-2}, Rumyantseva et al. (2015) estimated that this autumn storm supplied between 2.5% and 5% of the annual convective NO_3^- supply, making this storm quantitatively important for annual nutrient budgets. However, the surprising conclusion from our complementary study is that there was no obvious resulting biological impact on productivity despite low and limiting nutrient concentrations in surface waters before the storm being replaced with nutrient replete conditions thereafter. There clearly were biological changes, including the erosion of a subsurface chlorophyll maximum due to mixing, the appearance of silicoflagellates, an increase in small pennate diatom abundance and changes in the ratios of some particulate pools but there was no evidence of a significant increase in integrated chlorophyll or particulate biomass concentrations. We have been unable to firmly ascertain whether

there was an increase in the export of material to depth following the storm but our qualitative examination of chlorophyll fluorescence profiles suggests not.

Though we consider the post-storm oscillations in surface nutrient concentrations to be due to spatiotemporal variability (and possibly inertial currents) it is instructive to consider them in the context of biological utilization as a potential measure of productivity rates. We therefore calculated nutrient draw down rates based on the decrease in nutrient concentrations between days 272 (post-storm maximum) and day 274 (post-storm minimum) (Fig. 8). Over this 2-day period surface nutrient concentrations decreased by 0.38 μmol L^{-1} for NO_3^-, 0.15 μmol L^{-1} for $Si(OH)_4$ and 0.06 μmol L^{-1} for PO_4^{3-} equating to rates of 0.19 mmol m^{-3} d^{-1} for NO_3^-, 0.08 mmol m^{-3} d^{-1} for $Si(OH)_4$ and 0.03 mmol m^{-3} d^{-1} for PO_4^{3-}. Potential integrated rates are sensitive to the choice of mixed layer depth, which was deepening at this time from ~40 m to >60 m (Table 2) and to the assumption of a constant uptake rate with depth, but for a mixed layer of 50 m the approximate daily rates would be 9.5 mmol NO_3^- m^{-2} d^{-1}, 4 mmol $Si(OH)_4$ m^{-2} d^{-1} and 1.5 mmol PO_4^{3-} m^{-2} d^{-1}. Literature estimates of NO_3^- uptake measurements conducted between February and September range from 0.2 to 13.64 mmol m^{-2} d^{-1} (Bury et al., 2001; Donald et al., 2001; Fernandez et al., 2005; Painter et al., 2010b) indicating that our potential integrated rates are towards the upper end of previous observations. In fact they are larger than would be considered typical for the summer period and this result most likely occurred because of the assumption of a constant uptake rate with depth, which is unlikely (Painter et al., 2010b). Though there were no significant post-storm changes to the integrated biomass inventories we revisit the rapid changes observed over days 272–274 (Section 3.5.2). Integrated NO_3^- and PON concentrations show a reduction/increase with time respectively (Table 2), supporting both biological utilization of NO_3^- throughout the water column and the subsequent partitioning of this NO_3^- into new PON biomass. Consequently, there is tentative evidence showing productivity rates (or more accurately nutrient uptake rates) may have been enhanced for a 2 day period after the storm. The same cannot be said of carbon fixation rates as POC concentrations did not increase thus enhanced productivity cannot be substantiated. Subsequently we cannot definitively rule out the possibility that some of the oscillation seen in surface nutrient concentrations was the result of phytoplankton uptake.

A further consequence of this study concerns the growing trend for assessing storm impacts on ocean productivity levels from satellite measurements of chlorophyll fluorescence. Specifically such applications need to consider whether an observed increase in surface chlorophyll is the result of vertical mixing or of in situ growth. The former case is essentially neutral in its impact on productivity as pre-existing features are vertically relocated towards the surface whilst the latter case will have a positive impact on productivity rates. Debate over the biological impact of cyclones therefore is unlikely to reach consensus until additional in situ information can be obtained to complement the satellite record. This may be achievable through appropriate use of float and glider technologies (e.g. Perry et al., 2008; Hemsley et al., 2015). It is also evident from this study that there are likely to be many complex impacts within the phytoplankton community that cannot be easily resolved via remote platforms or through traditional sampling techniques that may be slow or weather dependent. Future in situ sampling efforts should therefore carefully consider sampling resolution.

Finally, one aspect that we can only speculate over is the role of grazing. During the late summer it is argued that microzooplankton herbivory broadly matches daily productivity rates leading to a steady-state system in the northeast Atlantic (Colebrook, 1984, 1986; Burkill et al., 1993). A deepening of the mixed layer in autumn, either due to storm activity or convective cooling is argued to dilute the concentrations of phytoplankton and grazers reducing the chance of grazer–prey interaction and thereby reducing grazing rates (Behrenfeld and Boss, 2014). Our dataset does not allow for the investigation of grazing rates but one could argue that with relatively constant integrated biomass levels pre-and post-storm that grazing rates were largely unchanged. Whether there were slower, longer-term impacts on herbivory however remains unclear.

5. Conclusions

The classical picture of in situ phytoplankton growth following the deepening of the mixed layer and the resupply of nutrients to the mixed layer in autumn leading to an autumn bloom is not consistent with the observations we report here. The passage of an unusually intense autumn storm through the temperate northeast Atlantic induced significant vertical mixing eroding an established subsurface chlorophyll maximum, whilst simultaneously resupplying surface waters with nutrients. A subsequent 50% increase in surface chlorophyll concentrations was not indicative of changes in column integrated chlorophyll concentrations, which were unchanged. This suggests that the surface increase in chlorophyll concentrations was due to the vertical redistribution of the subsurface chlorophyll maximum and not due to in situ growth by the phytoplankton community. Nanoplankton, particularly prymnesiophytes, dominated the community (~75%) but significant perturbations in all plankton size classes were observed over different time scales in response to wind-forcing. No significant changes were found in any particulate biomass pool suggesting negligible changes to productivity rates following nutrient enrichment but there is tentative evidence of enhanced nutrient uptake rates leading to subtle changes in PON pools. Imprinted onto these changes were slower seasonal changes in particulate pool concentrations and particulate ratios indicating that the biological system was winding down, most likely in response to seasonal changes in irradiance.

Acknowledgments

We thank Danielle Waters and Ben Barton for their assistance at sea, John Gittins, Richard Pearce and Mathew Cooper (all University of Southampton) for their assistance with analytical analyses and David Johns (Sir Alister Hardy Foundation for Ocean Science) for provision of Continuous Plankton Recorder data. MODIS Aqua data obtained from NASA via the Ocean Color webpage (http://oceancolor.gsfc.nasa.gov). SCP also thanks the organisers and participants of the 3rd International Phytoplankton Identification workshop jointly held at the Marine Biological Association/Sir Alister Hardy Foundation for Ocean Science in Plymouth, UK, July 2014. Cruise D381 was conducted in support of the OSMOSIS (Ocean Surface Mixing, Ocean Sub-mesoscale Interaction Study) project funded by NERC (Natural Environment Research Council) grant NE/1020083/1. Additional funding was provided by the EU Framework 7 project EuroBASIN (FP7-ENV-2010) and NERC National Capability.

Appendix A

A.1. Further details of the coccolithophore community

One rationale for the detailed examination of the phytoplankton community via Scanning Electron Microscopy (SEM) in this study was to provide support for trends in the pigment data. This task however was complicated by significant variation in the contribu-

tions of key species (e.g. coccolithophores), limitations of this analytical approach for larger species (e.g. dinoflagellates, diatoms) and restriction to a single depth level. Nevertheless whilst the SEM data are useful for disentangling the pigment and other biogeochemical data they also provided a wealth of data on the coccolithophore community of the Northeast Atlantic in autumn. In addition to the main aspects of the coccolithophore community described in the text we provide here some additional information on station-to-station variability and coccolith:coccosphere ratios for the dominant species. In particular, in Fig. A1 we present a summary of the coccolithophore community showing the proportion of the community represented by enumerated species. As described in the main text species contributing <5% to the total are grouped together under the heading 'other'.

The most abundant coccolithophore was *Emiliania huxleyi*. *E. huxleyi* coccosphere abundance ranged from 4.35 to 52.37 coccospheres mL^{-1} (Table 4), concentrations far below those considered indicative of bloom conditions (e.g. 5000–10,000 coccospheres mL^{-1}; Fernandez et al. (1993)) but comparable to estimates reported from the Bay of Biscay in winter by Daniels et al. (2012) (10.9 coccospheres mL^{-1}), or from the northeast Atlantic in mid summer by Poulton et al. (2014) (19.4–68.4 coccospheres mL^{-1}). There is a suggestion in the data that *E. huxleyi* coccosphere abundance may have been consistently higher (>20 coccospheres mL^{-1}) from station 18 onwards but variability at earlier stations and the low coccosphere abundances at stations 12 and 16 separated by the extremely high abundance at station 14 make it difficult to derive a direct causal link. Due to this variability and also due to high abundances at station 14 the mean coccosphere abundance for pre-storm stations 6–12 (8.36 coccospheres mL^{-1}) was not significantly lower than the mean abundance for post-storm stations 14–21 (29.92 coccospheres mL^{-1}) (*t*-test, $p > 0.05$). Removal of station 14 from the statistical test however resulted in a statistically significant difference in mean coccosphere abundance (8.36 coccospheres mL^{-1} vs 34.23 coccospheres mL^{-1}, *t*-test, $p < 0.01$) for those stations sampled pre- and post-storm suggesting that there was a real post-storm change in abundance.

We report in Table 4 loose *E. huxleyi* coccolith abundances and the coccolith:coccosphere ratio for each station. The abundance of loose coccoliths broadly mirrored the coccosphere abundance and varied from 187 liths mL^{-1} (station 12) to 1155 liths mL^{-1} (station 14). Coccolith abundance appears to have been higher at stations earlier (stations 1–4) and later (stations 14–21) in the cruise with a mid-cruise minimum (stations 6–12). Consequently, there was a statistically significant increase in the mean pre-storm and post-storm coccolith abundance (*t*-test, $p < 0.01$), a finding that was not altered by the inclusion/exclusion of station 14. In isolation this observation could indicate that wind-driven turbulent mixing broke apart *E. huxleyi* coccospheres but the simultaneous increase in coccosphere abundance suggests that entrainment from depth and/or spatial patchiness may also have contributed to the post-storm increase in coccolith abundance.

Despite the variation in individual coccosphere and coccolith abundances between stations (Fig. A1) the *E. huxleyi* coccolith:coccosphere ratio exhibited two quasi-stable periods but these periods were not necessarily indicative of pre- and post-storm sampling. At stations 1–10 the coccolith:coccosphere ratio was >30 (mean 38.1 ± 10; range 32–50), but for stations 12–21 (excluding station 16) the ratio was <30 (mean 23.07 ± 2.05; range 19–26). This difference was only significant (two-sample *t*-test, $p < 0.05$) following exclusion of station 16 from the statistical test. Station 16 had the highest coccolith:coccosphere ratio of 73:1 which was driven by low coccosphere abundance and strict application of the *t*-test to the data did not find a significant difference in the coccolith:coccosphere ratio between stations 1–10 and 12–21. Most interestingly the step-like change in the coccolith:coccosphere ratio did not cleanly separate pre-storm and post-storm stations. Although the coccolith:coccosphere ratio at station 12 was more similar to the ratios encountered at later stations it was actually

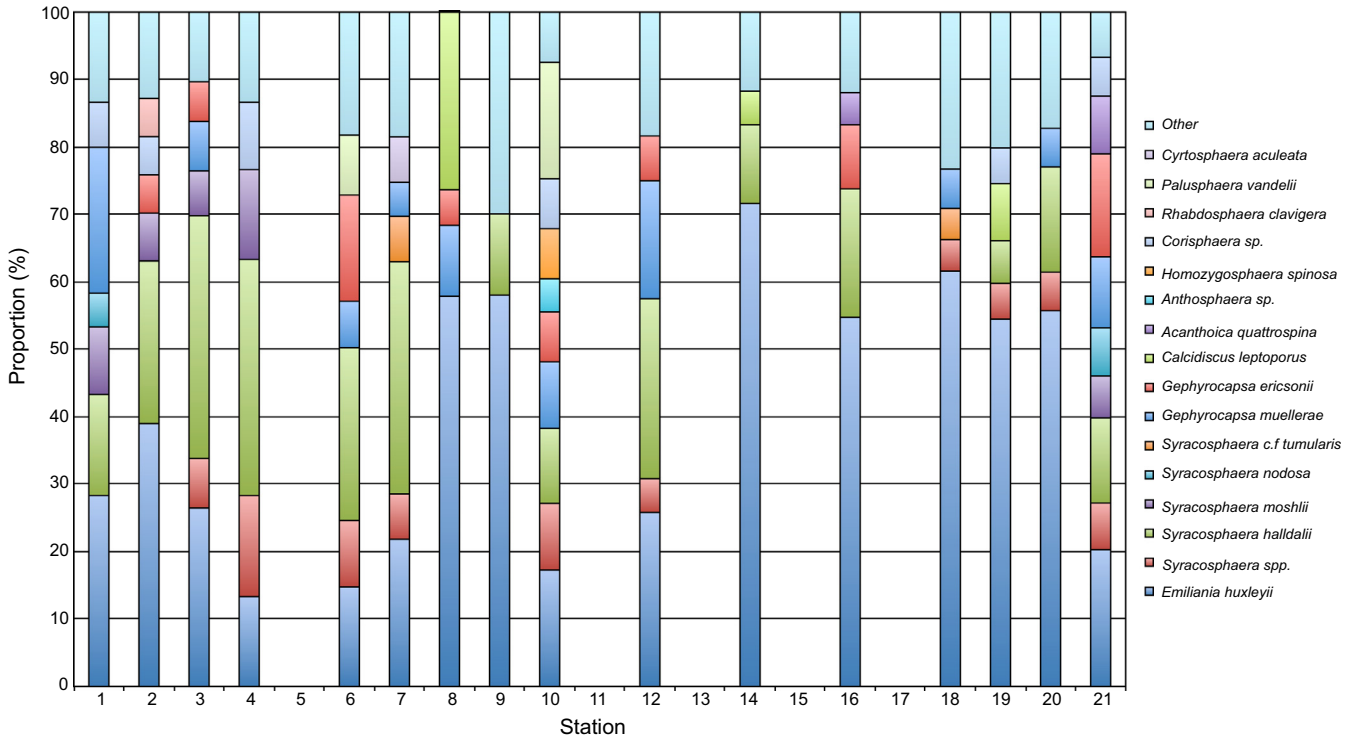

Fig. A1. Coccolithophore species contribution to total coccolithophore abundance in surface water samples (4–13 m) at the sampled stations (Fig. 1). Note the significant station-to-station variability that appears to characterise the observations.

sampled prior to the storm suggesting that the cause of the shift in the coccolith:coccosphere ratio may not be fully attributable to the impact of wind-mixing.

The lack of similar consistent changes in either coccolith or coccosphere abundances implies that variation in both must be considered in attempts to unravel the presence of two quasi-stable periods in the coccolith:coccosphere ratio. The mean coccosphere abundance for stations 1–10 was 10.1 ± 6.7 coccospheres mL^{-1}, whereas the mean coccolith abundance was 406 ± 249 coccolith mL^{-1}. In contrast, at stations 12–21 the mean coccosphere abundance was 27.0 ± 15.0 coccospheres mL^{-1} and the coccolith abundance 674 ± 292 coccolith mL^{-1}. The reduction in the coccolith:coccosphere ratio is therefore more likely to have been driven by an increase in coccosphere abundance, a finding consistent with the pre- and post-storm change in coccosphere abundance described above.

Similarly detailed examination of *Syracosphaera halldalii*, *S. moshlii*, *Gephyrocapsa muellerae*, *G. ericsonii* and *Calcidiscus leptoporus* abundances, as dominant species in our study site, did not find any similar patterns to those described above for *E. huxleyi* (Table 4). High inter-station variability in coccosphere or coccolith abundance (Fig. A1) for these species meant that a simple pre- and post-storm classification was inappropriate. The ratio of *S. halldalii* coccoliths:coccospheres perhaps contained the most comparable temporal pattern with the ratio for stations 1–7 (mean 19 cells mL^{-1}) generally lower than found at station 8–21 (mean 52 cells mL^{-1}) but this clearly could not be related to atmospheric forcing and suggests that other environmental factors must be considered.

References

Aiken, J., Bale, A.J., 2000. An introduction to the Atlantic Meridional Transect (AMT) Programme. Progress in Oceanography 45 (3–4), 251–256.

Aiken, J., Pradhan, Y., Barlow, R., Lavender, S., Poulton, A., Holligan, P., Hardman-Mountford, N., 2009. Phytoplankton pigments and functional types in the Atlantic Ocean: a decadal assessment, 1995–2005. Deep Sea Research Part II 56, 899–917.

Babin, S.M., Carton, J.A., Dickey, T.D., Wiggert, J.D., 2004. Satellite evidence of hurricane-induced phytoplankton blooms in an oceanic desert. Journal of Geophysical Research 109, C03043. http://dx.doi.org/10.1029/2003JC001938.

Bach, L.T., Riebesell, U., Sett, S., Febiri, S., Rzepka, P., Schulz, K.G., 2012. An approach for particle sinking velocity measurements in the 3–400 μm size range and considerations on the effect of temperature on sinking rates. Marine Biology 159, 1853–1864.

Balch, W.M., Bowler, B.C., Drapeau, D.T., Poulton, A.J., Holligan, P.M., 2010. Biominerals and the vertical flux of particulate organic carbon from the surface ocean. Geophysical Research Letters 37, L22605. http://dx.doi.org/10.1029/2010GL044640.

Balch, W.M., Gordon, H.R., Bowler, B.C., Drapeau, D.T., Booth, E.S., 2005. Calcium carbonate measurements in the surface global ocean based on Moderate-Resolution Imaging Spectroradiometer data. Journal of Geophysical Research 110, C07001. http://dx.doi.org/10.1029/2004JC002560.

Banse, K., 1994. Uptake of inorganic carbon and nitrate by marine plankton and the Redfield ratio. Global Biogeochemical Cycles 8 (1), 81–84.

Barlow, R.G., Cummings, D.G., Gibb, S.W., 1997. Improved resolution of mono- and divinyl chlorophylls *a* and *b* and zeaxanthin and lutein in phytoplankton extracts using reverse phase C-8 HPLC. Marine Ecology Progress Series 161, 303–307.

Barlow, R.G., Aiken, J., Moore, G.F., Holligan, P.M., Lavender, S., 2004. Pigment adaptations in surface phytoplankton along the eastern boundary of the Atlantic Ocean. Marine Ecology Progress Series 281, 13–26.

Barlow, R.G., Aiken, J., Holligan, P.M., Cummings, D.G., Maritorena, S., Hooker, S., 2002. Phytoplankton pigment and absorption characteristics along meridional transects in the Atlantic Ocean. Deep Sea Research I 47, 637–660.

Barlow, R.G., Mantoura, R.F.C., Gough, M.A., Fileman, T.W., 1993a. Phaeopigment distribution during the 1990 spring bloom in the northeastern Atlantic. Deep Sea Research I 40 (11/12), 2229–2242.

Barlow, R.G., Mantoura, R.F.C., Gough, M.A., Fileman, T.W., 1993b. Pigment signatures of the phytoplankton composition in the northeastern Atlantic during the 1990 spring bloom. Deep Sea Research Part II 40 (1/2), 459–477.

Batten, S.D., Clark, R., Flinkman, J., Hays, G., John, E., John, A.W.G., Jonas, T., Lindley, J. A., Stevens, D.P., Walne, A., 2003. CPR sampling: the technical background, materials and methods, consistency and comparability. Progress in Oceanography 58, 193–215.

Beaugrand, G., 2004. Continuous plankton records: plankton atlas of the North Atlantic Ocean (1958–1999). 1. Introduction and methodology. Marine Ecology Progress Series Supplement, 3–10.

Behrenfeld, M.J., 2010. Abandoning Sverdrup's Critical Depth Hypothesis on phytoplankton blooms. Ecology 91 (4), 977–989.

Behrenfeld, M.J., Boss, E.S., 2014. Resurrecting the ecological underpinnings of ocean plankton blooms. Annual Review of Marine Science 6, 167–194.

Bode, A., Varela, M., Casas, B., Gonzalez, N., 2002. Intrusions of eastern North Atlantic central waters and phytoplankton in the north and northwestern Iberian shelf during spring. Journal of Marine Systems 36, 197–218.

Burkill, P.H., Edwards, E.S., John, A.W.G., Sleigh, M.A., 1993. Microzooplankton and their herbivorous activity in the northeastern Atlantic Ocean. Deep Sea Research Part II 40 (1/2), 479–493.

Bury, S.J., Boyd, P.W., Preston, T., Savidge, G., Owens, N.J.P., 2001. Size-fractionated primary production and nitrogen uptake during a North Atlantic phytoplankton bloom: implications for carbon export estimates. Deep Sea Research Part I 48 (3), 689–720.

Castro, C.G., Perez, F.F., Holley, S.E., Rios, A.F., 1998. Chemical characterisation and modelling of water masses in the Northeast Atlantic. Progress in Oceanography 41, 249–279.

Chen, Y., Tang, D.L., 2012. Eddy-feature phytoplankton bloom induced by a tropical cyclone in the South China Sea. International Journal of Remote Sensing 33 (23), 7444–7457. http://dx.doi.org/10.1080/01431161.2012.685976.

Colebrook, J.M., 1984. Continuous plankton records: relationships between species of phytoplankton and zooplankton in the seasonal cycle. Marine Biology 83, 313–323.

Colebrook, J.M., 1986. Continuous plankton records: the distribution and standing crop of the plankton of the shelf and ocean to the west of the British Isles. Proceedings of the Royal Society of Edinburgh 88B, 221–237.

Colebrook, J.M., Robinson, G.A., 1961. The seasonal cycle of the plankton in the North Sea and the North-Eastern Atlantic. Journal Conseil International pour l'Exploration de la Mer 26 (2), 156–165.

Compo, G.P., Whitaker, J.S., Sardeshmukh, P.D., Matsui, N., Allan, R.J., Yin, X., Gleason Jr., B.E., Vose, R.S., Rutledge, G., Bessemoulin, P., Brönnimann, S., Brunet, M., Crouthamel, R.I., Grant, A.N., Groisman, P.Y., Jones, P.D., Kruk, M.C., Kruger, A.C., Marshall, G.J., Maugeri, M., Mok, H.Y., Nordli, Ø., Ross, T.F., Trigo, R.M., Wang, X. L., Woodruff, S.D., Worley, S.J., 2011. The twentieth century reanalysis project. Quarterly Journal of the Royal Meteorological Society 137, 1–28. http://dx.doi.org/10.1002/qj.1776.

Corlett, J., 1953. Net phytoplankton at Ocean Weather Stations "I" and "J". Journal du Conseil International pour l'Exploration de la Mer 19, 178–190.

Cros, L., Fortuno, J.-M., 2002. Atlas of northwestern Mediterranean coccolithophores. Scientia Marina 66 (S1), 1–186.

Cushing, D.H., 1959. The seasonal variation in oceanic production as a problem in population dynamics. Journal du Conseil International pour l'Exploration de la Mer 24, 455–464.

Daniels, C.J., Tyrrell, T., Poulton, A.J., Pettit, L., 2012. The influence of lithogenic material on particulate inorganic carbon measurements of coccolithophores in the Bay of Biscay. Limnology and Oceanography 57 (1), 145–153.

Dodge, J.D., 1985. Atlas of Dinoflagellates: A Scanning Electron Microscope Survey. Farrand Press, London, 119 pp.

Donald, K.M., Joint, I., Rees, A.P., Woodward, E.M.S., Savidge, G., 2001. Uptake of carbon, nitrogen and phosphorus by phytoplankton along the 20 degrees W meridian in the NE Atlantic between 57.5 degrees N and 37 degrees N. Deep-Sea Research Part II 48 (4–5), 873–897.

Ducklow, H.W., Harris, R.P., 1993. Introduction to the JGOFS North Atlantic bloom experiment. Deep Sea Research Part II 40 (1/2), 1–8.

Dugenne, M., Thyssen, M., Nerini, D., Mante, C., Poggiale, J-C, Garcia, N., Garcia, F., Grégori, G.J., 2014. Consequence of a sudden wind event on the dynamics of a coastal phytoplankton community: an insight into specific population growth rates using a single cell high frequency approach. Frontiers in Microbiology, 5 Article 485.

Fernandez, C., Raimbault, P., Garcia, N., Rimmelin, P., Caniaux, G., 2005. An estimation of annual new production and carbon fluxes in the northeast Atlantic Ocean during 2001. Journal of Geophysical Research 110, C07S13. http://dx.doi.org/10.1029/2004JC002616.

Fernandez, E., Boyd, P., Holligan, P.M., Harbour, D.S., 1993. Production of organic and inorganic carbon within a large-scale coccolithophore bloom in the northeast Atlantic Ocean. Marine Ecology Progress Series 97, 271–285.

Foltz, G.R., Balaguru, K., Leung, L.R., 2015. A reassessment of the integrated impact of tropical cyclones on surface chlorophyll in the western subtropical North Atlantic. Geophysical Research Letters 42, 1158–1164. http://dx.doi.org/10.1002/2015GL063222.

Gibb, S.W., Barlow, R.G., Cummings, D.G., Rees, N.W., Trees, C.C., Holligan, P., Suggett, D., 2000. Surface phytoplankton pigment distributions in the Atlantic Ocean: an assessment of basin scale variability between 50°N and 50°S. Progress in Oceanography 45, 339–368.

Gibb, S.W., Cummings, D.G., Irigoien, X., Barlow, R.G., Fauzi, R., Mantoura, C., 2001. Phytoplankton pigment chemataxonomy of the northeastern Atlantic. Deep Sea Research Part II 48, 795–823.

Goericke, R., Repeta, D.J., 1992. The pigments of *Prochlorococcus marinus*: the presence of divinyl chlorophyll a and b in a marine procaryote. Limnology and Oceanography 37 (2), 425–433.

Green, D.R.H., Cooper, M.J., German, C.R., Wilson, P.A., 2003. Optimization of an inductively coupled plasma-optical emission spectrometry method for the rapid determination of high-precision Mg/Ca and Sr/Ca in foraminiferal calcite.

Geochemistry, Geophysics, Geosystems 4 (6), 8404. http://dx.doi.org/10.1029/2002GC000488.
Hanshaw, M.N., Lozier, M.S., Palter, J.B., 2008. Integrated impact of tropical cyclones on sea surface chlorophyll in the North Atlantic. Geophysical Research Letters 35, L01601. http://dx.doi.org/10.1029/2007GL031862.
Hartman, S.E., Lampitt, R.S., Larkin, K.E., Pagnani, M., Campbell, J., Gkritzalis, T., Jiang, Z.-P., Pebody, C.A., Ruhl, H.A., Gooday, A.J., Bett, B.J., Bett, D.S.M., Provost, P., McLachlan, R., Turton, J.D., Lankester, S., 2012. The Porcupine Abyssal Plain fixed-point sustained observatory (PAP-SO): variations and trends from the Northeast Atlantic fixed-point time-series. ICES Journal of Marine Science 69 (5), 776–783.
Harvey, H.W., Cooper, L.H.N., Lebour, M.V., Russell, F.S., 1935. Plankton production and it control. Journal of the Marine Biological Association of the UK 20, 407–441.
Hasle, G.R., Syvertsen, E.E., 1997. Marine diatoms. In: Tomas, C.R. (Ed.), Identifying Marine Phytoplankton. Academic Press, San Diego, pp. 5–385.
Heimdal, B.R., 1997. Modern coccolithophores. In: Tomas, C.R. (Ed.), Identifying Marine Phytoplankton. Academic Press, San Diego, pp. 731–831.
Hemsley, V.S., Smyth, T.J., Martin, A.P., Frajka-Williams, E., Thompson, A.F., Damerell, G., Painter, S.C., 2015. Estimating oceanic primary production using vertical irradiance and chlorophyll profiles from ocean gliders in the North Atlantic. Environmental Science & Technology 49, 11612–11621.
Higgins, H.W., Wright, S.W., Schluter, L., 2011. Quantitative interpretation of chemotaxonomic pigment data. In: Roy, S., Llewellyn, C.A., Egeland, E.S., Johnsen, G. (Eds.), Phytoplankton Pigments: Characterization, Chemotaxonomy and Applications in Oceanography. Cambridge University Press, pp. 257–313.
Hulme, M., Jones, P.D., 1991. Temperatures and windiness over the United Kingdom during the winters of 1988/89 and 1989/90 compared with previous years. Weather 46, 126–136. http://dx.doi.org/10.1002/j.1477-8696.1991.tb05724.x.
Jeffrey, S.W., Wright, S.W., Zapata, M., 2011. Microalgal classes and their signature pigments. In: Roy, Suzanne, Llewellyn, C.A., Einar Skarstad, Egeland, Johnsen, G. (Eds.), Phytoplankton Pigments: Characterization, Chemotaxonomy and Applications in Oceanography. Cambridge University Press, New York, USA, pp. 3–77.
Jenkinson, A.F., Collison, F.P., 1977. An Initial Climatology of Gales over the North Sea. Synoptic Climatology Branch Memorandum No. 62, Meteorological Office, Bracknell.
Johns, D., 2014. Monthly Averaged Data for Phytoplankton Abundance (E5 Standard Area) 2000–2012 as Recorded by the Continuous Plankton Recorder. Sir Alister Hardy Foundation for Ocean Science, Plymouth, UK, http://dx.doi.org/10.7487/2014.27.1.7.
Joint, I., Pomroy, A., Savidge, G., Boyd, P., 1993. Size-fractionated primary productivity in the northeast Atlantic in May–July 1989. Deep Sea Research Part II 40 (1/2), 423–440.
Jones, P.D., Harpham, C., Briffa, K.R., 2013. Lamb weather types derived from reanalysis products. International Journal of Climatology 33, 1129–1139. http://dx.doi.org/10.1002/joc.3498.
Jones, P.D., Hulme, M., Briffa, K.R., 1993. A comparison of Lamb circulation types with an objective classification scheme. International Journal of Climatology 13, 655–663.
Kahler, P., Koeve, W., 2001. Marine dissolved organic matter: can its C:N ratio explain carbon overconsumption? Deep Sea Research I 48, 49–62.
Kalnay, E., Kanamitsu, M., Kistler, R., Collins, W., Deaven, D., Gandin, L., Iredell, M., Saha, S., White, G., Wollen, J., Zhu, Y., Chelliah, M., Ebisuzaki, W., Higgins, W., Janowiak, J., Mo, K.C., Ropelewski, C., Wang, J., Leetmaa, A., Reynolds, R., Jenne, R., Joseph, D., 1996. The NCEP/NCAR 40-year reanalysis project. Bulletin of the American Meteorological Society 77, 437–471.
Karayanni, H., Christaki, U., Wembeke, F.V., Denis, M., Moutin, T., 2005. Influence of ciliated protozoa and heterotrophic nanoflagellates on the fate of primary production in the northeast Atlantic Ocean. Journal of Geophysical Research 110, C07S15. http://dx.doi.org/10.1029/2004JC002602.
Kirk, J.T.O., 2010. Light and Photosynthesis in Aquatic Ecosystems. Cambridge University Press, Cambridge, 64 pp.
Kirkwood, D.S., 1996. Nutrients: practical notes on their determination in seawater. ICES Techniques in Marine Environmental Sciences Report 17. Copenhagen, International Council for the Exploration of the Seas, 25pp.
Klass, C., Archer, D.E., 2002. Association of sinking organic matter with various types of mineral ballast in the deep sea: implications for the rain ratio. Global Biogeochemical Cycles 16 (4), 1116. http://dx.doi.org/10.1029/2001GB001765.
Knutson, T.R., McBride, J.L., Chan, J., Emanuel, K., Holland, G., Landsea, C., Held, I., Kossin, J.P., Srivastava, A.K., Sugi, M., 2010. Tropical cyclones and climate change. Nature Geoscience 3, 157–163. http://dx.doi.org/10.1038/ngeo1779.
Koeve, W., 2002. Upper ocean carbon fluxes in the Atlantic Ocean: the importance of the POC:PIC ratio. Global Biogeochemical Cycles 16 (4), 1056. http://dx.doi.org/10.1029/2001GB001836.
Koeve, W., 2004. Spring bloom carbon to nitrogen ratio of net community production in the temperate N Atlantic. Deep Sea Research Part I 51, 1579–1600.
Koeve, W., 2006. C:N stoichiometry of the biological pump in the North Atlantic: constraints from climatological data. Global Biogeochemical Cycles 20, GB3018. http://dx.doi.org/10.1029/2004GB002407.
Koeve, W., Pollehne, F., Oschlies, A., Zeitzschel, B., 2002. Storm-induced convective export of organic matter during spring in the northeast Atlantic Ocean. Deep Sea Research I 49, 1431–1444.
Körtzinger, A., Koeve, W., Kahler, P., Mintrop, L., 2001. C:N ratios in the mixed layer during the productive season in the northeast Atlantic Ocean. Deep Sea Research Part I 48, 661–688.
Körtzinger, A., Send, U., Lampitt, R.S., Hartman, S., Wallace, D.W.R., Karstensen, J., Villagarcia, M.G., Llinas, O., DeGrandpre, M.D., 2008. The seasonal pCO_2 cycle at 49°N/16.5°W in the northeastern Atlantic Ocean and what it tells us about biological productivity. Journal of Geophysical Research 113, C04020. http://dx.doi.org/10.1029/2007JC004347.
Krause, J.W., Nelson, D.M., Lomas, M.W., 2009. Biogeochemical responses to late-winter storms in the Sargasso Sea, II: increased rates of biogenic silica production and export. Deep Sea Research Part I 56, 861–874.
Lamb, H.H., 1972. British Isles Weather Types and a Register of Daily Sequence of Circulation Patterns. Geophysical Memoir 116, HMSO, London, 85pp.
Leblanc, K., Leynaert, A., Fernandez, I., Rimmelin, P., Moutin, T., Raimbault, P., Ras, J., Queguiner, B., 2005. A seasonal study of diatom dynamics in the North Atlantic during the POMME experiment (2001): evidence for Si limitation of the spring bloom. Journal of Geophysical Research 110, C07S14. http://dx.doi.org/10.1029/2004JC002621.
Leblanc, K., Hare, C.E., Feng, Y., Berg, G.M., DiTullio, G.R., Neely, A., Benner, I., Sprengel, C., Beck, A., Sanudo-Wilhelmy, S.A., Passow, U., Klinck, K., Rowe, J.M., Wilhelm, S.W., Brown, C.W., Hutchins, D.A., 2009. Distribution of calcifying and silicifying phytoplankton in relation to environmental and biogeochemical parameters during the late stages of the 2005 North East Atlantic Spring Bloom. Biogeosciences 6, 2155–2179.
Lebour, M.V., 1925. The Dinoflagellates of Northern Seas. Marine Biological Association of the United Kingdom, Plymouth, 254 pp.
Lebour, M.V., 1930. The Planktonic Diatoms of Northern Seas. Ray Society, 244 pp. (Reprint 1978 Otto Koeltz Science Publishers).
Lessard, E.J., Merico, A., Tyrrell, T., 2005. Nitrate: phosphate ratios and *Emiliania huxleyi* blooms. Limnology and Oceanography 50 (3), 1020–1024.
Lindemann, C., St-John, M.A., 2014. A seasonal diary of phytoplankton in the North Atlantic. Frontiers in Marine Science 1 (37), 31–36.
Lochte, K., Pfannkuche, O., 1987. Cyclonic cold-core eddy in the eastern North Atlantic. II. Nutrients, phytoplankton and bacterioplankton. Marine Ecology Progress Series 39, 153–164.
Lomas, M.W., Lipschultz, F., Nelson, D.M., Krause, J.W., Bates, N.R., 2009a. Biogeochemical responses to late-winter storms in the Sargasso Sea, I: pulses of primary and new production. Deep Sea Research Part I 56, 843–860.
Lomas, M.W., Roberts, N., Lipschultz, F., Krause, J.W., Nelson, D.M., BAtaes, N.R., 2009b. Biogeochemical responses to late-winter storms in the Sargasso Sea, IV. Rapid succession of major phytoplankton groups. Deep Sea Research Part I 56, 892–908.
Longhurst, A., 1995. Seasonal cycles of pelagic production and consumption. Progress in Oceanography 36, 77–167.
Longhurst, A., 1998. Ecological Geography of the Sea. Academic Press, San Diego.
Luo, Y.-W., Doney, S.C., Anderson, L.A., Benavides, M., Bode, A., Bonnet, S., Bostrom, K.H., Bottjer, D., Capone, D.G., Carpenter, E.J., Chen, Y.L., Church, M.J., Dore, J.E., Falcon, L.I., Fernandez, A., Foster, R.A., Furuya, K., Gomez, F., Gundersen, K., Hynes, A.M., Karl, D.M., Kitajima, S., Langlois, R.J., LaRoche, J., Letelier, R.M., Maranon, E., McGillicuddy Jr., D.J., Moisander, P.H., Moore, C.M., Mourino-Carballido, B., Mulholland, M.R., Needoba, J.A., Orcutt, K.M., Poulton, A.J., Raimbault, P., Rees, A.P., Riemann, L., Shiozaki, T., Subramaniam, A., Tyrrell, T., Turk-Kubo, K.A., Varela, M., Villareal, T.A., Webb, E.A., White, A.E., Wu, J., Zehr, J. P., 2012. Database of diazotrophs in global ocean: abundance, biomass and nitrogen fixation rates. Earth System Science Data 4, 47–73.
Mackey, M.D., Mackey, D.J., Higgins, H.W., Jeffrey, S.W., 1996. CHEMTAX – a program for estimating class abundances from chemical markers: application to HPLC measurements of phytoplankton. Marine Ecology Progress Series 144, 265–283.
Mahadevan, A., D'Asaro, E., Lee, C., Perry, M.J., 2012. Eddy-driven stratification initiates North Atlantic spring phytoplankton blooms. Science 337, 54–58.
Maiti, K., Benitez-Nelson, C.R., Lomas, M.W., Krause, J.W., 2009. Biogeochemical responses to late-winter storms in the Sargasso Sea, III – estimates of export production using ^{234}Th:^{238}U disequilibria and sediment traps. Deep Sea Research Part I 56, 875–891.
Maixandeau, A., Lefevre, D., Karayanni, H., Christaki, U., Van Wambeke, F., Thyssen, M., Denis, M., Fernandez, I., Uitz, J., Leblanc, K., Queguiner, B., 2005. Microbial community production, respiration and structure of the microbial foodweb of an ecosystem in the northeastern Atlantic Ocean. Journal of Geophysical Research 110, C07S17. http://dx.doi.org/10.1029/2004JC002694.
Mantoura, R.F.C., Wright, S.W., Jeffrey, S.W., Barlow, R.G., Cummings, D.E., 1997. Filtration and storage of pigments from microalgae. In: Jeffrey, S.W., Mantoura, R.F.C., Wright, S.W. (Eds.), Phytoplankton Pigments in Oceanography. UNESCO Publishing, Paris, pp. 283–305.
Margalef, R., 1969. Composición especifica del fitoplancton de la costa catalano-levantina (Mediterráneo occidental) en 1962–1967. Investigaćion Pesquera 33 (1), 345–380.
Margalef, R., 1978. Life-forms of phytoplankton as survival alternatives in an unstable environment. Oceanologica Acta 1 (4), 493–509.
Martinez, E., Antoine, D., D'Ortenzio, F., de Boyer Montegut, C., 2011. Phytoplankton spring and fall blooms in the North Atlantic in the 1980s and 2000s. Journal of Geophysical Research 116, C11029. http://dx.doi.org/10.1029/2010JC006836.
McIntyre, A., Bé, A.W.H., 1967. Modern coccolithophoridae of the Atlantic Ocean – I. Placoliths and cyrtoliths. Deep Sea Research 14, 561–597.

McQuatters-Gollop, A., Raitsos, D.E., Edwards, M., Attrill, M.J., 2007. Spatial patterns of diatom and dinoflagellate seasonal cycle in the NE Atlantic Ocean. Marine Ecology Progress Series 339, 301–306.

Mojica, K.D.A., van de Poll, W.H., Kehoe, M., Huisman, J., Timmermans, K.R., Buma, A. G.J., van der Woerd, H.J., Hahn-Woernle, L., Dijkstra, H.A., Brussaard, C.P.D., 2015. Phytoplankton community structure in relation to vertical stratification along a north-south gradient in the Northeast Atlantic Ocean. Limnology and Oceanography 60, 1498–1521.

Monterey, G., Levitus, S., 1997. Seasonal Variability of Mixed Layer Depth for the World Ocean. NOAA Atlas NESDIS 14. U.S. Gov Printing Office, Washington, DC, 96pp.

Morozov, E., Kondrik, D., Fedorova, A., Pozdnyakov, D., Tang, D.L., Pettersson, L., 2015. A spaceborne assessment of cyclone impacts on Barents Sea surface temperature and chlorophyll. International Journal of Remote Sensing 36 (7), 1921–1941.

Okada, H., McIntyre, A., 1977. Modern coccolithophores of the Pacific and North Atlantic Oceans. Micropaleontology 23 (1), 1–55.

Painter, S.C., Pidcock, R.E., Allen, J.T., 2010a. A mesoscale eddy driving spatial and temporal heterogeneity in the productivity of the euphotic zone of the northeast Atlantic. Deep Sea Research Part II 57, 1281–1292.

Painter, S.C., Lucas, M.I., Stinchcombe, M.C., Bibby, T.S., Poulton, A.J., 2010b. Summertime trends in pelagic biogeochemistry at the Porcupine Abyssal Plain study site in the northeast Atlantic. Deep Sea Research Part II 57, 1313–1323.

Peloquin, J., Swan, C., Gruber, N., Vogt, M., Claustre, H., Ras, J., Uitz, J., Barlow, R., Behrenfeld, M., Bidigare, R., Dierssen, H., Ditullio, G., Fernandez, E., Gallienne, C., Gibb, S., Goericke, R., Harding, L., Head, E., Holligan, P., Hooker, S., Karl, D., Landry, M., Letelier, R., Llewellyn, C.A., Lomas, M., Lucas, M., Mannino, A., Marty, J.-C., Mitchell, B.G., Muller-Karger, F., Nelson, N., O'Brien, C., Prezelin, B., Repeta, D., Smith Jr., W.O., Smythe-Wright, D., Stumpf, R., Subramaniam, A., Suzuki, K., Trees, C., Vernet, M., Wasmund, N., Wright, S., 2013. The MAREDAT global database of high performance liquid chromatography marine pigment measurements. Earth System Science Data 5, 109–123. http://dx.doi.org/10.5194/essd-5-109-2013.

Perry, M.J., Sackmann, B.S., Eriksen, C.C., Lee, C.M., 2008. Seaglider observations of blooms and subsurface chlorophyll maxima off the Washington coast. Limnology and Oceanography 53 (5 part 2), 2169–2179.

Pollard, R., 1980. Properties of near-surface inertial oscillations. Journal of Physical Oceanography 10 (3), 385–398.

Pollard, R.T., Griffiths, M.J., Cunningham, S.A., Read, J.F., Perez, F.F., Rios, A.F., 1996. Vivaldi 1991 – a study of the formation, circulation and ventilation of Eastern North Atlantic Central Water. Progress in Oceanography 37, 167–192.

Poulton, A.J., Stinchcombe, M.C., Achterberg, E.P., Bakker, D.C.E., Dumousseaud, C., Lawson, H.E., Lee, G.A., Richier, S., Suggett, D.J., Young, J.R., 2014. Coccolithophores on the north-west European shelf: calcification rates and environmental controls. Biogeosciences 11, 3919–3940. http://dx.doi.org/10.5194/bg-11-3919-2014.

Poulton, A.J., Young, J.R., Bates, N.R., Balch, W.M., 2011. Biometry of detached *Emiliania huxleyi* coccoliths along the Patagonian Shelf. Marine Ecology Progress Series 443, 1–17.

Ragueneau, O., Treguer, P., 1994. Determination of biogenic silica in coastal waters: applicability and limits of the alkaline digestion method. Marine Chemistry 45, 43–51.

Redfield, A.C., Ketchum, B.H., Richards, F.A., 1963. The influence of organisms on the composition of sea-water. In: Hill, M.N. (Ed.), The Sea: Composition of Seawater Comparative and Descriptive Oceanography, vol. 2. Interscience, London, pp. 26–77.

Reid, P.C., Colebrook, J.M., Matthews, J.B.L., Aiken, J., Team, C.P.R., 2003. The Continuous Plankton Recorder: concepts and history, from Plankton Indicator to undulating recorder. Progress in Oceanography 58, 117–173.

Richardson, A.J., Walne, A.W., John, A.W.G., Jonas, T.D., Lindley, J.A., Sims, D.W., Stevens, D., Witt, M., 2006. Using continuous plankton recorder data. Progress in Oceanography 68, 27–74.

Rios, A.F., Perez, F.F., Fraga, F., 1992. Water masses in the upper and middle North Atlantic Ocean east of the Azores. Deep Sea Research 39 (3/4), 645–658.

Rippeth, T.P., Wiles, P., Palmer, M.R., Sharples, J., Tweddle, J., 2009. The diapycnal nutrient flux and shear-induced diapycnal mixing in the seasonally stratified western Irish Sea. Continental Shelf Research 29 (13), 1580–1587.

Robinson, C., Poulton, A.J., Holligan, P.M., Baker, A.R., Forster, G., Gist, N., Jickells, T. D., Malin, G., Upstill-Goddard, R., Williams, R.G., Woodward, E.M.S., Zubkov, M. V., 2006. The Atlantic Meridional Transect (AMT) Programme: a contextual view 1995–2005. Deep Sea Research Part II 53 (14–16), 1485–1515.

Robinson, C., Holligan, P., Jickells, T., Lavender, S., 2009. Foreward: the Atlantic Meridional Transect Programme (1995–2012). Deep Sea Research Part II 56, 895–898.

Rumyantseva, A., Lucas, N., Rippeth, T., Martin, A., Painter, S.C., Boyd, T.J., Henson, S., 2015. Ocean nutrient pathways associated with the passage of a storm. Global Biogeochemical Cycles 29, 1179–1189. http://dx.doi.org/10.1002/2015GB005097.

Russell, F.S., Yonge, C.M., 1928. The Seas: Our Knowledge of Life in the Sea and How It is Gained. Frederick Warne and Co. Ltd., London, 379 pp.

Sambrotto, R.N., Savidge, G., Robinson, C., Boyd, P., Takahashi, T., Karl, D.M., Langdon, C., Chipman, D., Marra, J., Codispoti, L., 1993a. Elevated consumption of carbon relative to nitrogen in the surface ocean. Nature 363, 248–250.

Sambrotto, R.N., Martin, J.H., Broenkow, W.W., Carlson, C., Fitzwater, S.E., 1993b. Nitrate utilization in surface waters of the Iceland Basin during spring and summer of 1989. Deep Sea Research Part II 40 (1/2), 441–457.

Savidge, G., Williams, P.J.I.B., 2001. The PRIME 1996 cruise: an overview. Deep Sea Research II 48, 687–704.

Smayda, T.J., 1957. Phytoplankton studies in lower Narragansett Bay. Limnology and Oceanography 2 (4), 342–359.

Steidinger, K.A., Tangen, K., 1997. Dinoflagellates. In: Tomas, C.R. (Ed.), Identifying Marine Phytoplankton. Academic Press, San Diego, pp. 387–584.

Steinhoff, T., Friedrich, T., Hartman, S.E., Oschlies, A., Wallace, D.W.R., Kortzinger, A., 2010. Estimating mixed layer nitrate in the North Atlantic Ocean. Biogeosciences 7, 795–807.

Sverdrup, H.U., 1953. On conditions for the vernal blooming of phytoplankton. Journal du Conseil Permanent International Pour L'Exploration de la Mer 18, 287–295.

Taylor, J.R., Ferrari, R., 2011. Shutdown of turbulent convection as a new criterion for the onset of spring phytoplankton blooms. Limnology and Oceanography 38 (6), 2293–2307.

Thyssen, M., Mathieu, D., Garcia, N., Denis, M., 2008. Short-term variation of phytoplankton assemblages in Mediterranean coastal waters recorded with an automated submerged flow cytometer. Journal of Plankton Research 30 (9), 1027–1040.

Thyssen, M., Grégori, G.J., Grisoni, J.-M., Pedrotti, M.L., Mousseau, L., Artigas, L.F., Marro, S., Garcia, N., Passafiume, O., Denis, M.J., 2014. Onset of the spring bloom in the northwestern Mediterranean Sea: influence of environmental pulse events on the in situ hourly-scale dynamics of the phytoplankton community structure. Frontiers in Microbiology, 5 Article 387.

Toggweiler, J.R., 1993. Carbon overconsumption. Nature 363, 210–211.

Torres-Valdes, S., Painter, S.C., Martin, A.P., Sanders, R., Felden, J., 2014. Data compilation of fluxes of sedimenting material from sediment traps in the Atlantic Ocean. Earth System Science Data 6, 123–145.

Trees, C.C., Clark, D.K., Bidigare, R.R., Ondrusek, M.E., Mueller, J.L., 2000. Accessory pigments versus chlorophyll *a* concentrations within the euphotic zone: a ubiquitous relationship. Limnology and Oceanography 45 (5), 1130–1143.

Tyrrell, T., Maranon, E., Poulton, A.J., Bowie, A.R., Harbour, D.S., Woodward, E.M.S., 2003. Large-scale latitudinal distribution of *Trichodesmium* spp. in the Atlantic Ocean. Journal of Plankton Research 25 (4), 405–416.

Tyrrell, T., Merico, A., 2004. Emiliania huxleyi: bloom observations and the conditions that induce them. In: Thierstein, H.R., Young, J.R. (Eds.), Coccolithophores: From Molecular Processes to Global Impact. Springer-Verlag, Berlin, pp. 75–97.

Uitz, J., Claustre, H., Morel, A., Hooker, S.B., 2006. Vertical distribution of phytoplankton communities in open ocean: an assessment based on surface chlorophyll. Journal of Geophysical Research 111, C08005. http://dx.doi.org/10.1029/2005JC003207.

Van Bleijswijk, J., Kempers, R., Van Der Wal, P., Westbroek, P., Egge, J., Lukk, T., 1994. Standing stocks of PIC, POC, PON and *Emiliania huxleyi* coccospheres and liths in seawater enclosures with different phosphate loadings. Sarsia 79, 307–318.

van de Poll, W.H., Kulk, G., Timmermans, K.R., Brussaard, C.P.D., van der Woerd, H.J., Kehoe, M.J., Mojica, K.D.A., Visser, R.J.W., Rozema, P.D., Buma, A.G.J., 2013. Phytoplankton chlorophyll a biomass, composition, and productivity along a temperature and stratification gradient in the northeast Atlantic Ocean. Biogeosciences 10, 4227–4240.

Vidussi, F., Claustre, H., Manca, B.B., Luchetta, A., Marty, J.C., 2001. Phytoplankton pigment distribution in relation to upper thermocline circulation in the eastern Mediterranean Sea during winter. Journal of Geophysical Research 106 (C9), 19939–19956.

Vogt, M., O'Brien, C., Peloquin, J., Schoemann, V., Breton, E., Estrada, M., Gibson, J., Karentz, D., Van Leeuwe, M.A., Stefels, J., Widdicombe, C., Peperzak, L., 2012. Global marine plankton functional type biomass distributions: *Phaeocystis* spp. Earth System Science Data 4, 107–120.

Warner, A.J., Hays, G.C., 1994. Sampling by the Continuous Plankton Recorder survey. Progress in Oceanography 34, 237–256.

Welschmeyer, N.A., 1994. Fluorometric analysis of chlorophyll a in the presence of chlorophyll b and phaeopigments. Limnology and Oceanography 39 (8), 1985–1992.

Williams, R., Claustre, H., 1991. Photosynthetic pigments as biomarkers of phytoplankton populations and processes involved in the transformation of particulate organic matter at the biotrans site (47°N, 20°W). Deep Sea Research 38 (3), 347–355.

Winter, A., Jordan, R.W., Roth, P.H., 1994. Biogeography of living coccolithophores in ocean waters. In: Winter, A., Siesser, W.G.E. (Eds.), Coccolithophores. Cambridge University Press, Cambridge, pp. 161–177.

Winter, A., Siesser, W.G., 1994. Atlas of living coccolithophores. In: Winter, A., Siesser, W.G.E. (Eds.), Coccolithophores. Cambridge University Press, Cambridge, pp. 107–159.

Young, J., Geisen, M., Cros, L., Kleijne, A., Sprengel, C., Probert, I., Østergaard, J., 2003. A guide to extant coccolithophore taxonomy. Journal of Nannoplankton Research Special Issue 1, 1–125.